Inorganic Chemistry

Article

pubs.acs.org/IC

# A Polyaromatic Terdentate Binding Unit with Fused 5,6-Membered Chelates for Complexing s-, p-, d-, and f-Block Cations

Thi Nhu Y Hoang,*[,†] Marie Humbert-Droz,[†] Thibault Dutronc,[†] Laure Guénée,[‡] Céline Besnard,[‡] and Claude Piguet*[,†]

[†]Department of Inorganic, Analytical and Applied Chemistry, University of Geneva, 30 quai E. Ansermet, CH-1211 Geneva 4, Switzerland

[‡]Laboratory of Crystallography, University of Geneva, 24 quai E. Ansermet, CH-1211 Geneva 4, Switzerland

Supporting Information

**ABSTRACT:** The polyaromatic terdentate ligand 6-(azaindol-1-yl)-2,2′-bipyridine (**L7**) combines one 5-membered chelate ring with a fused 6-membered chelate ring. It is designed to provide complexation properties intermediate between 2,2′;6′,2″-terpyridine (**L1**) (two fused 5-membered chelate rings) and 2,6-bis(azaindol-1-yl)pyridine (**L6**) (two fused 6-membered chelate rings). In polar organic solvents, **L7** displays remarkable affinities for the successive fixation of two small univalent cations M = $H^+$ or $Li^+$, leading to stable $[M_m(\mathbf{L7})]^{m+}$ ($m$ = 1−2) complexes. Upon reaction with M = $Mg^{2+}$ or $Zn^{2+}$ cations, the large positive charge densities borne by the metals result in the successive cooperative complexation of two ligands to give $[M(\mathbf{L7})_n]^{n+}$ ($n$ = 1−2). For small $Sc^{3+}$, unavoidable traces of water favor the formation of the protonated ligand at millimolar concentrations in acetonitrile, but the use of larger $Y^{3+}$ cations leads to $[Y(\mathbf{L7})_n]^{n+}$ ($n$ = 1, 2), for which stability constants of $\log(\beta_{1,1}^{Y,L7})$ = 2.9(5) and $\log(\beta_{1,2}^{Y,L7})$ = 5.3(4) are estimated. The complexation behaviors are supported by speciations in solution, thermodynamic analyses, and solution and solid-state structures.

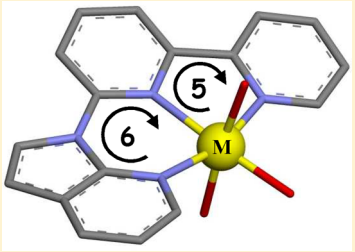


## INTRODUCTION

Molecular mechanics have established that aliphatic 5-membered chelate rings were geometrically adapted for catching large cations, whereas six-membered analogues matched smaller metals (see Figure S1 in the Supporting Information).[1] In order to improve structural control and light-harvesting properties, aromatic rings were incorporated into the chelating ligands and numerous large tervalent lanthanide cations, Ln(III), acting as luminescent[2] or magnetic[3] probes, were successfully coordinated not only with 5-, but also with 6- or even with 7-membered polyaromatic chelates, in contradiction with the original rule of thumb.[2] However, we note that 6- and 7-membered chelates, which are geometrically poorly adapted for large Ln(III), systematically relied on negatively charged ligands in order to benefit from the considerable entropic driving force produced by the charge neutralization accompanying the complexation process in polar solvents.[1b,4] For neutral polyaromatic terdentate ligands, only fused 5-membered chelates are known to give stable complexes with tervalent Ln(III), among which the terdentate ligands **L1**,[5] **L2**,[6] **L3**,[7] **L4**,[8] and **L5**[9] are the archetypes (see Scheme 1).

Beyond the investigation of these neutral soft receptors for the selective extraction of actinides over lanthanides in acidic nuclear wastes, only slight interest was focused on their potential selectivity along the lanthanide series. For terpyridine **L1**, the fixation of the first binding unit gives moderately stable $[Ln(\mathbf{L1})(H_2O)_n]^{3+}$ complexes in water, whose formation constants stepwise increase along the series ($\log(\beta_{1,1}^{Ln,L7})$ = 2.08−2.80 for Ln = La, Eu, Lu).[5r] In less-polar acetonitrile, the stability is improved by 5 orders of magnitude ($\log(\beta_{1,1}^{Ln,L1})$ = 7.5−7.7), but the size-discriminating effects are leveled out.[5h] To the best of our knowledge, only the third successive thermodynamic constants $K_{1,3}^{Ln,L5}$, transforming $[Ln(\mathbf{L5})_2(CH_3CN)_3]^{3+}$ into $[Ln(\mathbf{L5})_3]^{3+}$, display some noticeable size selectivity along the lanthanide series. These constants decrease by 3 orders of magnitude in going from Ln = Gd(III) to Lu(III), because of the steric constraints produced by the helical wrapping of the three strands in the final complexes.[5t,9d] With this in mind, we suspect that the large distortion of the polyaromatic backbone detected upon meridional ter-coordination of **L6** (fused 6,6-membered chelate) to Zn(II)[10] or Cu(II),[11] compared with the coplanar arrangement found for **L1** (fused 5,5-membered chelate) in $[Zn(\mathbf{L1})Br_2]$,[12] could produce unusual thermodynamic effects. Along this line of reasoning, we note that **L6** indeed reacts with $YI_3$ under anhydrous conditions to give $[Y(\mathbf{L6})_n]^{3+}$ ($n$ = 1, 2), despite its claimed reluctance for large cations; however, the extreme sensitivity of these complexes to moisture and their low solubility prevent further investigations.[10] Pushing forward this strategy, we report here on the preparation of the unsymmetrical terdentate aromatic ligands **L7**, which are made of a 5-membered bipyridine chelate fused with a 6-membered pyridine-azaindole ring,[13] and we also explore its complexation properties with spherical cations possessing various $Z^2/R$

**Received:** March 1, 2013
**Published:** April 19, 2013

   dx.doi.org/10.1021/ic400526j | Inorg. Chem. 2013, 52, 5570−5580

**Scheme 1. Chemical Structures of the Terdentate Polyaromatic Ligands L1−L7 in Their Relaxed *trans−trans* Conformations**

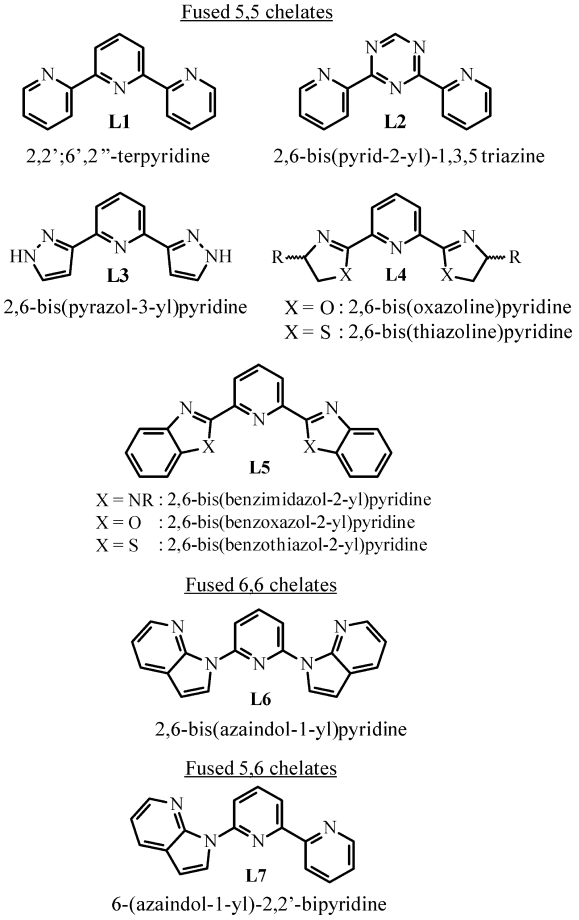


electrostatic factors ($Z$ is the charge of the cation in electrostatic units and $R$ is its ionic radius).

## RESULTS AND DISCUSSION

**Synthesis of Ligand L7, and Complexation with Univalent $H^+$ and $Li^+$ Cations.** The terdentate ligand **L7** is obtained in two steps from 2-(tributylstannyl) pyridine (**1**) with a 47% global yield (see Scheme 2). The initial Stille coupling reaction uses commercially available 2,6-dibromopyridine to give 6-bromo-2,2′-bipyridine (**2**),[14] which is transformed to **L7** via a catalyzed Ullmann-type coupling reaction with 7-azaindole.[15] The 12 aromatic $^1$H NMR signals of **L7** (see Figure 2 and Figures S2−S5 in the Supporting Information) are compatible with an average planar $C_s$ symmetry, where the distal N atoms adopt *trans−trans* conformations, with respect to the nitrogen of the central pyridine ring, as shown in Scheme 2. The low-field resonances of H2−H3 and H8−H9 pairs are diagnostic for their location close to the electronegative N atoms of the adjacent heterocyclic ring (see Tables S1 and S2 in the Supporting Information), while the lack of a nuclear Overhauser enhancement effect between the H atoms of each hydrogen pair precludes *cis−cis* geometry.

$^1$H NMR titrations of **L7** in $CD_3CN/CDCl_3$ (1:1) or in $CD_3CN$ with $CF_3SO_3H$ (Figures S2 and S3 in the Supporting Information) or with $LiClO_4$ (Figures S4 and S5 in the Supporting Information) exhibit fast-exchange processes on the

**Scheme 2. Synthesis of Ligand L7 with Numbering Scheme for NMR Data**

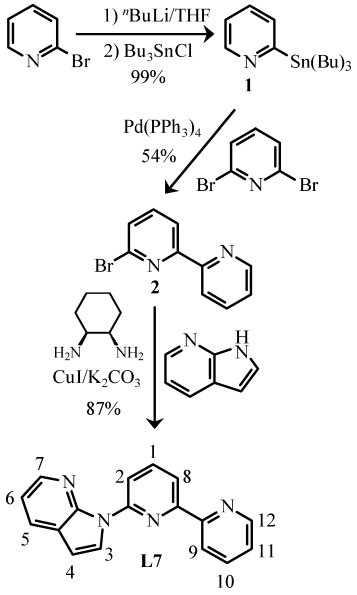


NMR time scale with end points for M:**L7** = 1.0 and 2.0, in agreement with the formation of the $[ML7]^+$ and $[M_2(L7)]^{2+}$ complexes detected by ESI-MS in the gas phase (see Table S3 in the Supporting Information). The complete set of dynamically average chemical shifts can be satisfyingly fitted to eqs 1 and 2, using nonlinear least-squares techniques, to give $\log(\beta_{1,1}^{M,L7})$ and $\log(\beta_{2,1}^{M,L7})$ (Table 1),[16] ligand distributions (Figure 1 and Figure S6 in the Supporting Information) and individual $^1$H NMR spectra (see Figure 2, as well as Figure S7, Table S1, and Table S2 in the Supporting Information).

$$M^+ + L7 \rightleftharpoons [ML7]^+ \qquad \beta_{1,1}^{M,L7} \tag{1}$$

$$2M^+ + L7 \rightleftharpoons [M_2L7]^{2+} \qquad \beta_{2,1}^{M,L7} \tag{2}$$

As expected, the formation constants $\beta_{m,1}^{M,L7}$ are reduced by a factor of 5−10 in pure $CD_3CN$, because of the larger solvation of the free cations in a more polar solvent. Compared with **L1** ($\log(\beta_{1,1}^{H,L1})$ = 3.4(1) and $\log(\beta_{2,1}^{H,L1})$ = 5.3(3)) and with **L6** ($\log(\beta_{1,1}^{H,L6})$ = 5.3(3) and $\log(\beta_{2,1}^{H,L6})$ = 8.9(3)) in $CD_3CN/CDCl_3$ (1:1),[10] **L7** displays the largest affinity for protons ($\log(\beta_{1,1}^{H,L7})$ = 5.7(1) and $\log(\beta_{2,1}^{H,L7})$ = 9.5(5)), together with non-negligible formation constants with $Li^+$, for which **L1** and **L6** exhibited nonmesurable stability constants at millimolar concentrations. The careful analysis of the individual $^1$H NMR spectra gives pertinent structural information. Upon titration with $H^+$, the concomitant downfield shift of the signals of H2, H3, and H5 indicates a decrease in electronic density upon protonation, but the *trans* conformation of the azaindol-pyridine unit is not seriously affected by the fixation of the first proton in $[HL7]^+$ (red arrows in Figure 2).

In contrast, the upfield shift of H8 (−0.15 ppm) points to a *cis* conformation of the 2,2′-bipyridine unit in $[HL7]^+$, because H8 is no more influenced by the N atom of the adjacent pyridine ring,[10] while the concomitant downfield shift of H10 (0.73 ppm) demonstrates that protonation occurs on the distal pyridine ring (blue arrows in Figure 2).[17] The second protonation occurs at the azaindol ring and leads to a twisted *cis−cis* conformation for the terdentate ligand in $[H_2L7]^{2+}$. With M = $Li^+$, the concomitant downfield shift of the signals of


dx.doi.org/10.1021/ic400526j | Inorg. Chem. 2013, 52, 5570−5580

Table 1. Cumulative Thermodynamic Constants ($\log(\beta_{m,n}^{M,L7})$, Associated Microscopic Affinities ($\log(j_{connect}^{M,L7})$ and $\Delta G_{connect}^{M,L7}$), Intramolecular Intermetallic ($\log(u_{L7}^{M,M})$ and $\Delta G_{interaction}^{M,M,L7}$) and Interligand ($\log(u_{M}^{L7,L7})$ and $\Delta G_{interaction}^{L7,L7,M}$) Interactions and Allosteric Cooperativity Factors ($\alpha$) Obtained by $^1$H NMR for the Titrations of L7 with $CF_3SO_3H$, $LiClO_4$, $Mg(ClO_4)_2$, $Zn(CF_3SO_3)_2$, and $Y(CF_3SO_3)_3$·diglyme at 298 K

| | $H^+$ | | $Li^+$ | | $Mg^{2+}$ | | $Zn^{2+}$ | | $Y^{3+}$ |
|---|---|---|---|---|---|---|---|---|---|
| | $CD_3CN/CDCl_3$ (1:1) | $CD_3CN$ | $CD_3CN/CDCl_3$ (1:1) | $CD_3CN$ | $CD_3CN/CDCl_3$ (1:1) | $CD_3CN$ | $CD_3CN/CDCl_3$ (1:1) | $CD_3CN$ | $CD_3CN$ |
| $\log(\beta_{1,1}^{M,L7})$ | 5.7(1) | 5.3(2) | 3.4(1) | 2.6(1) | 4.1(3) | 3.1(4) | 4.0(2) | 3.8(2) | 2.9(5) |
| $\log(\beta_{2,1}^{M,L7})$ | 9.5(5) | 9.1(2) | 6.5(2) | 5.5(2) | 8.8(2) | 7.6(5) | 6.2(2) | 6.3(1) | 5.3(4) |
| $\log(j_{connect}^{M,L7})$ | 5.4(1) | 4.8(2) | 2.3(2) | 1.5(1) | 2.7(3) | 1.8(4) | 2.6(2) | 2.4(2) | 2.1(4) |
| $\Delta G_{connect}^{M,L7}$ (kJ mol$^{-1}$) | −30.8(6) | −28.5(1.1) | −13.2(1.1) | −8.7(6) | −15.4(1.9) | −10.0(2.0) | −15.0(1.1) | −13.8(1.1) | −12.1(2.9) |
| $\log(u_{L7}^{M,M})$ | −1.4(5) | −1.2(4) | −0.3(4) | 0.3(2) | 2.0(2.0) | 3.0(8) | −0.4(4) | 0.1(3) | 0.3(8) |
| $\Delta E_{interaction}^{M,M,L7}$ (kJ mol$^{-1}$) | 9.1(3.0) | 6.8(2.0) | 1.7(2.0) | −1.7(1.4) | −11.7(11.4) | −17.3(4.3) | 2.4(2.0) | −0.5(1.7) | −1.6(4.6) |
| $\alpha^a$ | 0.03(5) | 0.06(5) | 0.5(4) | 2.0(1.1) | $\alpha^b$ | 100(460) | 1000(1840) | 0.4(4) | 1.3(9) | 2.0(3.7) |

$^a$Equation taken from ref 21. $\alpha = [(\omega_{1,1}^{M,L7})^2/\omega_{2,1}^{M,L7}] \times [\beta_{2,1}^{M,L7}/(\beta_{1,1}^{M,L7})^2] = u_{L7}^{M,M}$. $^b$Equation taken from ref 21. $\alpha = [(\omega_{1,1}^{M,L7})^2/\omega_{1,2}^{M,L7}] \times [\beta_{1,2}^{M,L7}/(\beta_{1,1}^{M,L7})^2] = u_{M}^{L7,L7}$.




**Figure 1.** Computed ligand speciation (mole fraction (%) of the ligand in the various species) for the titrations of **L7** with (a) $CF_3SO_3H$ and (b) $LiClO_4$ in $CD_3CN/CDCl_3$ (1:1) at 298 K. Total ligand concentration $|\mathbf{L7}|_{tot} = 7.5 \times 10^{-3}$ M.

H2−H3 and of H8−H9 in $[LiL7]^{2+}$ implies a *cis*−*cis* conformation for the ligand upon fixation of the first $Li^+$ cation. The affinity for a second $Li^+$ cation remains modest and does further significantly affect the $^1$H NMR spectrum (see Figure 2 and Figure S7 in the Supporting Information).

X-ray crystal structures solved for $[HL7](CF_3SO_3)$ (**3**), $[H_2L7](ClO_4)_2$ (**4**), and $[Li(L7)(ClO_4)(H_2O)]$ (**5**) confirm the solution data with the coordinated polyaromatic terdentate unit adopting coplanar *trans*−*cis* $[HL7]^+$, twisted *cis*−*cis* $[H_2L7]^{2+}$, and coplanar *cis*−*cis* $[LiL7]^+$ conformations (see Figure 3, as well as Figure S8 and Tables S4−S13 in the Supporting Information). The protonated cations $[HL7]^+$ and $[H_2L7]^{2+}$ are involved in weak intramolecular and intermolecular hydrogen bonds in the crystals of **3** and **4** (see Tables S7 and S10 in the Supporting Information). In **5**, the univalent Li metal displays standard Li−N distances[18] and its coordination sphere is completed with one water molecule and one unidentate perchlorate counteranion to give the five-coordinated pseudo-trigonal bypyramidal complex $[Li(L7)(ClO_4)(H_2O)]$.[19] Taking the molecular structures of *cis*−*cis* $[H_2L7]^{2+}$ as a rough model for the meridional ter-coordination of this ligand around multivalent cations, we conclude that the shape of the irregular triangle drawn by the three donor N atoms (Figure 4) is intermediate between the pseudo-isosceles triangles reported for $[H_2L1]^{2+}$ (adapted for large cations)[20] and $[H_2L6]^{2+}$ (adapted for small cations).[10]


dx.doi.org/10.1021/ic400526j | Inorg. Chem. 2013, 52, 5570−5580

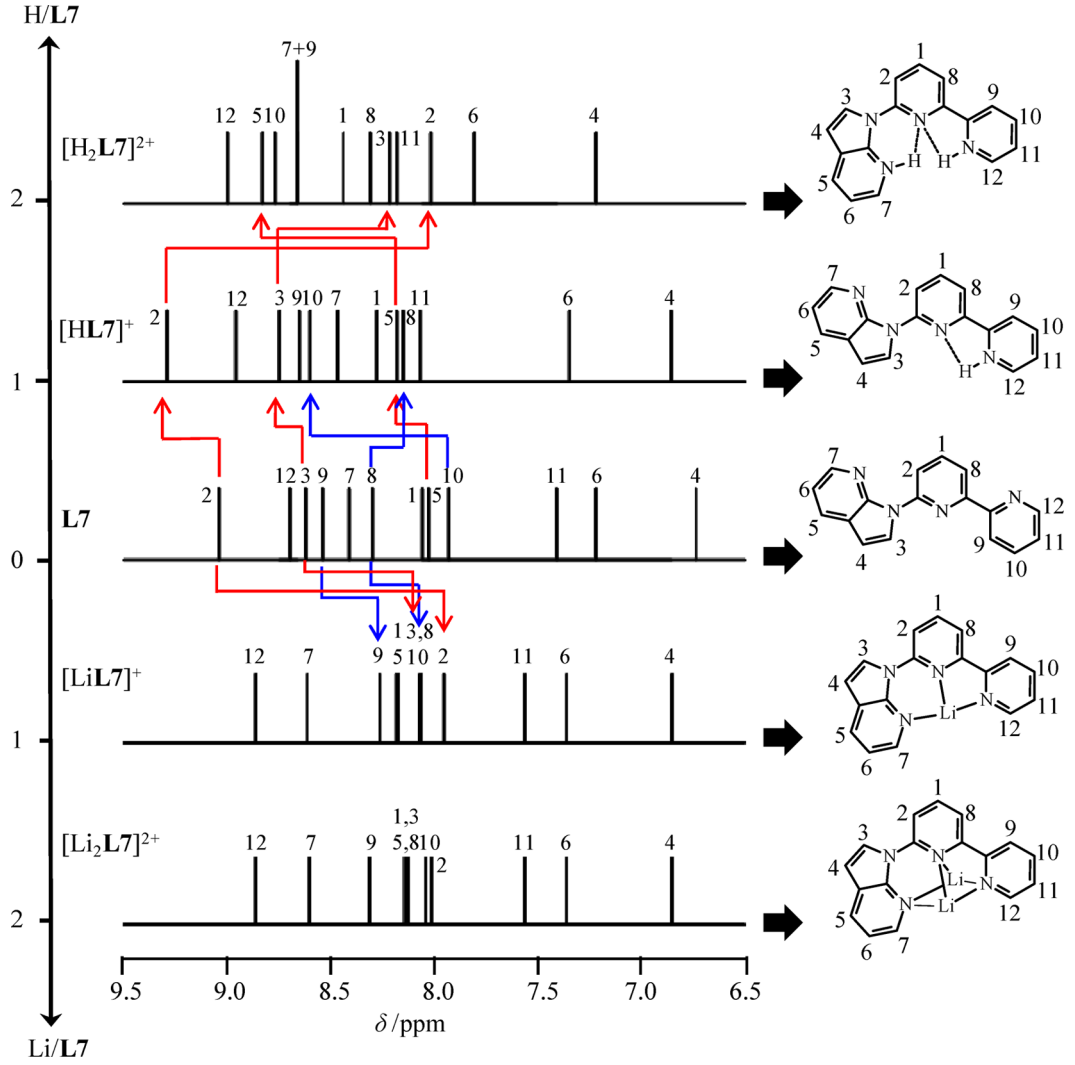


**Figure 2.** Computed individual $^1$H NMR spectra for **L7** (middle), $[H\mathbf{L7}]^+$ and $[H_2\mathbf{L7}]^{2+}$ (top), and $[Li\mathbf{L7}]^+$ and $[Li_2\mathbf{L7}]^{2+}$ (bottom) in $CD_3CN/CDCl_3$ (1:1) with associated solution structures. Red arrows highlight diagnostic variations in the chemical shifts for establishing the conformation of the azaindol-pyridine unit, whereas blue arrows hold for the bipyridine unit (see text).

Within the frame of the site-binding approach,[22] the cumulative formation macroconstants (eqs 1 and 2) can be modeled with eqs 3 and 4, respectively.

$$\beta_{1,1}^{M,\mathbf{L7}} = \sum_i \omega_{1,1(N_i)}^{H,\mathbf{L7}} f_{N_i}^{M,\mathbf{L7}} \tag{3}$$

$$\beta_{2,1}^{M,\mathbf{L7}} = \sum_{i\neq j} \omega_{2,1(N_iN_j)}^{M,\mathbf{L7}} (f_{N_i}^{M,\mathbf{L7}})(f_{N_j}^{M,\mathbf{L7}}) u_{\mathbf{L7}(N_iN_j)}^{M,M} \tag{4}$$

In these equations, the sums run over all microspecies possessing the same stoichiometry but differing by the precise location of the metallic cations bound to each specific nitrogen atom $N_i$ (and $Nj$) in ligand **L7**. $\omega_{m,n}^{M,\mathbf{L7}}$ takes into account the pure statistical (i.e., entropic) contribution due to change in molecular rotational entropies occurring upon complexation for each microspecies.[23] Once the point group of each partner contributing to eqs 1 and 2 is at hand, $\omega_{m,n}^{M,\mathbf{L7}}$ are easily computed using the method of symmetry numbers (see Figures S9 and S10 in the Supporting Information). $f_{N_i}^{M,\mathbf{L7}}$ corresponds to the absolute affinities of the $N_i$ atom of the heterocyclic aromatic ring involved in the coordination of the cation. Application of the van't Hoff isotherm transforms these thermodynamic descriptions into free energies of connection $\Delta G_{\text{connect, N}_i}^{M,\mathbf{L7}} = -RT \ln(f_{N_i}^{M,\mathbf{L7}})$, which include desolvation processes (the standard concentration of the reference state is set to 1 M).[24] Finally, $u_{\mathbf{L7}}^{M,M} = e^{-(\Delta E_{\mathbf{L7}}^{M,M}/RT)}$ is the Boltzmann factor correcting for the free energy of connection for any intramolecular M···M interactions resulting from the close location of the two cations in $[M_2\mathbf{L7}]^{2+}$. Assuming that the affinity of distal and central N donors are identical ($f_{\text{N-central}}^{M,\mathbf{L7}} = f_{\text{N-distal}}^{M,\mathbf{L7}} = f_{\text{connect}}^{M,\mathbf{L7}}$), the application of eqs 3 and 4 provides eqs 5 and 6 for $M = H^+$ (see Figures S9 and S10 in the Supporting Information) and eqs 7 and 8 for $M = Li^+$ (see Figure S11 in the Supporting Information), from which pertinent microscopic thermodynamic descriptions can be computed (see Table 1, entries 3–6).[25]

$$\beta_{1,1}^{H,\mathbf{L7}} = 2 f_{\text{connect}}^{H,\mathbf{L7}} \tag{5}$$

$$\beta_{2,1}^{H,\mathbf{L7}} = 2 (f_{\text{connect}}^{H,\mathbf{L7}})^2 u_{\mathbf{L7}}^{H,H} \tag{6}$$

$$\beta_{1,1}^{Li,\mathbf{L7}} = 12 f_{\text{connect}}^{Li,\mathbf{L7}} \tag{7}$$


dx.doi.org/10.1021/ic400526j | Inorg. Chem. 2013, 52, 5570−5580

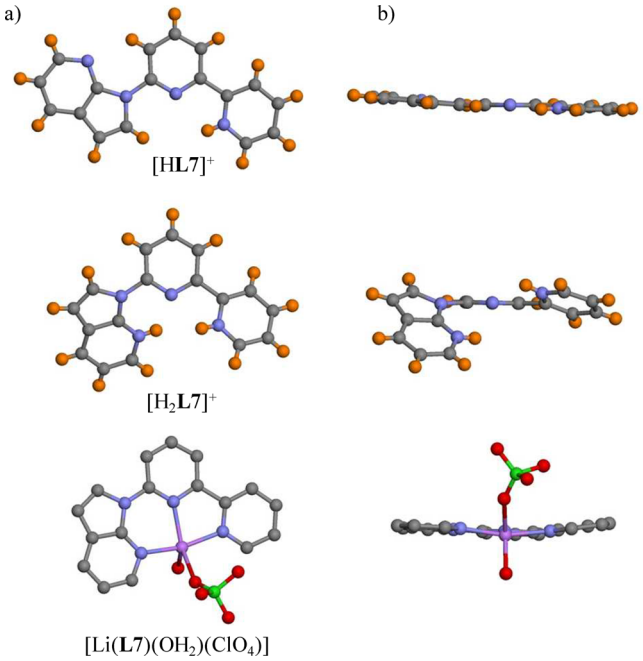


**Figure 3.** Perspective views (a) perpendicular and (b) parallel to the central pyridine ring of the molecular structures of $[HL7]^+$, $[H_2L7]^{2+}$ and $[Li(L7)(OH_2)(ClO_4)]$ observed in the crystal structures of $[HL7](CF_3SO_3)$ (**3**), $[H_2L7](ClO_4)_2$ (**4**) and $[Li(L7)(ClO_4)(H_2O)]$ (**5**). Color code: gray = C, blue = N, orange = H, violet = Li. Hydrogen atoms are omitted for $[Li(L7)(OH_2)(ClO_4)]$.

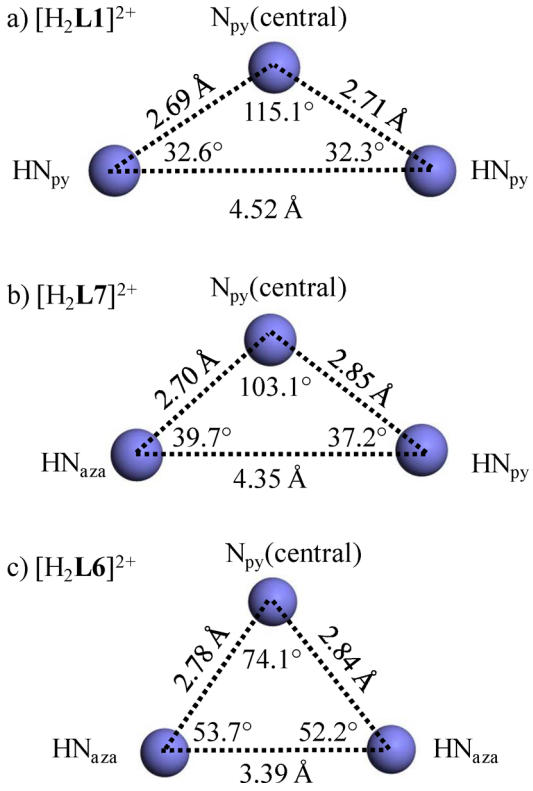


**Figure 4.** Geometries of the triangles formed by the donor N atoms in the molecular structures of (a) $[H_2L1]^{2+}$,[20] (b) $[H_2L7]^{2+}$, and (c) $[H_2L6]^{2+}$.[10]

$$\beta_{2,1}^{Li,L7} = 144(f_{connect}^{Li,L7})^2 u_{L7}^{Li,Li} \quad (8)$$

The free energy of connection is much larger for the $H^+$ cation than for the $Li^+$ cation, because of the increase in size, which reduces the electrostatic factor to $Z^2/R$ = 2.8 eu/Å for five-coordinated Li(I).[26] Interestingly, the unsymmetrical fused 5,6-membered chelate ligand **L7** displays the largest affinity for small univalent cation ($\Delta G_{connect}^{H,L7}$ = −30.8(6) kJ/mol and $\Delta G_{connect}^{Li,L7}$ = −13.2.(1.1) kJ/mol) compared with **L1** (fused 5,5-membered chelates, $\Delta G_{connect}^{H,L1}$ = −16.7(6) kJ/mol and $\Delta G_{connect}^{Li,L1}$ > −5 kJ/mol) and **L6** (fused 6,6-membered chelates, $\Delta G_{connect}^{H,L6}$ = −27.5(1.7) kJ/mol and $\Delta G_{connect}^{Li,L6}$ > −5 kJ/mol).[10] The successive protonations of **L1**, **L6**, and **L7** follow anticooperative protocols with a reluctance of 6 < $\Delta E_{interaction}^{M,M,Lk}$ < 9 kJ/mol for the fixation of the second proton, while multilithiation in $[Li_2L7]^{2+}$ is statistically within experimental uncertainties.

**Complexation of L7 with Bivalent $Mg^{2+}$ and $Zn^{2+}$ Cations.** Electron spin ionization−mass spectroscopy (ESI-MS) titrations of **L7** with $M^{2+}$ cation in acetonitrile show the initial formation of $[M(L7)]^{2+}$ ($[Mg(L7)(CH_3CN)]^{2+}$ at $m/z$ = 168.0 and $[Zn(L7)]^{2+}$ at $m/z$ = 169.4), followed by the fixation of a second ligand to the divalent metal to give saturated $[M(L7)_2]^{2+}$ complexes ($[Mg(L7)_2]^{2+}$ at $m/z$ = 284.0 and $[Zn(L7)_2]^{2+}$ at $m/z$ = 304.6). $^1H$ NMR titrations recorded in $CDCl_3$:$CD_3CN$ or in $CD_3CN$ operate under intermediate (M = Mg; see Figure S12 in the Supporting Information) or slow (M = Zn, Figure S13 in the Supporting Information) exchange rate on the NMR time scale, which easily demonstrate that **L7**, $[ML7]^{2+}$, and $[M(L7)_2]^{2+}$ are the only ligand-containing species. Integration of the $^1H$ NMR signals of the same proton in the different species provides quantitative speciations, from which the macroscopic stability constants for eqs 9 and 10 are deduced (see Table 1, columns 7−10, as well as Appendix I in the Supporting Information), together with ligand distributions (see Figure 5 and Figure S14 in the Supporting Information) and individual $^1H$ NMR spectra (see Figure 6, as well as Figures S15 and S16 and Tables S1 and S2 in the Supporting Information). For M = $Mg^{2+}$, the considerable broadening of the signal at 298 K forced us to solve the speciations at 253 and 263 K (see Figures S17−S19 and Table S14 in the Supporting Information), from which the formation constants at 298 K collected in Table 1 were estimated by using linear van't Hoff plots with $\ln(\beta_{1,n}^{Mg,L7}) = -(\Delta H_{1,n}^{Mg,L7})/RT + (\Delta S_{1,n}^{Mg,L7})/R$ ($\Delta H_{1,n}^{Mg,L7}$ and $\Delta S_{1,n}^{Mg,L7}$ are gathered in Table S14 in the Supporting Information).

$$M^{2+} + L7 \rightleftharpoons [ML7]^{2+} \qquad \beta_{1,1}^{M,L7} \quad (9)$$

$$M^{2+} + 2L7 \rightleftharpoons [M(L7)_2]^{2+} \qquad \beta_{1,2}^{M,L7} \quad (10)$$

The complexation of **L7** with either $Mg^{2+}$ or $Zn^{2+}$ is similar and shows the stepwise meridional tercoordination of two terdentate ligands to give the dynamically average $C_s$-symmetrical $[M(L7)]^{2+}$ and $C_2$-symmetrical $[M(L7)_2]^{2+}$ complexes on the NMR time scale. The systematic upfield shifts of H2, H3 and H9 are diagnostic for the transformation of the original *trans*−*trans* into *cis*−*cis* conformation for **L7** upon complexation, while the global downfield shifts of the protons bound at the para position of the pyridine rings (H1, H5 and H10) point to the complexation of the three N-donors to $M^{2+}$ (see Figure 6 and Figures S15 and S16 in the Supporting Information).[17] It is worth noting here the unusual, but expected, upfield shifts by more than 1.0 ppm for H7 and H12 in $[M(L7)_2]^{2+}$, which results from the location of these protons in the shielding


dx.doi.org/10.1021/ic400526j | Inorg. Chem. 2013, 52, 5570−5580

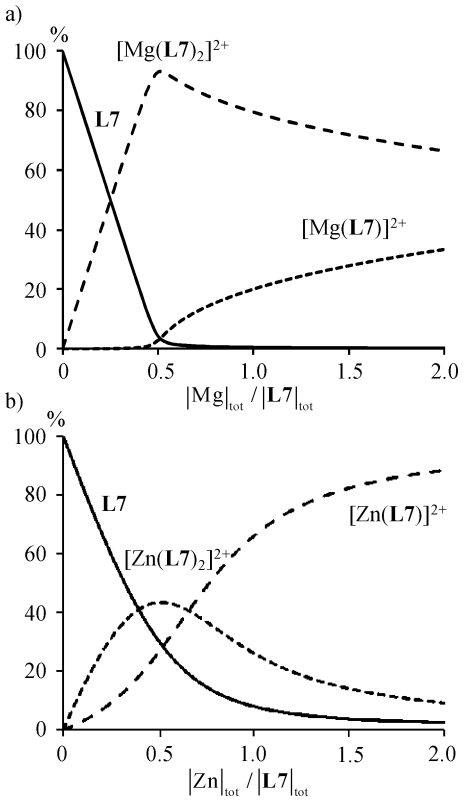


**Figure 5.** Computed ligand speciation (mole fraction (%) of the ligand in the various species) for the titrations of **L7** with (a) $Mg(ClO_4)_2$ and (b) $Zn(CF_3SO_3)_2$ in $CD_3CN/CDCl_3$ (1:1) at 298 K. Total ligand concentration $|\mathbf{L7}|_{tot} = 7.5 \times 10^{-3}$ M.

domain of the pyridine ring of the adjacent ligand (see Figure 6, top).

X-ray crystal structures were solved for $[Mg(\mathbf{L7})(OH_2)_3](ClO_4)_2$ (**6**), $[Zn(\mathbf{L7})(THF)(CF_3SO_3)_2]$ (**7**) and $[Zn(\mathbf{L7})_2](CF_3SO_3)_2 \cdot 0.13H_2O$ (**8**). Each terdentate ligand is meridionally coordinated to the central cation in agreement with the solution structures deduced by NMR (see Figure 7, as well as Figure S20 and Tables S15−S21 in the Supporting Information). The bivalent metals are six-coordinated in pseudo-octahedral environments as found for analogous $[Mg(\mathbf{L1})(OH_2)_3]Cl_2$,[27] $[Zn(\mathbf{L1})(S)X_2]$[28] and $[Zn(\mathbf{L1})_2]X_2$ complexes.[29] However, the adjacent five- and six-membered chelates in **L7** (instead of fused 5,5-membered chelates in **L1**) induces 15−20° helical twists along the polyaromatic strand in **6** and **7** as similarly observed for $[Li(\mathbf{L7})(ClO_4)(H_2O)]$ (**5**), a distortion raised to 35°−45° in $[Zn(\mathbf{L7})_2]^{2+}$, whereas the coordinated **L1** ligands in $[Zn(\mathbf{L1})_2]^{2+}$ are essentially planar (Figure 7 and Figure S21 in the Supporting Information).[29] The average Mg−N and Zn−N bond distances are comparable for complexes with **L1** and **L7**, but their specific distributions are different. With fused 5,5-membered chelates in **L1**, M(II) is located closer to the central pyridine ring (for instance $Mg-N_{pycentral}$ = 2.12 Å, $Mg-N_{pydistal}$ = 2.20 Å in $[Mg(\mathbf{L1})(OH_2)_3]^{2+}$), whereas fused 5,6-membered chelate rings in **L7** put M(II) at a remote distance from the central pyridine nitrogen donor atom, while the distal M−N interactions are shortened ($Mg-N_{pycentral}$ = 2.20 Å, $Mg-N_{pydistal}$ = 2.13 Å ≈ $Mg-N_{azadistal}$ = 2.12 Å in $[Mg(\mathbf{L7})(OH_2)_3]^{2+}$).[13a] This effect is further amplified when two fused 6,6-membered chelate rings are coordinated to Zn(II) as reported for $[Zn(\mathbf{L6})(CF_3SO_3)_2]$ ($Zn-N_{pycentral}$ = 2.25 Å, $Zn-N_{azadistal}$ = 2.00 Å).[10]

The thermodynamic analysis of eqs 9 and 10 within the frame of the site-binding model[22] gives eqs 11 and 12 (see Figure S22 in the Supporting Information), from which the microscopic describers $\Delta G^{M,L7}_{connect}$ and $\Delta E^{L7,L7M}_{interaction}$ are computed (see Table 1, entries 3−6).

$$\beta^{M,L7}_{1,1} = 24 f^{M,L7}_{connect} \quad (11)$$

$$\beta^{M,L7}_{1,2} = 24 (f^{M,L7}_{connect})^2 u^{L7,L7}_{M} \quad (12)$$

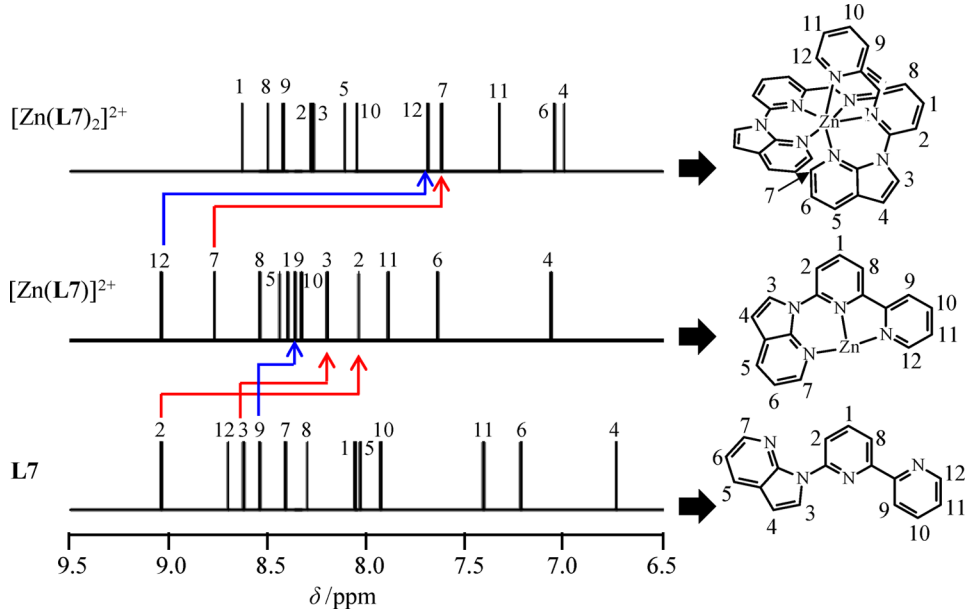


**Figure 6.** Computed individual $^1H$ NMR spectra for **L7**, $[Zn(\mathbf{L7})]^+$, and $[Zn(\mathbf{L7})_2]^{2+}$ in $CD_3CN/CDCl_3$ (1:1) with associated solution structures. Red arrows highlight chemical shifts variations diagnostic for establishing the conformation of the azaindol-pyridine unit, whereas blue arrows hold for the bipyridine unit (see text).


dx.doi.org/10.1021/ic400526j | Inorg. Chem. 2013, 52, 5570−5580

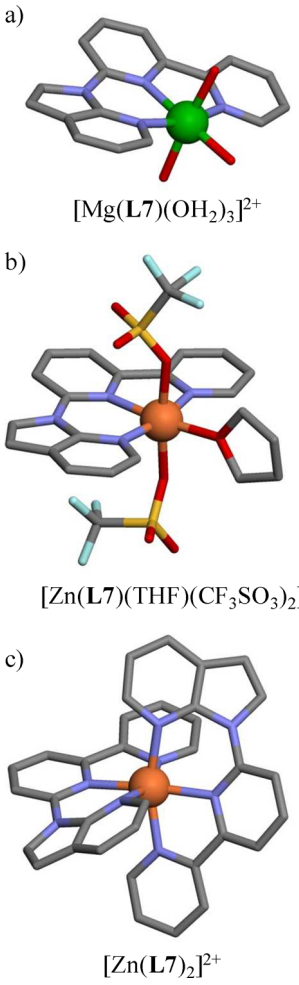


**Figure 7.** Perspective views of the molecular structures of (a) $[Mg(\mathbf{L7})(OH_2)_3]^{2+}$, (b) $[Zn(\mathbf{L7})(THF)(CF_3SO_3)_2]$, and (c) $[Zn(\mathbf{L7})_2]^{2+}$ observed in the crystal structures of $[Mg(\mathbf{L7})(OH_2)_3](ClO_4)_2$ (**6**), $[Zn(\mathbf{L7})(THF)(CF_3SO_3)_2]$ (**7**), and $[Zn(\mathbf{L7})_2](CF_3SO_3)_2{\cdot}0.13H_20$ (**8**). Color code: gray = C, blue = N, red = O, yellow = S, light blue = F, green = Mg, pink = Zn. Hydrogen atoms are omitted for clarity.

Since the ionic radius of six-coordinate $Mg^{2+}$ (0.72 Å) and $Zn^{2+}$ (0.74 Å) are comparable,[26] their affinity for **L7** is similar with $\Delta G^{M,L7}_{connect} \approx -15$ kJ/mol in $CDCl_3$:$CD_3CN$ (1:1), a value reduced by 20%–30% in more-polar $CD_3CN$. Surprisingly, the free energy of connection increases only slightly when going from M = $Li^+$ to $Mg^{2+}$, despite the doubling of both positive charge and electrostatic factor. This suggests that solvation processes play a major role in the complexation reactions occurring in polar organic solvents, a statement substantiated by the enthalpy-penalized ($\Delta H^{M,L7}_{1,n} > 0$), but entropy-driven complexation processes ($\Delta S^{Mg,L7}_{1,n} \gg 0$) revealed by vant' Hoff plots for $Mg^{2+}$ (see Table S14 in the Supporting Information). We also notice that the fixation of the second terdentate ligand in $[M(\mathbf{L7})_2]^{2+}$ is much more favorable for $Mg^{2+}$ (positive cooperativity $\Delta E^{L7,L7M}_{interaction} \approx -15$ kJ/mol), while a rough statistical behavior is found for $Zn^{2+}$, but the large uncertainties affecting this parameter for M = Mg prevent more-detailed interpretations.

**Complexation of L7 with Trivalent $Sc^{3+}$, $La^{3+}$, and $Y^{3+}$ Cations.** Titration of **L7** with hygroscopic $Sc(CF_3SO_3)_3$ in $CD_3CN$ shows the exclusive formation of the protonated ligand $[H\mathbf{L7}]^+$ and $[H_2\mathbf{L7}]^{2+}$ produced by the severe hydrolysis of small $Sc^{3+}$ with a trace of water, according to eq 13 (six-coordinate ionic radius $R^{CN=6}_{Sc} = 0.75$ Å and $pK^1_{a,Sc} = 10^{-4.55}$ in water; see Figure S23 in the Supporting Information).[26,30]

$$M^{3+} + H_2O \rightleftharpoons [M(OH)]^{2+} + H^+ \qquad K^1_{a,M} \tag{13}$$

In order to minimize water content, $Sc(CF_3SO_3)_3$ was replaced with anhydrous ternary complexes $[La(hfac)_3(diglyme)]$[31] and $[Y(CF_3SO_3)_3(diglyme)]$[32] containing larger $La^{3+}$ (nine-coordinate ionic radius $R^{CN=9}_{La} = 1.36$ Å, $pK^1_{a,La} = 10^{-9.01}$ in water, hfac = hexafluoroacetylacetonate) and $Y^{3+}$ cations ($R^{CN=9}_{Y} = 1.08$ Å, $pK^1_{a,Y} = 10^{-8.81}$ in water).[26,30] Titration of **L7** with $[La(hfac)_3(diglyme)]$ at millimolar concentrations in $CD_3CN$ displays only weak interactions and $|La|_{tot}/|\mathbf{L7}|_{tot}$ ratios larger than 5.0 are required for recording reliable changes in the $^1H$ NMR spectra (see Figure S24 in the Supporting Information).

The situation is different with $[Y(CF_3SO_3)_3(diglyme)]$, for which significant quantities of $[Y(\mathbf{L7})]^{3+}$ and $[Y(\mathbf{L7})_2]^{3+}$ (slow exchange on the NMR time scale) are formed together with comparable amounts of protonated ligands $[H\mathbf{L7}]^+$ and $[H_2\mathbf{L7}]^{2+}$ (fast exchange on the NMR time scale; see Figure S25 in the Supporting Information). The complete titration process can be satisfyingly modeled in $CD_3CN$ by simultaneously considering eqs 1, 2, 9, 10, and 13, adapted for M = $Y^{3+}$ (eqs 14–18), together with eq 19 for taking into account partial water dissociation in pure acetonitrile.[33] The fitting process used multi-Lorentzien deconvolutions of the complete $^1H$ NMR spectra, and it converged to $\log(\beta^{Y,L7}_{1,1}) = 2.9(5)$ and $\log(\beta^{Y,L7}_{1,2}) = 5.3(4)$ with the ligand distribution depicted in Figure 8 (see Appendix 2 in the Supporting Information).

$$H^+ + \mathbf{L7} \rightleftharpoons [H\mathbf{L7}]^+ \qquad \beta^{H,L7}_{1,1} = 10^{5.3} \tag{14}$$

$$2H^+ + \mathbf{L7} \rightleftharpoons [H_2\mathbf{L7}]^{2+} \qquad \beta^{H,L7}_{2,1} = 10^{9.1} \tag{15}$$

$$Y^{3+} + \mathbf{L7} \rightleftharpoons [Y\mathbf{L7}]^{3+} \qquad \beta^{Y,L7}_{1,1} \tag{16}$$

$$Y^{3+} + 2\mathbf{L7} \rightleftharpoons [Y(\mathbf{L7})_2]^{3+} \qquad \beta^{Y,L7}_{1,2} \tag{17}$$

$$Y^{3+} + H_2O \rightleftharpoons [Y(OH)]^{2+} + H^+ \qquad K^1_{a,Y} = 10^{-8.81} \tag{18}$$

$$H_2O \rightleftharpoons OH^- + H^+ \qquad K_s = 10^{-16.35} \tag{19}$$

According to the complicated speciation observed in solution, the isolation of pure yttrium complexes is difficult, but brownish X-ray quality crystals of $[Y(\mathbf{L7})_2Cl_2]I_3{\cdot}CH_2Cl_2$ (**9**) slowly deposited during the air evaporation of a $CH_3CN/CH_2Cl_2$ (1:8) solution containing $YI_3(THF)_{3.5}$ (1 equiv)[34] and **L7** (2 equiv; see Figure 9, as well as Figures S26 and S27, in addition to Tables S22–S24 in the Supporting Information).[35]

The 8-coordinated Y(III) metal in the $[Y(\mathbf{L7})_2Cl_2]^+$ cation is sandwiched between the two twisted terdentate ligands, with the two $Cl^-$ anions completing a pseudo-square antiprism (Figure 9). The Y–N bond distances (2.462–2.613 Å, average 2.54(7) Å) are similar to those reported for $[Y(\mathbf{L1})(OH_2)_4Cl]^{2+}$ (8-coordinate: 2.52(3) Å),[36] $[Y(\mathbf{L1})(OH_2)_2(NO_3)_2]^+$ (9-coordinate: 2.49(2) Å)[37] and $[Y(\mathbf{L1})_3]^{3+}$ (9-coordinate: 2.52(3) Å).[38] However, the yttrium atom, which is located within the plane defined by the three coordinated donor N atoms for complexes with **L1**, lies at 1.187 and 1.197 Å from the related coordination planes in $[Y(\mathbf{L7})_2Cl_2]^+$ (Figure


dx.doi.org/10.1021/ic400526j | Inorg. Chem. 2013, 52, 5570–5580

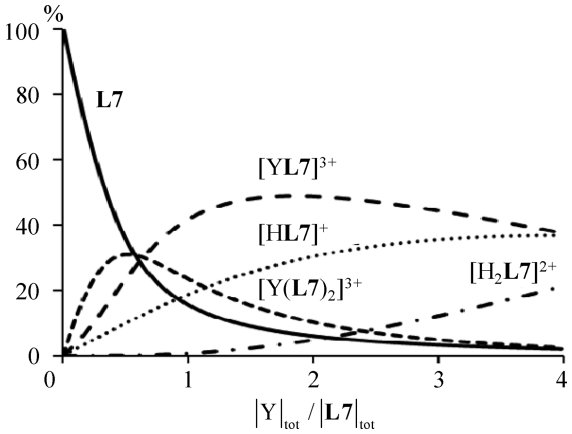


**Figure 8.** Computed ligand speciation for the titrations of **L7** with $[Y(CF_3SO_3)_3(diglyme)]$ in $CD_3CN$ at 298 K. Total ligand concentration $|\mathbf{L7}|_{tot} = 7.5 \times 10^{-3}$ M.

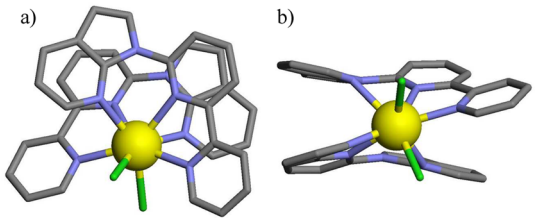


**Figure 9.** Perspective views (a) perpendicular and (b) parallel to the central pyridine ring of the terdentate ligands in the molecular structure of $[Y(\mathbf{L7})_2Cl_2]^+$ observed in the crystal structure of $[Y(\mathbf{L7})_2Cl_2]I_3{\cdot}CH_2Cl_2$ (**9**). Color code: gray = C, blue = N, green = Cl, yellow = Y. Hydrogen atoms are omitted for clarity.

9). This specific geometry is not the simple result of using 6-membered polyaromatic chelate rings, since a strictly planar $YN_3$ core was recently reported for the complexation of a terdentate carbazole-bis(oxazoline) ligand possessing two fused 6,6-membered chelate rings.[39] We however note the operation of various intramolecular and intermolecular $\pi$-stacking interactions in $[Y(\mathbf{L7})_2Cl_2]^+$, which could contribute to the stabilization of the observed sandwich conformation (see Figure S27 in the Supporting Information). The thermodynamic analysis of eqs 16 and 17 within the frame of the site-binding model[22] gives eqs 20 and 21 (Figure S28 in the Supporting Information), from which we can calculate a microscopic free energy of connection of $\Delta G^{Y,L7}_{connect} = -12.1(2.9)$ kJ/mol for a noncooperative complexation process in $CD_3CN$; this is a behavior very similar to that previously described for $Zn^{2+}$ (Table 1, entries 3–6), but much less efficient than $\Delta G^{Y,L1}_{connect} \approx \Delta G^{Y,L5}_{connect} = -30(3)$ kJ/mol reported for terdentate-fused 5,5-membered chelates in acetonitrile.[2f]

$$\beta^{Y,L7}_{1,1} = 6f^{Y,L7}_{connect} \quad (20)$$

$$\beta^{Y,L7}_{1,2} = 6(f^{Y,L7}_{connect})^2 u^{L7,L7}_{Y} \quad (21)$$

## CONCLUSION

The coordination chemistry of the semirigid polyaromatic terdentate ligands **L1** (fused 5,5-chelates)[5r] and **L6** (fused 6,6-chelates)[10] follows the geometrical rules established during the 1990s claiming that 5-membered chelate rings prefer large cations, whereas the reverse situation holds for 6-membered chelates (see Figure S1 in the Supporting Information),[1] The intermediate structural characteristics provided by **L7** (i.e., two fused 5,6-membered chelates) remove this effect in polar organic solvents. The terdentate ligand **L7** indeed efficiently reacts with $H^+$ ($\Delta G^{H,L7}_{connect} \approx -30$ kJ/mol), and it displays significant affinities for M = $Li^+$, $Mg^{2+}$, $Zn^{2+}$, and $Y^{3+}$ ($\Delta G^{M,L7}_{connect} \approx -15$ kJ/mol to $-10$ kJ/mol) without exhibiting pertinent dependence on the cationic electrostatic factors $Z^2/R$. Under these conditions, the use of easily hydrolyzed cations such as $Sc^{3+}$ or $Y^{3+}$, in the presence of a trace of water, leads to unavoidable competition with protonation. Structurally speaking, this rough invariance of the affinity for various cations is correlated with their close interactions with the two distal donor N atoms, while the central N atom is remote. The opposite situation occurs for coordinated **L1**, which better encapsulates the incoming cations, thus optimizing enthalpic contributions. Therefore, it is not so suprising that the fixation of $Mg^{2+}$ to **L7** proved to be strictly entropy-driven with deleterious positive enthalpic contributions. This limitation could be overcome by using less-coordinating anhydrous organic solvents, as suggested by the systematic increase in binding affinity observed upon going from $CH_3CN$ to $CH_3CN$:$CDCl_3$ (1:1), and cyclic ethers are currently investigated for pushing this strategy forward. We finally note that the successive fixation of two monovalent cations to **L7** is anticooperative, but the alternative binding of two ligands **L7** to a single bivalent or tervalent cation may be driven by remarkable positive cooperativities.

## EXPERIMENTAL SECTION

Chemicals were purchased from Strem, Acros, Fluka AG, and Aldrich, and used without further purification, unless otherwise stated. $La(hfac)_3{\cdot}$diglyme,[31] $Y(CF_3SO_3)_3{\cdot}$diglyme[32] and $YI_3(THF)_{3.5}$[10,34] were prepared according to literature procedures. Silicagel plates Merck 60 $F_{254}$ were used for thin layer chromatography (TLC) and Fluka silica gel 60 (0.04–0.063 mm) or Acros neutral activated alumina (0.050–0.200 mm) was used for preparative column chromatography.

**Preparation of 2-(tributylstannyl) Pyridine (1).** *n*-BuLi (8 mL, 1.6 M in hexane, 12.5 mmol) was added dropwise to a solution of 2-bromo pyridine (1.99 g, 12.5 mmol) in dry THF (5 mL) at −78 °C, and the mixture was stirred for 1 h. Tributyltin chloride (3.4 mL, 12.65 mmol) was quickly added to the solution at −78 °C, and stirring continued for 3 h at −78 °C, then 30 min at room temperature. The reaction was quenched with saturated aqueous $NH_4Cl$ solution (10 mL) and extracted with ethylacetate (3 × 25 mL). The combined organic layers were washed with brine, then water and finally dried over anhydrous $Na_2SO_4$. The solvent was evaporated under reduced pressure to give 2.7 g of 2-(tributylstannyl) pyridine (**1**, 12.5 mmol, yield = 99%) as a dark brown liquid.

$^1$H NMR ($CDCl_3$, 400 MHz): $\delta$ (ppm) 8.74–8.72 (m, 1H); 7.49 (dt, 1H); 7.40 (m, 1H); 7.09–7.13 (m, 1H); 1.57 (t, 6H,); 1.30–1.35 (m, 6H); 1.10–1.14 (m, 6H); 0.88 (t, 9H). ESI-MS *m*/*z*: 370.18 $[M+H]^+$.

**Preparation of 6-bromo-2,2′-bipyridine (2).** 2-(tributylstannyl) pyridine (**1**) (3.8 g, 10.32 mmol) was added to a degassed solution of 2,6-dibromo pyridine (2.6 g, 10.97 mmol) and $Pd(PPh_3)_4$ (608 mg, 0.53 mmol) in toluene (4 mL). The mixture was refluxed under an inert atmosphere for 12 h, the solvent evaporated and the resulting residue disolved in $CH_2Cl_2$ (10 mL). Extraction with 6 M aq HCl (3 × 10 mL) provided an aqueous layer, which was carefully neutralized with 10% aq ammonia (60 mL) at 0 °C, then extracted with dichloromethane (3 × 30 mL). The combined organic layers were washed with water and dried over anhydrous $Na_2SO_4$. The solvent was evaporated and the resulting solid residue was purified by column chromatography ($CH_2Cl_2$/MeOH: 99.5/0.5 → 99/1) yielded 1.3 g of


dx.doi.org/10.1021/ic400526j | Inorg. Chem. 2013, 52, 5570−5580

6-bromo-2,2′-bipyridine (**2**, 5.5 mmol, yield = 53%) as a white solid. $^1$H NMR ($CDCl_3$, 400 MHz): $\delta$ (ppm) 8.69 (m, 1H); 8.43 (td, 1H, $^3J$ = 8.0 Hz); 8.40 (dd, 1H, $^3J$ = 7.6 Hz, $^4J$ = 0.8 Hz); 7.84 (dt, 1H, $^3J$ = 7.6 Hz, $^4J$ = 2 Hz); 7.69 (t, 1H, $^3J$ = 8.0 Hz); 7.51 (dd, 1H, $^3J$ = 8.0 Hz, $^4J$ = 0.8 Hz); 7.35 (m, 1H). ESI-MS, *m/z*: 235.1 $[M+H]^+$.

**Preparation of 6-(azaindol-1-yl)-2,2′-bipyridine (L7).** 6-Bromo-2,2′-bipyridine (866 mg, 3.6 mmol), 7-azaindole (390 mg, 3.30 mmol), $K_2CO_3$ (993 mg, 7.2 mmol), trans-1,2-diaminocyclohexane (41 mg, 0.36 mmol), and CuI (35 mg, 0.18 mmol) in dioxane (10 mL) were degassed with $N_2$ for 30 min. The mixture was then refluxed under an inert atmosphere for 72 h. The solvent was evaporated, and the resulting brown residue was extracted with $CH_2Cl_2$ (3 × 40 mL) and washed with water. The organic layer was dried over $MgSO_4$, and the solvent was evaporated under reduced pressure. The resulting solid was purified by column chromatography ($CH_2Cl_2$/MeOH: 99/1) to yield 787 mg of 6-(azaindol-1-yl)-2,2′-bipyridine (**L7**, 2.9 mmol, yield = 87%) as a white solid. $^1$H NMR ($CDCl_3$, 400 MHz): $\delta$ 9.02 (dd, 1H, $^3J$ = 8.2 Hz, $^4J$ = 0.8 Hz); 8.73 (m, 1H); 8.60 (d, 1H, $^3J$ = 3.6 Hz); 8.53 (td, 1H, $^3J$ = 7.6 Hz, $^4J$ = 1.2 Hz); 8.45 (dd, 1H, $^3J$ = 4.8 Hz, $^4J$ = 1.6 Hz); 8.32 (dd, 1H, $^3J$ = 7.6 Hz, $^4J$ = 0.8 Hz); 8.03 (t, 1H, $^3J$ = 8.0 Hz); 8.0 (dd, 1H, $^3J$ = 8.0 Hz, $^4J$ = 1.6 Hz); 7.88 (dt, 1H, $^3J$ = 7.6 Hz, $^4J$ = 2 Hz); 7.36 (d, 1H, $^3J$ = 4.8 Hz); 7.20 (dd, 1H, $^3J$ = 8.0 Hz, $^4J$ = 4.8 Hz); 6.70 (d, 1H, $^3J$ = 4 Hz). $^{13}$C NMR ($CDCl_3$, 100 MHz): $\delta$ 156.82 (Cquat); 154.58 (Cquat); 150.16 (Cquat); 149.21 (C12); 147.69 (Cquat); 143.16 (C7); 139.35 (C1); 136.88 (C10); 129.07 (C5); 126.44 (C3); 123.84 (C11); 123.39 (Cquat); 121.23 (C9); 117.42 (C8); 117.20 (C6); 115.63 (C2); 102.56 (C4). ESI-MS ($CH_2Cl_2$): *m/z* 272.93 $[M+H]^+$. Elemental analyses: Calcd for $C_{17}H_{12}N_4$: C 74.98%, H 4.44%, N 20.58%. Found C 74.63%, H 4.31%, N 20.30%.

**Preparation of the Complexes.** *[HL7](CF$_3$SO$_3$) (**3**).* Diethyl ether was slowly diffused into a concentrated solution containing **L7** (1 equiv) and $HCF_3SO_3$ (1 equiv) in $CH_3CN/CH_2Cl_2$ (1:1) to give X-ray quality prisms of $[HL7](CF_3SO_3)$.

*[H$_2$L7](ClO$_4$)$_2$ (**4**).* The dissolution of **L7** (10 mg, 0.037 mmol) in acetonitrile/dichloromethane (1:1, 1 mL), followed by the addition of 6 M aq $HClO_4$ (16 $\mu$L, 0.093 mmol) resulted in the precipitation of $[H_2L7](ClO_4)_2$. The solid was filtered, washed with dichloromethane, diethyl ether and dried under vacuum to afford a 13 mg of $[H_2L7](ClO_4)_2$ (0.027 mmol, yield 74%) as a white solid. Slow diffusion of THF into a concentrated solution containing **L7** (1 equiv) and $HClO_4$ (2 equiv) in $CH_3CN/CH_2Cl_2$ (1:1) gave X-ray quality prisms of $[H_2L7](ClO_4)_2$ (**4**). $^1$H NMR ($CD_3CN$, 400 MHz): $\delta$ 8.94 (d, $^3J$ = 3.6 Hz, 1H); 8.88 (dd, $^3J$ = 8.0 Hz, $^4J$ = 1.0 Hz, 1H); 8.82 (dt, $^3J$ = 7.8 Hz, 1H); 8.71 (d, $^3J$ = 7.8 Hz, 1H); 8.60 (d, $^3J$ = 6.0 Hz, 1H); 8.48 (t, $^3J$ = 8.1 Hz, 1H); 8.35 (d, $^3J$ = 7.8 Hz, 1H); 8.28 (d, $^3J$ = 3.8 Hz, 1H); 8.22 (t, $^3J$ = 7.2 Hz, 1H); 8.07 (d, $^3J$ = 8.3 Hz, 1H, H2); 7.83 (dd, $^3J$ = 7.9 Hz, $^4J$ = 6.0 Hz, 1H, H6), 7.26 (d, $^3J$ = 3.8 Hz, 1H, H4). Elemental analysis: Calcd: $C_{17}H_{14}N_4Cl_2O_8$ ($[H_2L7](ClO_4)_2$): C, 43.15; H, 2.98; N, 11.83. Found: C, 43.00; H, 3.00; N, 11.90.

*[Li(L7)(OH$_2$)(ClO$_4$)] (**5**).* Heptane was slowly diffused into a concentrated solution containing **L7** (1 equiv) and $LiClO_4$ (1 equiv) in $CH_3CN/CH_2Cl_2$ (1:1) to give X-ray quality prisms of $[Li(L7)(OH_2)(ClO_4)]$.

*[MgL7](ClO$_4$)$_2$·3H$_2$O (**6**).* Stoichiometric amounts of **L7** (10 mg, 0.037 mmol) and $Mg(ClO_4)_2$ (8.3 mg, 0.037 mmol) were dissolved in acetonitrile/dichloromethane (1:1, 1 mL). The solvent was partially evaporated and slow diffusion of diethyl ether afforded 5 mg of X-ray quality prisms of $[MgL7](ClO_4)_2·3H_2O$ (0.009 mmol, yield 25%). $^1$H NMR ($CD_3CN$, 400 MHz): $\delta$ 8.87 (d, $^3J$ = 4.5 Hz, 1H); 8.63 (dd, $^3J$ = 5.3 Hz, $^4J$ = 1.4 Hz, 1H); 8.54 (d, $^3J$ = 8.2 Hz, 1H), 8.45 (dd, $^3J$ = 7.8 Hz, $^4J$ = 1.5 Hz, 1H); 8.42 (t, $^3J$ = 8.1 Hz, H1); 8.40 (dt, $^3J$ = 8.0 Hz, $^4J$ = 1.5 Hz, 1H); 8.34 (dt, $^3J$ = 7.7 Hz, $^4J$ = 1.6 Hz, 1H); 8.22 (d, $^3J$ = 4.1 Hz, 1H); 8.05 (dd, $^3J$ = 7.7 Hz, $^4J$ = 1.5 Hz, 1H); 7.85 (ddd, $^3J$ = 7.6 Hz, $^4J$ = 5.2 Hz, $^5J$ = 0.9 Hz, 1H); 7.62 (dd, $^3J$ = 7.9, $^4J$ = 5.3 Hz, 1H); 7.09 (d, $^3J$ = 4.1 Hz, 1H). Elemental analysis: Calcd for $MgC_{17}H_{18}N_4Cl_2O_{11}$: C, 37.15; H, 3.30; N, 10.19. Found: C, 37.28; H, 3.32; N, 10.04.

*[Zn(L7)](CF$_3$SO$_3$)$_2$ (**7**).* Stoichiometric amounts of **L7** (10 mg, 0.037 mmol) and $Zn(CF_3SO_3)_2$ (13.45 mg, 0.037 mmol) were dissolved in acetonitrile (0.5 mL). The slow diffusion of tetrahydrofuran (THF), followed by filtration and drying, afforded 12 mg $[ZnL7](CF_3SO_3)_2$ (0.019 mmol, yield 51%) as a white microcrystalline powder. Slow diffusion of THF into a concentrated solution containing **L7** (1 equiv) and $Zn(CF_3SO_3)$ (1 equiv) in $CH_3CN$ gave X-ray quality prisms of $[Zn(L7)](CF_3SO_3)_2$ (**7**). $^1$H NMR ($CD_3CN$, 400 MHz): $\delta$ 9.04 (d, $^3J$ = 6 Hz, 1H); 8.78 (dd, $^3J$ = 5.4 Hz, $^4J$ = 1.4 Hz, 1H); 8.60 (td, $^3J$ = 7.3 Hz, 1H); 8.50 (dd, $^3J$ = 7.8 Hz, $^4J$ = 1.5 Hz, 1H); 8.44 (t, $^3J$ = 7.7 Hz, 1H); 8.42 (dt, $^3J$ = 7.7 Hz, $^4J$ = 2 Hz, 1H); 8.40 (dt, $^3J$ = 7.6 Hz, $^4J$ = 1.6 Hz, 1H); 8.27 (d, $^3J$ = 4.1 Hz, 1H); 8.09 (dd, $^3J$ = 7.7 Hz, $^4J$ = 1.6 Hz, 1H); 7.93 (ddd, $^3J$ = 7.7 Hz, $^4J$ = 5.3 Hz, $^5J$ = 1.0 Hz, 1H); 7.68 (dd, $^3J$ = 7.8, $^4J$ = 5.4 Hz, 1H); 7.12 (d, $^3J$ = 4.08 Hz, 1H). Elemental analysis: Calcd for $ZnC_{19}H_{17}N_4S_2F_6O_6$: C, 35.89; H, 1.90; N, 8.81. Found: C, 35.50; H, 2.19; N, 8.71.

*[Zn(L7)$_2$](CF$_3$SO$_3$)$_2$ (**8**).* Stoichiometric amounts of **L7** (10 mg, 0.037 mmol) and $Zn(CF_3SO_3)_2$ (6.7 mg, 0.019 mmol) were dissolved in acetonitrile/dichloromethane (1:1, 1 mL). The solvent was then partially evaporated. Slow diffusion of THF afforded 4 mg of X-ray-quality prisms of $[Zn(L7)_2](CF_3SO_3)_2$ (0.004 mmol, yield 24%). $^1$H NMR ($CD_3CN$, 400 MHz) $\delta$ 8.64 (7, $^3J$ = 8.1 Hz, 1H,); 8.51 (d, $^3J$ = 7.8 Hz, 1H); 8.43 (d, $^3J$ = 8.2 Hz, 1H); 8.30−8.27 (m, 2H, H2); 8.13 (dd, $^3J$ = 7.8 Hz, $^4J$ = 1.4 Hz, 1H); 8.05 (dt, $^3J$ = 8.0 Hz, $^4J$ = 1.6 Hz, 1H); 7.76 (d, $^3J$ = 5.0 Hz, 1H); 7.71 (d, $^3J$ = 6.6 Hz, 1H); 7.33 (dd, $^3J$ = 6.8 Hz, $^4J$ = 5.8 Hz, 1H); 7.04 (dd, $^3J$ = 7.8 Hz, $^4J$ = 5.3 Hz, 1H); 7.02 (d, $^3J$ = 4.1 Hz, 1H). Elemental analysis: Calcd for $ZnC_{36}H_{24}N_8S_2F_6O_6$: C, 47.61; H, 2.66; N, 12.33. Found: C, 46.75; H, 3.00; N, 11.60.

*[Y(L7)$_2$Cl$_2$]I$_3$·CH$_2$Cl$_2$ (**9**).* Brownish X-ray quality crystals of $[Y(L7)_2Cl_2]I_3·CH_2Cl_2$ (**9**) slowly deposited during the air evaporation of a concentrated $CH_3CN/CH_2Cl_2$ (1:8) solution containing $YI_3(THF)_{3.5}$ (1 equiv) and **L7** (2 equiv).

**Spectroscopic Measurements.** $^1$H and $^{13}$C NMR spectra were recorded on a Bruker Avance 400 MHz spectrometer. Chemical shifts are given in parts per million (ppm), with respect to TMS. In a typical $^1$H NMR tiration experiment, 500 $\mu$L of a 7.5 × $10^{-3}$ M solution of ligand **L7** in $CD_3CN/CDCl_3$ (1:1) were reacted with successive aliquots of solutions of $CF_3SO_3H$, $LiClO_4$, $Mg(ClO_4)_2$, $Zn(CF_3SO_3)_2$, or $Y(CF_3SO_3)$·diglyme in the same solvent mixture. After each aliquot, the $^1$H NMR spectrum was recorded at 298 K and the global chemical shifts matrix was fitted to pertinent equilibria using the HypNMR-2008 software.[16] Pneumatically assisted electrospray ionization−mass spectroscopy (ESI-MS) spectra were recorded from $10^{-4}$ M solutions on an Applied Biosystems API 150EX LC/MS System equipped with a Turbo Ionspray source. Elemental analyses were performed by K. L. Buchwalder from the Microchemical Laboratory of the University of Geneva.

**X-ray Crystallography.** Summary of crystal data, intensity measurements, and structure refinements for $[HL7](CF_3SO_3)$ (**3**), $[H_2L7](ClO_4)_2$ (**4**), $[Li(L7)(OH_2)(ClO_4)]$ (**5**), $Mg(L7)(OH_2)_3](ClO_4)_2$ (**6**), $[Zn(L7)(THF)(CF_3SO_3)_2]$ (**7**), $[Zn(L7)_2](CF_3SO_3)_2·0.13H_2O$ (**8**), and $[Y(L7)_2Cl_2]I_3·CH_2Cl_2$ (**9**) were collected in Tables S4, S15, and S22 in the Supporting Information). All crystals were mounted on quartz fibers with protection oil. Cell dimensions and intensities were measured at 180 or 293 K on a Agilent Supernova diffractometer with mirror-monochromated Cu-[K$\alpha$] radiation ($\lambda$ = 1.54184 Å). Data were corrected for Lorentz and polarization effects and for absorption. The structures were solved by direct methods (SIR97),[40] all other calculation were performed with ShellX97[41] systems and ORTEP3[42] programs. CCDC-926740 to CCDC-926747 (**3**-**9**) contain the supplementary crystallographic data. The CIF files can be obtained free of charge via www.ccdc.cam.ac.uk/conts/retrieving.html (or from the Cambridge Crystallographic Data Centre, 12 Union Road, Cambridge CB2 1EZ, U.K.; fax: (+44) 1223-336-033; or deposit@ccdc.cam.ac.uk).

## ■ ASSOCIATED CONTENT

### Ⓢ Supporting Information

Methods of speciation (Appendixes 1 and 2). Tables of $^1$H NMR chemical shifts, crystal data, geometric parameters, bond


dx.doi.org/10.1021/ic400526j | Inorg. Chem. 2013, 52, 5570−5580

distances and bond angles, and thermodynamic data. Figures showing molecular structures with numbering schemes and crystal packing, $^1$H NMR titrations, ligand speciations and applications of the site binding model. A CIF file for compounds [HL7]($CF_3SO_3$) (**3**), [$H_2$L7]($ClO_4$)$_2$ (**4**), [Li(L7)($OH_2$)($ClO_4$)] (**5**), Mg(L7)($OH_2$)$_3$]($ClO_4$)$_2$ (**6**), [Zn(L7)(THF)($CF_3SO_3$)$_2$] (**7**), [Zn(L7)$_2$]($CF_3SO_3$)$_2$·0.13$H_2$0 (**8**), and [Y(L7)$_2$$Cl_2$]$I_3$·$CH_2Cl_2$ (**9**). This material is available free of charge via the Internet at http://pubs.acs.org.

## AUTHOR INFORMATION

### Corresponding Author

*E-mail addresses: Claude.Piguet@unige.ch (C.P.), Thi.Hoang@unige.ch (T.H.Y.H.).

### Notes

The authors declare no competing financial interest.

## ACKNOWLEDGMENTS

Financial support from the Swiss National Science Foundation is gratefully acknowledged.

## REFERENCES

(1) (a) Hancock, R. D. *J. Chem. Educ.* **1992**, *69*, 615−621. (b) Motekaitis, R. J.; Martell, A. E.; Hancock, R. D. *Coord. Chem. Rev.* **1994**, *133*, 39−65 and references therein.

(2) For reviews, see: (a) Bünzli, J.-C. G. In *Handbook on the Physics and Chemistry of Rare Earths*, Vol. *10*; Gschneider, K. A., Jr., Eyring, L., Eds.: Elsevier: Amsterdam, 1987; pp 322−394. (b) Sabbatini, N.; Guardigli, M.; Lehn, J.-M. *Coord. Chem. Rev.* **1993**, *123*, 201−228. (c) Gawryszewska, P.; Sokolnicki, J.; Legendziewicz, J. *Coord. Chem. Rev.* **2005**, *249*, 2489−2509. (d) Bünzli, J.-C. G. *Acc. Chem. Res.* **2006**, *39*, 53−61. (e) Comby, S.; Bünzli, J.-C. G. In *Handbook on the Physics and Chemistry of Rare Earths*, Vol. *37*; Gschneider, K. A., Jr., Bünzli, J.-C. G., Pecharsky, V. K., Eds.; Elsevier Science: Amsterdam, 2007; pp 217−470. (f) Piguet, C.; Bünzli, J.-C. G. In *Handbook on the Physics and Chemistry of Rare Earths*, Vol. *40*; Gschneider, K. A., Jr., Bünzli, J.-C. G., Pecharsky, V. K., Eds.; Elsevier Science: Amsterdam, 2009; pp 301−553. (g) Moore, E. G.; Samuel, A. P. S.; Raymond, K. N. *Acc. Chem. Res.* **2009**, *42*, 542−552. (h) Eliseeva, S. V.; Bünzli, J.-C. G. *Chem. Soc. Rev.* **2010**, *39*, 189−227. (i) Eliseeva, S. V.; Bünzli, J.-C. G. *New J. Chem.* **2011**, *35*, 1165−1176. (j) Xu, J.; Corneillie, T. M.; Moore, E. G.; Law, G.-L.; Butlin, N. G.; Raymond, K. N. *J. Am. Chem. Soc.* **2011**, *133*, 19900−19910.

(3) For reviews, see: (a) Benelli, C.; Gatteschi, D. *Chem. Rev.* **2002**, *102*, 2369−2387. (b) Sorace, L.; Benelli, C.; Gatteschi, D. *Chem. Soc. Rev.* **2011**, *40*, 3092−3104. (c) Luzon, J.; Sessoli, R. *Dalton Trans.* **2012**, *41*, 13556−13567.

(4) (a) Senegas, J.-M.; Bernardinelli, G.; Imbert, D.; Bünzli, J.-C. G.; Morgantini, P.-Y.; Weber, J.; Piguet, C. *Inorg. Chem.* **2003**, *42*, 4680−4695. (b) Zou, J.; Berg, D. J.; Stuart, D.; McDonald, R.; Twamley, B. *Organometallics* **2011**, *30*, 4958−4967.

(5) (a) Durham, D. A.; Frost, G. H.; Hart, F. A. *J. Inorg. Nucl. Chem.* **1969**, *31*, 833−838. (b) Chapman, R. D.; Loda, R. T.; Riehl, J. P.; Schwartz, R. W. *Inorg. Chem.* **1984**, *23*, 1652−1657. (c) Fréchette, M.; Bensimon, C. *Inorg. Chem.* **1995**, *34*, 3520−3527. (d) Semenova, L. I.; White, A. H. *Aust. J. Chem.* **1999**, *52*, 507−517. (e) Semenova, L. I.; Sobolev, A. N.; Skelton, B. W.; White, A. H. *Aust. J. Chem.* **1999**, *52*, 519−529. (f) Bekiari, V.; Lianos, P. *Adv. Mater.* **2000**, *12*, 1603−1605. (g) Drew, M. G. B.; Iveson, P. B.; Hudson, M. J.; Liljenzin, J. O.; Spjuth, L.; Cordier, P.-Y.; Enarsson, A.; Hill, C.; Madic, C. *J. Chem. Soc., Dalton Trans.* **2000**, 821−830. (h) Mürner, H.-R.; Chassat, E.; Thummel, R. P.; Bünzli, J.-C. G. *J. Chem. Soc., Dalton Trans.* **2000**, 2809−2816. (i) Rabbe, C.; Mikhalko, V.; Dognon, J.-P. *Theor. Chem. Acc.* **2000**, *104*, 280−283. (k) Ahrens, B.; Cotton, S., A.; Feeder, N.; Noy, O. E.; Raithby, P. R.; Teat, S. J. *J. Chem. Soc., Dalton Trans.* **2002**, 2027−2030. (l) Berthet, J.-C.; Rivière, C.; Miquel, Y.; Nierlich, M.; Madic, C.; Ephritikhine, M. *Eur. J. Inorg. Chem.* **2002**, 1439−1446. (l) Fukuda, Y.; Nakao, A.; Hayashi, K. *J. Chem. Soc., Dalton Trans.* **2002**, 527−533. (m) Cotton, S. A.; Franckevicius, V.; How, R. E.; Ahrens, B.; Ooi, L. L.; Mahon, M. F.; Raithby, P. R.; Teat, S. J. *Polyhedron* **2003**, *22*, 1489−1497. (n) Guillaumont, D. *J. Phys. Chem. A* **2004**, *108*, 6893−6900. (o) Berthet, J.-C.; Nierlich, M.; Miquel, Y.; Madic, C.; Ephritikhine, M. *Dalton Trans.* **2005**, 369−379. (p) Sénéchal-David, K.; Hemeryck, A.; Tancrez, N.; Toupet, L.; Williams, J. A. G.; Ledoux, I.; Zyss, J.; Boucekkine, A.; Guégan, J.-P.; Le Bozec, H.; Maury, O. *J. Am. Chem. Soc.* **2006**, *128*, 12243−12255. (q) Petit, L.; Daul, C.; Adamo, C.; Maldivi, P. *New J. Chem.* **2007**, *31*, 1738−1745. (r) Hamilton, J. M.; Anhorn, M. J.; Oscarson, K. A.; Reibenspies, J. H.; Hancock, R. D. *Inorg. Chem.* **2011**, *50*, 2764−2770. (s) de Bettencourt-Dias, A.; Bauer, S.; Viswanathan, S.; Maull, B. C.; Ako, A. M. *Dalton Trans.* **2012**, *41*, 11212−11218. (t) Di Bernardo, P.; Melchior, A.; Tolazzi, M.; Zanonato, P. L. *Coord. Chem. Rev.* **2012**, *256*, 328−351.

(6) (a) Drew, M. G. B.; Hudson, M. J.; Iveson, P. B.; Madic, C.; Russel, M. L. *J. Chem. Soc., Dalton Trans.* **2000**, 2711−2720. (b) Boubals, N.; Drew, M. G. B.; Hill, C.; Hudson, M. J.; Iveson, P. B.; Madic, C.; Russell, M. L.; Youngs, T. G. A. *J. Chem. Soc., Dalton Trans.* **2002**, 55−62. (c) Karmazin, L.; Mazzanti, M.; Gateau, C.; Hill, C.; Pécaut, J. *Chem. Commun.* **2002**, 2892−2893. (d) Drew, M. G. B.; Hill, C.; Hudson, M. J.; Iveson, P. B.; Madic, C.; Youngs, T. G. A. *Dalton Trans.* **2004**, 244−251. (e) Foreman, M. R. S.; Hudson, M. J.; Drew, M. G. B.; Hill, C.; Madic, C. *Dalton Trans.* **2006**, 1645−1653. (f) Hudson, M. J.; Boucher, C. E.; Braekers, D.; Desreux, J. F.; Drew, M. G. B.; Foreman, M. R. S. J.; Harwood, L. M.; Hill, C.; Madic, C.; Marken, F.; Youngs, T. G. A. *New J. Chem.* **2006**, *30*, 1171−1183. (g) Hubscher-Bruder, V.; Haddaoui, J.; Bouhroum, S.; Arnaud-Neu, F. *Inorg. Chem.* **2010**, *49*, 1363−1371.

(7) (a) Bardwell, D. A.; Jeffery, J. C.; Jones, P. L.; McCleverty, J. A.; Psillakis, E.; Reeves, Z.; Ward, M. D. *J. Chem. Soc., Dalton Trans.* **1997**, 2079−2086. (b) Kadjane, P.; Starck, M.; Camerel, F.; Hill, D.; Hildebrandt, N.; Ziessel, R.; Charbonnière, L. J. *Inorg. Chem.* **2009**, *48*, 4601−4603. (c) Bremer, A.; Ruff, C. M.; Girnt, D.; Müllich, U.; Rothe, J.; Roesky, P. W.; Panak, P. J.; Karpov, A.; Müller, T. J. J.; Denecke, M. A.; Geist, A. *Inorg. Chem.* **2012**, *51*, 5199−5207.

(8) (a) de Bettencourt-Dias, A.; Barber, P. S.; Viswanathan, S.; de Lill, D. T.; Rollett, A.; Ling, G.; Altun, S. *Inorg. Chem.* **2010**, *49*, 8848−8861. (b) Matsumoto, K.; Suzuki, K.; Tsukuda, T.; Tsubomura, T. *Inorg. Chem.* **2010**, *49*, 4717−4719. (c) Yuasa, J.; Ohno, T.; Miyata, K.; Tsumatori, H.; Hasegawa, Y.; Kawai, T. *J. Am. Chem. Soc.* **2011**, *133*, 9892−9902. (d) Ward, M. D.; Gade, L. H. *Chem. Commun.* **2012**, *48*, 10587−10599.

(9) (a) Piguet, C.; Williams, A. F.; Bernardinelli, G.; Moret, E.; Bünzli, J.-C. G. *Helv. Chim. Acta* **1992**, *75*, 1697−1717. (b) Piguet, C.; Bünzli, J.-C. G.; Bernardinelli, G.; Williams, A. F. *Inorg. Chem.* **1993**, *32*, 4139−4149. (c) Piguet, C.; Bünzli, J.-C. G.; Bernardinelli, G.; Bochet, C. G.; Froidevaux, P. *J. Chem. Soc., Dalton Trans.* **1995**, 83−97. (d) Petoud, S.; Bünzli, J.-C. G.; Renaud, F.; Piguet, C.; Schenk, K. J.; Hopfgartner, G. *Inorg. Chem.* **1997**, *36*, 5750−5760. (e) Petoud, S.; Bünzli, J.-C. G.; Schenk, K. J.; Piguet, C. *Inorg. Chem.* **1997**, *36*, 1345−1353. (f) Ionova, G.; Rabbe, C.; Guillaumont, R.; Ionov, S.; Madic, C.; Krupa, J.-C.; Guillaneux, D. *New J. Chem.* **2002**, *26*, 234−242. (g) Froidevaux, P.; Harrowfield, J. M.; Sobolev, A. N. *Inorg. Chem.* **2000**, *39*, 4678−4687. (h) Nozary, H.; Piguet, C.; Rivera, J.-P.; Tissot, P.; Bernardinelli, G.; Vulliermet, N.; Weber, J.; Bünzli, J.-C. G. *Inorg. Chem.* **2000**, *39*, 5286−5298. (i) Muller, G.; Bünzli, J.-C. G.; Schenk, K. J.; Piguet, C.; Hopfgartner, G. *Inorg. Chem.* **2001**, *40*, 2642−2651. (j) Muller, G.; Riehl, J. P.; Schenk, K. J.; Hopfgartner, G.; Piguet, C.; Bünzli, J.-C. G. *Eur. J. Inorg. Chem.* **2002**, 3101−3110. (k) Beck, J. B.; Rowan, S. J. *J. Am. Chem. Soc.* **2003**, *125*, 13922−13923. (l) Drew, M. G. B.; Hill, C.; Hudson, M. J.; Iveson, P. B.; Madic, C.; Vaillant, L.; Youngs, T. G. A. *New J. Chem.* **2004**, *28*, 462−470. (m) Terazzi, E.; Torelli, S.; Bernardinelli, G.; Rivera, J.-P.; Bénech, J.-M.; Bourgogne, C.; Donnio, B.; Guillon, D.; Imbert, D.; Bünzli, J.-C. G.; Pinto, A.; Jeannerat, D.; Piguet, C. *J. Am. Chem. Soc.* **2005**, *127*, 888−903. (n) Knapton, D.; Iyer, P. K.; Rowan, S. J.; Weder, C. *Macromolecules*

**2006**, *39*, 4069−4075. (o) Burnworth, M.; Knapton, D.; Rowan, S. J.; Weder, C. J. *Inorg. Organomet. Polym. Mater.* **2007**, *17*, 91−103. (p) Escande, A.; Guénée, L.; Buchwalder, K.-L.; Piguet, C. *Inorg. Chem.* **2009**, *48*, 1132−1147. (q) Shavaleev, N. M.; Scopelliti, R.; Gumy, F.; Bünzli, J.-C. G. *Inorg. Chem.* **2009**, *48*, 2908−2918. (r) Shavaleev, N. M.; Scopelliti, R.; Gumy, F.; Bünzli, J.-C. G. *Inorg. Chem.* **2009**, *48*, 6178−6191. (s) Shavaleev, N. M.; Scopelliti, R.; Gumy, F.; Bünzli, J.-C. G. *Inorg. Chem.* **2009**, *48*, 7937−7946. (t) Shavaleev, N. M.; Gumy, F.; Scopelliti, R.; Bünzli, J.-C. G. *Inorg. Chem.* **2009**, *48*, 5611−5613. (u) Shavaleev, N. M.; Eliseeva, S. V.; Scopelliti, R.; Bünzli, J.-C. G. *Inorg. Chem.* **2010**, *49*, 3929−3936.

(10) Hoang, T. N.; Lathion, T.; Guénée, L.; Terazzi, E.; Piguet, C. *Inorg. Chem.* **2012**, *51*, 8567−8575.

(11) Collins, S. N.; Taylor, S.; Krause, J. A.; Connick, W. B. *Acta Crystallogr., Sect. C: Cryst. Struct. Commun.* **2007**, *C63*, m436−m439.

(12) Zhao, Q.-L.; Li, G.-P. *Acta Crystallogr., Sect. E: Struct. Rep. Online* **2009**, *E65*, m693.

(13) The related, but less-flexible, aromatic fused 5−6 membered terdentate ligand 2-(8′quinolinyl)-1,10-phenanthroline has been reported to react with Pt(II) and Ru(II) to give distorted tetragonal and pseudo-octahedral complexes. (a) Hu, Y.-Z.; Wilson, M. H.; Zong, R.; Bonnefous, C.; McMillin, D. R.; Thummel, R. P. *Dalton Trans.* **2005**, 354−358. (b) Kaveevivitchai, N.; Zong, R.; Tseng, H.-W.; Chitta, R.; Thummel, R. P. *Inorg. Chem.* **2012**, 2930−2939.

(14) Shin, D.; Switzer, C. *Chem. Commun.* **2007**, 4401−4403.

(15) (a) Sperotto, E.; van Klink, G. P. M.; van Koten, G.; de Vries, J. G. *Dalton Trans.* **2010**, *39*, 10338−10351. (b) Garner, K. L.; Parkes, J. F.; Piper, J. D; Williams, J. A. G. *Inorg. Chem.* **2010**, *49*, 476−487.

(16) HypNMR-2008 software: (a) Frassineti, C.; Ghelli, S.; Gans, P.; Sabatini, A.; Moruzzi, M. S.; Vacca, A. *Anal. Biochem.* **1995**, *231*, 374−382. (b) Frassineti, C.; Alderighi, L.; Gans, P.; Sabatini, A.; Vacca, A.; Ghelli, S. *Bioanal Chem.* **2003**, *376*, 1041−1052.

(17) Lavallee, D. K.; Baughman, M. D.; Phillips, M. D. *J. Am. Chem. Soc.* **1977**, *99*, 718−724.

(18) (a) Reimers, J. R.; Hall, L. E. *J. Am. Chem. Soc.* **1999**, *121*, 3730−3744. (b) Constable, E. C.; Doyle, M. J.; Healy, J.; Raithby, P. R. *J. Chem. Soc., Chem. Commun.* **1988**, 1262−1263.

(19) The nitrogen atom of the central pyridine and the two coordinated oxygen atoms form the trigonal basis.

(20) (a) Kepert, C. J.; Skelton, B. W.; White, A. H. *Aust. J. Chem.* **1994**, *47*, 391−396. (b) Drew, M. G. B.; Hudson, M. J.; Iveson, P. B.; Russell, M. L.; Lilijenzin, J.-O.; Skalberg, M.; Spjuth, L.; Madic, C. *J. Chem. Soc., Dalton Trans.* **1998**, 2973−2980. (c) Berthon, C.; Grigoriev, M. S. *Acta Crystallogr., Sect. E: Struct. Rep. Online* **2005**, *E61*, o1216−o1217.

(21) Ercolani, G.; Schiaffino, L. *Angew. Chem., Int. Ed.* **2011**, *50*, 1762−1768.

(22) (a) Hamacek, J.; Borkovec, M.; Piguet, C. *Chem.—Eur. J.* **2005**, *11*, 5227−5237. (b) Hamacek, J.; Borkovec, M.; Piguet, C. *Chem.—Eur. J.* **2005**, *11*, 5217−5226. (c) Hamacek, J.; Borkovec, M.; Piguet, C. *Dalton Trans.* **2006**, 1473−1490. (d) Piguet, C. *Chem. Commun.* **2010**, *46*, 6209−6231.

(23) Ercolani, G.; Piguet, C.; Borkovec, M.; Hamacek, J. *J. Phys. Chem. B* **2007**, *111*, 12195−12203.

(24) (a) Schwarzenbach, G. *Helv. Chim. Acta* **1952**, *35*, 39−65. (b) Adamson, A. W. *J. Am. Chem. Soc.* **1954**, *76*, 1578−1579. (c) Martell, A. E. *Adv. Chem. Ser.* **1966**, *62*, 272−294. (d) Munro, D. *Chem. Brit.* **1977**, *13*, 100−105. (e) Simmons, E. L. *J. Chem. Educ.* **1979**, *56*, 578−579. (f) Chung, C.-S. *J. Chem. Educ.* **1984**, *61*, 1062−1064.

(25) In eqs 5 and 6, we assume that $f^{H,L7}_{connect} = f^{H,L7}_{N_{py}distal} = f^{H,L7}_{N_{py}central} = f^{H,L7}_{N_{aza}distal}$, and $u^{H,H}_{L7} = u^{H_{Npycentral},H_{Nazadistal}}_{L7} = u^{H_{Npydistal},H_{Nazadistal}}_{L7}$.

(26) (a) Shannon, R. D. *Acta Crystallogr., Sect. A: Cryst. Phys., Diffr., Theor. Gen. Crystallogr.* **1976**, *A32*, 751−767. (b) D'Angelo, P.; Zitolo, A.; Migliorati, V.; Chillemi, G.; Duvail, M.; Vitorge, P.; Abadie, S.; Spezia, R. *Inorg. Chem.* **2011**, *50*, 4572−4579.

(27) (a) Waters, A. F.; White, A. H. *Aust. J. Chem.* **1996**, *49*, 147. (b) Bock, C. W. *Inorg. Chem.* **1994**, *33*, 419−427.

(28) (a) Einstein, F. W. B.; Penfold, B. R. *Acta Crystallogr.* **1966**, *20*, 924−926. (b) Vlasse, M.; Rojo, T.; Beltran-Porter, D. *Acta Crystallogr., Sect. C: Cryst. Struct. Commun.* **1983**, *C39*, 560−563. (c) Harrison, P. G.; Begley, M. J.; Kikabhai, T.; Killer, F. *J. Chem. Soc., Dalton Trans.* **1986**, 929−934. (d) Tamasi, G.; Cini, R. *Dalton Trans.* **2003**, 2928−2936. (e) Finn, R. C.; Zubieta, J. *J. Chem. Soc., Dalton Trans.* **2002**, 856−861. (f) Shalumova, T.; Tanski, J. M. *Acta Crystallogr., Sect. E: Struct. Rep. Online* **2009**, *E65*, m1325. (g) Zhao, Q.-L.; Li, G.-P. *Acta Crystallogr., Sect. E: Struct. Rep. Online* **2009**, *E65*, m693.

(29) (a) Harvey, M. A.; Baggio, S.; Ibanez, A.; Baggio, R. *Acta Crystallogr., Sect. C: Cryst. Struct. Commun.* **2004**, *C60*, m375−m381. (b) Dumitru, F.; Petit, E.; Van der Lee, A.; Barboiu, M. *Eur. J. Inorg. Chem.* **2005**, 4255−4262. (c) Tang, L.; Yang, X.-G.; Li, D.-S.; Wang, J.-J.; Gao, X.-M.; Wang, J.-W.; Kristallogr, Z. *New Cryst. Struct.* **2007**, *222*, 59. (d) Goforth, A. M.; Tershansy, M. A.; Smith, M. D.; Peterson, L.; Kelley, J. G.; DeBenedetti, W. J. I. H.; Loye, C. Z *J. Am. Chem. Soc.* **2011**, *133*, 603−612.

(30) Baes, C. F. J.; Mesmer, R., E. *Hydrolysis of Cations*; Wiley−Interscience: New York, 1976; Ch. 7, p 129.

(31) (a) Evans, W. J.; Giarikos, D. G.; Johnston, M. A.; Greci, M. A.; Ziller, J. W. *J. Chem. Soc., Dalton Trans.* **2002**, *4*, 520−526. (b) Malandrino, G.; Nigro, R. L.; Fragala, I. L.; Cristiano, B. *Eur. J. Inorg. Chem.* **2004**, *3*, 500−509.

(32) Aspinall, H. C.; Greeves, N.; McIver, E. G. *J. Alloys Compd.* **1998**, *275−277*, 773−776.

(33) Kilic, E.; Aslan, N. *Michrochim. Acta* **2005**, *151*, 89−92.

(34) Izod, K.; Liddle, S. T.; Clegg, W. *Inorg. Chem.* **2004**, *43*, 214−218.

(35) The noncoordinated triiodide $I_3^-$ counteranion is produced by air oxidation of iodide, whilst the chloride anion probably results from halide exchange reactions between $CH_2Cl_2$ and $I^-$.

(36) Kepert, C. J.; Weimin, L.; Skelton, B. W.; White, A. H. *Aust. J. Chem.* **1994**, *47*, 365−384.

(37) Semenova, L. I.; White, A. H. *Aust. J. Chem.* **1999**, *52*, 507−517.

(38) Semenova, L. I.; Sobolev, A. N.; Skelton, B. W.; White, A. H. *Aust. J. Chem.* **1999**, *52*, 519−529.

(39) Zou, J.; Berg, D. J.; Stuart, D.; McDonald, R.; Twamley, B. *Organometallics* **2011**, *30*, 4958−4967.

(40) Altomare, A.; Burla, M. C.; Camalli, M.; Cascarano, G.; Giacovazzo, C.; Guagliardi, A.; Moliterni, G.; Polidori, G.; Spagna, R. *J. Appl. Crystallogr.* **1999**, *32*, 115−119.

(41) Sheldrick, G. M. *SHELXL97 Program for the Solution and Refinement of Crystal Structures*; University of Göttingen, Göttingen, Germany, 1997.

(42) ORTEP3 for Windows: Farrugia, L. J. *J. Appl. Crystallogr.* **1997**, *30*, 565−566.

# A Polyaromatic Terdentate Binding Unit with Fused 5,6-Membered Chelates for Complexing s, p, d and f-Block Cations.

---

**Thi Nhu Y Hoang,[*] Marie Humbert-Droz, Thibault Dutronc, Laure Guénée, Céline Besnard and Claude Piguet[*]**

## Supporting Information

(49 pages)

**Appendix 1**. **Speciation obtained from $^1$H NMR titrations of L7 with $Mg(ClO_4)_2$ and $Zn(CF_3SO_3)_2$.**

For a given stoichiometric $|M|_{tot} / |\mathbf{L7}|_{tot}$ ratio, the integrated intensities of the $^1$H NMR signals recorded for the same proton in **L7** ($I_L$), $[M(\mathbf{L7})]^{2+}$ ($I_{M\text{-}L}$) and $[M(\mathbf{L7})_2]^{2+}$ ($I_{M\text{-}2L}$) can be combined and scaled with respect to $|[M(\mathbf{L7})]|$ by using eqns (S1)-(S2).

$$|\mathbf{L7}| = \left(\frac{I_L}{I_{M\text{-}L}}\right)|[M(\mathbf{L7})]| \quad \text{(S1)}$$

$$|[M(\mathbf{L7})_2]| = \left(\frac{I_{M\text{-}2L}}{2I_{M\text{-}L}}\right)|[M(\mathbf{L7})]| \quad \text{(S2)}$$

Introducing eqns (S1)-(S2) into the mass balance eqn (S3) yields eqn (S4) after straightforward algebraic transformations.

$$|\mathbf{L7}|_{tot} = |\mathbf{L7}| + |[M(\mathbf{L7})]| + 2|[M(\mathbf{L7})_2]| \quad \text{(S3)}$$

$$|[M(\mathbf{L7})]| = |\mathbf{L7}|_{tot}\left(\frac{I_{M\text{-}L}}{I_L + I_{M\text{-}L} + I_{M\text{-}2L}}\right) \quad \text{(S4)}$$

Introducing eqn (S4) into eqns (S1)-(S2) gives the speciation of the free ligand (eqn S5) and of $[M(\mathbf{L7})_2]^{2+}$ (eqn S6).

$$|\mathbf{L7}| = |\mathbf{L7}|_{tot}\left(\frac{I_L}{I_L + I_{M\text{-}L} + I_{M\text{-}2L}}\right) \quad \text{(S5)}$$

$$|[M(\mathbf{L7})_2]| = \frac{|\mathbf{L7}|_{tot}}{2}\left(\frac{I_{M\text{-}2L}}{I_L + I_{M\text{-}L} + I_{M\text{-}2L}}\right) \quad \text{(S6)}$$

The missing concentration $|M|$ (eqn S9) can be deduced from the mass balance written for the metal concentrations (eqn S8).

$$|M| = |M|_{tot} - |[M(\mathbf{L7})]| - |[M(\mathbf{L7})_2]| \quad \text{(S8)}$$

$$|M| = |M|_{tot} - \frac{|\mathbf{L7}|_{tot}}{2}\left(\frac{2I_{M\text{-}L} + I_{M\text{-}2L}}{I_L + I_{M\text{-}L} + I_{M\text{-}2L}}\right) \quad \text{(S9)}$$

The final introduction of eqns (S4)-(S6) and (S9) into the laws of mass action associated with equilibrium (9) and (10) yields eq (S10) and (S11), respectively (the standard concentration of the reference state is set at 1 M).

$$\beta_{1,1}^{M,\mathbf{L7}} = \frac{|[M(\mathbf{L7})]|}{|M|\cdot|\mathbf{L7}|} = \frac{I_{M\text{-}L}}{I_L}\left(\frac{I_L + I_{M\text{-}L} + I_{M\text{-}2L}}{|M|_{tot}(I_L + I_{M\text{-}L} + I_{M\text{-}2L}) - |\mathbf{L7}|_{tot}(I_{M\text{-}L} + I_{M\text{-}2L})}\right) \quad \text{(S10)}$$

$$\beta_{1,2}^{\mathrm{M},\mathbf{L7}} = \frac{\left|[\mathrm{M}(\mathbf{L7})_2]\right|}{\left|\mathrm{M}\right|\cdot\left|\mathbf{L7}\right|^2} = \frac{I_{\mathrm{M\text{-}2L}}}{\left(I_{\mathrm{L}}\right)^2\left|\mathbf{L7}\right|_{\mathrm{tot}}}\left(\frac{\left(I_{\mathrm{L}}+I_{\mathrm{M\text{-}L}}+I_{\mathrm{M\text{-}2L}}\right)^2}{2\left|\mathrm{M}\right|_{\mathrm{tot}}\left(I_{\mathrm{L}}+I_{\mathrm{M\text{-}L}}+I_{\mathrm{M\text{-}2L}}\right)-\left|\mathbf{L7}\right|_{\mathrm{tot}}\left(2I_{\mathrm{M\text{-}L}}+I_{\mathrm{M\text{-}2L}}\right)}\right) \quad \text{(S11)}$$

In the case of M = Zn, the concentration of free ligand can be detected ($I_{\mathrm{L}} > 0$) only in default of metal for $\left|\mathrm{Zn}\right|_{\mathrm{tot}} / \left|\mathbf{L7}\right|_{\mathrm{tot}}$ = 0.1-0.5, a domain in which $I_{\mathrm{M\text{-}L}} = 0$ and only $\beta_{1,2}^{\mathrm{M},\mathbf{L7}}$ can be estimated with eqn (S11). $\beta_{1,1}^{\mathrm{M},\mathbf{L7}}$ is alternatively computed from the exchange equilibrium (S12), which is easily quantified by using eqn (S13) in excess of metal ($I_{\mathrm{M\text{-}L}} > 0$, $I_{\mathrm{M\text{-}2L}} > 0$ and $I_{\mathrm{L}} = 0$).

$$\mathrm{Zn}^{2+} + [\mathrm{Zn}(\mathbf{L7})_2]^{2+} \rightleftharpoons 2\,[\mathrm{Zn}(\mathbf{L7})_2]^{2+} \qquad K_{\mathrm{exch}}^{\mathrm{Zn},\mathbf{L7}} \quad \text{(S12)}$$

$$K_{\mathrm{exch}}^{\mathrm{Zn},\mathbf{L7}} = \frac{\left(\beta_{1,1}^{\mathrm{Zn},\mathbf{L7}}\right)^2}{\beta_{1,2}^{\mathrm{Zn},\mathbf{L7}}} = \frac{\left|[\mathrm{Zn}(\mathbf{L7})]\right|^2}{\left|\mathrm{Zn}\right|\cdot\left|[\mathrm{Zn}(\mathbf{L7})_2]\right|} = \frac{4\left(I_{\mathrm{M\text{-}L}}\right)^2\left|\mathbf{L7}\right|_{\mathrm{tot}}}{\left(I_{\mathrm{M\text{-}2L}}\right)\left[2\left|\mathrm{M}\right|_{\mathrm{tot}}\left(I_{\mathrm{L}}+I_{\mathrm{M\text{-}L}}+I_{\mathrm{M\text{-}2L}}\right)-\left|\mathbf{L7}\right|_{\mathrm{tot}}\left(2I_{\mathrm{M\text{-}L}}+I_{\mathrm{M\text{-}2L}}\right)\right]} \quad \text{(S13)}$$

**Appendix 2. Speciation obtained from $^1$H NMR titration of L7 with Y(CF$_3$SO$_3$)$_3$·diglyme**.

$$H^+ + \mathbf{L7} \rightleftharpoons [H\mathbf{L7}]^+ \qquad \beta_{1,1}^{H,\mathbf{L7}} = 5.3(2) \tag{14}$$

$$2H^+ + \mathbf{L7} \rightleftharpoons [H_2\mathbf{L7}]^{2+} \qquad \beta_{2,1}^{H,\mathbf{L7}} = 9.1(2) \tag{15}$$

$$Y^{3+} + \mathbf{L7} \rightleftharpoons [Y\mathbf{L7}]^{3+} \qquad \beta_{1,1}^{Y,\mathbf{L7}} \tag{16}$$

$$Y^{3+} + 2\,\mathbf{L7} \rightleftharpoons [Y(\mathbf{L7})_2]^{3+} \qquad \beta_{2,1}^{Y,\mathbf{L7}} \tag{17}$$

$$Y^{3+} + H_2O \rightleftharpoons [Y(OH)]^{2+} + H^+ \qquad K_{a,Y}^1 = 10^{-8.81} \tag{18}$$

$$H_2O \rightleftharpoons OH^- + H^+ \qquad K_s = 10^{-16.35} \tag{19}$$

The application of the law of mass action for equilibria (14)-(19) gives (standard concentration of the reference state $c^\theta$ = 1 M):

$$\beta_{1,1}^{H,\mathbf{L7}} = \frac{|HL7|}{|L7||H|} \tag{S14}$$

$$\beta_{2,1}^{H,\mathbf{L7}} = \frac{|HL7|}{|L7||H|^2} \tag{S15}$$

$$\beta_{1,1}^{Y,\mathbf{L7}} = \frac{|Y(L7)|}{|Y||L7|} \tag{S16}$$

$$\beta_{1,2}^{Y,\mathbf{L7}} = \frac{|Y(L7)|}{|Y||L7|^2} \tag{S17}$$

$$K_{a,Y}^1 = \frac{|Y(OH)||H|}{|Y||H_2O|} \tag{S18}$$

$$K_s = \frac{|OH||H|}{|H_2O|} \tag{S19}$$

The mass balances lead to

$$|L7|_{tot} = |L7| + |HL7| + |H_2L7| + |LnL7| + 2|Ln(L7)_2| \tag{S20}$$

$$|Y|_{tot} = |Y| + |Y(OH)| + |YL7| + |Y(L7)_2| \tag{S21}$$

$$|H_2O|_{tot} = |H_2O| + |Y(OH)| + |OH| \tag{S22}$$

The charge balance provides

$$3|Y| + 2|Y(OH)| + 3|YL7| + 3|Y(L7)_2| + |HL7| + 2|H_2L7| + |H| = |OH| + |CF_3SO_3| \tag{S23}$$

We first take advantage of the fast exchange process characterizing the NMR regime for the protonation of 'free' **L7**. In these conditions, the chemical shift of the time-average signal for a proton *i* in the 'free' ligand $\delta_{obs}^i$ can be written as eqn (S24), in which $\delta_{L7}^i$, $\delta_{HL7}^i$ and $\delta_{H2L7}^i$ are taken from Table S2.

$$\delta^i_{obs} = \frac{\delta^i_{L7}\left|L7\right| + \delta^i_{HL7}\left|HL7\right| + \delta^i_{H2L7}\left|H_2L7\right|}{\left|L7\right| + \left|HL7\right| + \left|H_2L7\right|} \quad \text{(S24)}$$

The introduction of $\left|HL7\right|$ from eqn (S14) and $\left|H_2L7\right|$ from eqn (S15) into eqn (S24) provides eqn (S25), from which the free concentration $\left|H\right|$ can be easily deduced.

$$\delta^i_{obs} = \frac{\delta^i_{L7} + \delta^i_{HL7}\beta^{H,\mathbf{L7}}_{1,1}\left|H\right| + \delta^i_{H2L7}\beta^{H,\mathbf{L7}}_{2,1}\left|H\right|^2}{1 + \beta^{H,\mathbf{L7}}_{1,1}\left|H\right| + \beta^{H,\mathbf{L7}}_{2,1}\left|H\right|^2}$$

$$\Rightarrow \left|H\right|^2\beta^{H,\mathbf{L7}}_{2,1}\left(\delta^i_{obs} - \delta^i_{H2L7}\right) + \left|H\right|\beta^{H,\mathbf{L7}}_{1,1}\left(\delta^i_{obs} - \delta^i_{HL7}\right) + \left(\delta^i_{obs} - \delta^i_{L7}\right) = 0 \quad \text{(S25)}$$

We now focuse on the ratio of the $^1$H NMR integrations of the signals measured for $[Y(\mathbf{L7})]^{3+}$ ($I_{YL7,}$ slow exchange), $[Y(\mathbf{L7})_2]^{3+}$ ($I_{Y(L7)2}$, slow exchange) and for the sum of the protons in the free and protonated ligand ($I_{sum}$, fast exchange).

$$\frac{\left|YL7\right|}{\left|Y(L7)_2\right|} = \frac{2I_{YL7}}{I_{Y(L7)2}} \quad \text{(S26)}$$

$$\frac{\left|YL7\right|}{\left|L7\right| + \left|HL7\right| + \left|H_2L7\right|} = \frac{I_{YL7}}{I_{sum}} \quad \text{(S27)}$$

The introduction of the masse balance for **L7** (eqn S20) into the denominator of eqn (S27) gives

$$\frac{\left|YL7\right|}{\left|L7\right|_{tot} - \left|YL7\right| - 2\left|Y(L7)_2\right|} = \frac{I_{YL7}}{I_{sum}} \quad \text{(S28)}$$

The simultaneous solution of eqns (S26) and (S28) eventually leads to the estimation of the concentration of the two complexes-

$$\left|YL7\right| = \left|L7\right|_{tot}\frac{I_{YL7}}{I_{sum} + I_{YL7} + I_{Y(L7)2}} \quad \text{(S29)}$$

$$\left|Y(L7)_2\right| = \left|L7\right|_{tot}\frac{I_{Y(L7)2}}{2\left(I_{sum} + I_{YL7} + I_{Y(L7)2}\right)} \quad \text{(S30)}$$

The concentration of free ligand then results from the the mass balance written in eqn S20

$$\left|L7\right| = \frac{\left|L7\right|_{tot} - \left|YL7\right| - 2\left|Y(L7)_2\right|}{1 + \beta^{H,\mathbf{L7}}_{1,1}\left|H\right| + \beta^{H,\mathbf{L7}}_{2,1}\left|H\right|^2} \quad \text{(S31)}$$

Finally, the missing free concentration in metal is deduced from the charge balance (eqn S23), in which eqns (14)-(15) and (S21) were introduced reminding that $\left|CF_3SO_3\right| = 3\left|Y\right|_{tot}$.

$$\left|Y\right| = K_s/\left|H\right| + \left|Y\right|_{tot} - \left|YL7\right| - \left|Y(L7)_2\right| - \beta^{H,\mathbf{L7}}_{1,1}\left|L7\right|\left|H\right| - 2\beta^{H,\mathbf{L7}}_{2,1}\left|L7\right|\left|H\right|^2 - \left|H\right| \quad \text{(S32)}$$

The ultimate introduction of the free concentrations obtained with eqns (S29)-(S32) into eqns (16)-(17) provides the estimates of $\beta^{Y,\mathbf{L7}}_{1,1}$ and $\beta^{Y,\mathbf{L7}}_{1,2}$ collected in Table 1.

**Table S1** $^{1}$H NMR Chemical Shifts Computed for **L7**, [H**L7**]$^{+}$, [$H_2$**L7**]$^{2+}$, [Li**L7**]$^{+}$, [$Li_2$**L7**]$^{2+}$, [M(**L7**)]$^{2+}$ and [M(**L7**)$_2$]$^{2+}$ (M = Mg(II), Zn(II)) in $CD_3CN/CDCl_3$ (1:1) at 298 K.

| Ligand | H1 | H2 | H3 | H4 | H5 | H6 | H7 | H8 | H9 | H10 | H11 | H12 |
|---|---|---|---|---|---|---|---|---|---|---|---|---|
| **L7** | 8.06 | 9.04 | 8.62 | 6.74 | 8.03 | 7.22 | 8.41 | 8.30 | 8.54 | 7.93 | 7.41 | 8.70 |
| [H**L7**]$^{+}$ | 8.28 | 9.29 | 8.75 | 6.86 | 8.18 | 7.35 | 8.47 | 8.15 | 8.60 | 8.65 | 8.07 | 8.96 |
| [$H_2$**L7**]$^{2+}$ | 8.44 | 8.02 | 8.22 | 7.22 | 8.83 | 7.81 | 8.66 | 8.31 | 8.66 | 8.77 | 8.18 | 9.00 |
| [Li**L7**]$^{+}$ | 8.18 | 7.95 | 8.07 | 6.85 | 8.17 | 7.36 | 8.61 | 8.06 | 8.26 | 8.06 | 7.56 | 8.86 |
| [$Li_2$**L7**]$^{2+}$ | 8.13 | 8.01 | 8.14 | 6.85 | 8.13 | 7.36 | 8.60 | 8.12 | 8.31 | 8.04 | 7.56 | 8.86 |
| [Mg(**L7**)]$^{2+}$ | 8.37 | 7.99 | 8.16 | 7.03 | 8.38 | 7.56 | 8.55 | 8.48 | 8.35 | 8.28 | 7.79 | 8.79 |
| [Mg(**L7**)$_2$]$^{2+}$ | 8.62 | 8.33 | 8.30 | 6.98 | 8.10 | 7.03 | 7.63 | 8.45 | 8.42 | 8.03 | 7.30 | 7.65 |
| [Zn(**L7**)]$^{2+}$ | 8.40 | 8.04 | 8.20 | 7.07 | 8.44 | 7.64 | 8.77 | 8.54 | 8.36 | 8.33 | 7.89 | 9.04 |
| [Zn(**L7**)$_2$]$^{2+}$ | 8.63 | 8.28 | 8.27 | 7.00 | 8.11 | 7.05 | 7.62 | 8.50 | 8.42 | 8.05 | 7.33 | 7.96 |

**Table S2** $^{1}$H NMR Chemical Shifts Computed for **L7**, $[H\mathbf{L7}]^{+}$, $[H_2\mathbf{L7}]^{2+}$, $[Li\mathbf{L7}]^{+}$, $[Li_2\mathbf{L7}]^{2+}$, $[M(\mathbf{L7})]^{2+}$ and $[M(\mathbf{L7})_2]^{2+}$ (M = Mg(II), Zn(II)) in $CD_3CN$ at 298 K.

| Ligand | H1 | H2 | H3 | H4 | H5 | H6 | H7 | H8 | H9 | H10 | H11 | H12 |
|---|---|---|---|---|---|---|---|---|---|---|---|---|
| **L7** | 8.13 | 9.07 | 8.68 | 6.8 | 8.09 | 7.28 | 8.45 | 8.34 | 8.59 | 7.97 | 7.46 | 8.95 |
| $[H\mathbf{L7}]^{+}$ | 8.28 | 9.48 | 8.85 | 6.85 | 8.07 | 7.29 | 8.47 | 8.18 | 8.65 | 8.62 | 8.02 | 8.89 |
| $[H_2\mathbf{L7}]^{2+}$ | 8.48 | 8.07 | 8.28 | 7.26 | 8.88 | 7.83 | 8.60 | 8.35 | 8.71 | 8.82 | 8.22 | 8.73 |
| $[Li\mathbf{L7}]^{+}$ | 8.21 | 8.06 | 8.2 | 6.89 | 8.21 | 7.40 | 8.63 | 8.17 | 8.3 | 8.09 | 7.59 | 8.88 |
| $[Li_2\mathbf{L7}]^{2+}$ | 8.17 | 8.32 | 8.31 | 6.86 | 8.17 | 7.36 | 8.59 | 8.22 | 8.41 | 8.05 | 7.56 | 8.84 |
| $[Mg(\mathbf{L7})]^{2+}$ | 8.43 | 8.04 | 8.21 | 7.08 | 8.38 | 7.61 | 8.61 | 8.54 | 8.40 | 8.33 | 7.84 | 8.85 |
| $[Mg(\mathbf{L7})_2]^{2+}$ | 8.64 | 8.33 | 8.26 | 7.01 | 8.14 | 7.03 | 7.74 | 8.40 | 8.41 | 8.05 | 7.30 | 7.74 |
| $[Zn(\mathbf{L7})]^{2+}$ | 8.44 | 8.09 | 8.27 | 7.12 | 8.5 | 7.68 | 8.78 | 8.6 | 8.42 | 8.40 | 7.93 | 9.14 |
| $[Zn(\mathbf{L7})_2]^{2+}$ | 8.64 | 8.30 | 8.28 | 7.02 | 8.13 | 7.04 | 7.71 | 8.51 | 8.43 | 8.05 | 7.33 | 7.76 |

**Table S3** Major Positive-Mode ESI-MS Peaks Observed during the Titration of **L7** with $LiClO_4$ in $CH_3CN$ ($|\mathbf{L7}|_{tot} = 5 \cdot 10^{-4}$ M).

| $\left\|[Li]^+\right\|_{tot} / \|\mathbf{L7}\|_{tot}$ | *+m/z* | | | |
|---|---|---|---|---|
| | $[\mathbf{L7}+H]^+$ | $[\mathbf{L7}+2H_3O]^{2+}$ | $[\mathbf{L7}+Li]^+$ | $[\mathbf{L7}+2Li+CH_3CN]^{2+}$ |
| 0 | 273.95 | 155.03 | - | - |
| 1.0 | 272.81 | 155.03 | 279.02 | 164.02 |
| 2.0 | 272.99 | 154.97 | 279.34 | 164.02 |
| 3.0 | 272.93 | 155.01 | 279.37 | 164.02 |

**Table S4** Summary of Crystal Data, Intensity Measurements and Structure Refinements for [H**L7**]($CF_3SO_3$) (**3**), [$H_2$**L7**]($ClO_4$)$_2$ (**4**) and [Li(**L7**)($OH_2$)($ClO_4$)] (**5**).

| | **3** | **4** | **5** |
|---|---|---|---|
| Empirical formula | $C_{18}H_{13}F_3N_4O_3S$ | $C_{17}H_{14}Cl_2N_4O_8$ | $C_{17}H_{14}ClLiN_4O_5$ |
| Formula weight | 422.38 | 473.22 | 396.71 |
| Temperature /K | 293(2) | 180(2) | 180 |
| Wavelength /Å | 1.54184 | 1.54184 | 1.5418 |
| Crystal System, Space group | Monoclinic | Monoclinic | Triclinic |
| | $P2_1/c$ | $Cc$ | $P$-1 |
| $a$ /Å | 6.94004(12) | 21.8972(10) | 7.4188(5) |
| $b$/Å | 11.60676(13) | 15.3474(3) | 10.2066(10) |
| $c$ /Å | 22.9171(3) | 15.1806(7) | 12.4306(8) |
| $\alpha$ /° | 90 | 90 | 111.463(8) |
| $\beta$ /° | 98.1622(15) | 130.218(8) | 94.292(6) |
| $\gamma$ /° | 90 | 90 | 101.089(7) |
| Volume / Å$^3$ | 1827.30(5) | 3895.6(3) | 869.40(12) |
| $Z$, Calculated density / Mg·m$^{-3}$ | 4 | 8 | 2 |
| | 1.535 | 1.614 | 1.515 |
| Absorption coefficient /mm$^{-1}$ | 2.122 | 3.520 | 2.299 |
| $F$(000) | 864 | 1936 | 408 |
| Theta range for data collection /° | 3.9 to 73.20 | 3.91 to 73.42 | 7.68 to 147.18 |
| Limiting indices | -8<=$h$<=5 | -26<=$h$<=27 | -8<=$h$<=9 |
| | -14<=$k$<=14 | -18<=$k$<=18 | -12<=$k$<=12 |
| | -28<=$l$<=28 | -18<=$l$<=18 | -8<=$l$<=15 |
| Reflections collected / unique | 10624 / 3588 | 11149 / 6067 | 5441 / 3365 |
| $R$(int) | 0.0289 | 0.0371 | 0.0131 |
| Completeness to theta / °/ % | 67/ 100 | 67/ 100 | 67.0/ 99.8 |
| Data / restraints / parameters | 3588 / 0 / 267 | 6067 / 11 / 562 | 3365 / 33 / 296 |
| Goodness-of-fit on $F^2$ | 1.123 | 1.025 | 1.061 |
| Final $R$ indices [$I$>2σ($I$)] | 0.0573 | 0.0637 | 0.0546 |
| | 0.1733 | 0.1729 | 0.1499 |
| $R$ indices (all data) | 0.0639 | 0.0654 | 0.0599 |
| | 0.1804 | 0.1761 | 0.1499 |
| Largest diff. peak and hole / e.Å$^{-3}$ | 0.351 and -0.394 | 0.776 and -0.536 | 0.620 and -0.431 |

**Table S5** Selected Bond Distances (Å), Bond Angles (°) in [H**L7**]($CF_3SO_3$) (**3**).[a]

Bond Distances (Å)

| Atom 1 | Atom 2 | Distance | Atom 1 | Atom 2 | Distance |
|---|---|---|---|---|---|
| C7 | N1 | 1.333(3) | C7 | N2 | 1.406(3) |
| C8 | N2 | 1.405(3) | C8 | N3 | 1.330(3) |
| C12 | N3 | 1.343(4) | C12 | C13 | 1.476(3) |
| C13 | N4 | 1.339(3) | | | |

Angles (°)

| Atom 1 | Atom 2 | Atom 3 | Angle | Atom 1 | Atom 2 | Atom 3 | Angle |
|---|---|---|---|---|---|---|---|
| N1 | C7 | N2 | 125.7(2) | C7 | N2 | C8 | 128.9(2) |
| N2 | C8 | N3 | 115.4(2) | N3 | C12 | C13 | 114.8(2) |
| C12 | C13 | N4 | 117.2(2) | | | | |

[a] Numbering scheme in Fig. S8

**Table S6** Selected Least-Squares Planes Data for [H**L7**]($CF_3SO_3$) (**3**).[a]

Least-Squares Planes

| Least-squares planes description | Abbreviation | Max. deviation/Å | Atom |
|---|---|---|---|
| Azaindol | Az | | |
| N1 C1 C2 C3 C4 C5 C6 N2 C7 | | 0.004(1) | C7 |
| Pyridine central | Py1 | | |
| N3 C8 C9 C10 C11 C12 | | 0.01(1) | C8 |
| Pyridine | Py2 | | |
| N4 C13 C14 C15 C16 C17 | | 0.004(1) | C15 |

[a] Numbering scheme in Fig. S8a

Interplanar angles (°) (esd < 0.1°)

| | Py1 | Py2 |
|---|---|---|
| Az | 4.40 | 3.77 |
| Py1 | | 2.84 |

**Table S7** Hydrogen bonds in [H**L7**]($CF_3SO_3$) (**3**).[a]

| D-H···A | *d*(D-H) /Å | *d*(H···A) /Å | *d*(D···A) /Å | <(DHA)/ ° |
|---|---|---|---|---|
| N4-H···O [b] | 0.77(3) | 2.13(3) | 2.787(3) | 144(3) |
| N4-H···N3 [c] | 0.77(3) | 2.27(3) | 2.649(3) | 111(3) |

[a] Numbering scheme in Fig. S8a. [b] Intermolecular hydrogen bond between the N-atom of the distal pyridine ring and one oxygen atom of the triflate counter-anion. [c] Intramolecular hydrogen bond between the two nitrogen atoms of the adjacent pyridine rings.

**Table S8** Selected Bond Distances (Å), Bond Angles (°) in [$H_2$**L7**]($ClO_4$)$_2$ (4).[a]

Bond Distances (Å)

| Atom 1 | Atom 2 | Distance | Atom 1 | Atom 2 | Distance |
|---|---|---|---|---|---|
| C7 | N1 | 1.319(7) | C7B | N1B | 1.329(6) |
| C7 | N2 | 1.338(8) | C7B | N2B | 1.344(7) |
| C8 | N2 | 1.425(7) | C8B | N2B | 1.384(8) |
| C8 | N3 | 1.325(6) | C8B | N3B | 1.312(7) |
| C12 | N3 | 1.341(6) | C12B | N3B | 1.407(8) |
| C13 | N4 | 1.329(6) | C13B | N4B | 1.358(6) |
| C13 | C12 | 1.478(7) | C13B | C12B | 1.512(8) |

Angles (°)

| Atom 1 | Atom 2 | Atom 3 | Angle | Atom 1 | Atom 2 | Atom 3 | Angle |
|---|---|---|---|---|---|---|---|
| N1 | C7 | N2 | 129.4(2) | N1B | C7B | N2B | 130.7(5) |
| C7 | N2 | C8 | 125.8(4) | C7B | N2B | C8B | 126.0(5) |
| N2 | C8 | N3 | 114.1(4) | N2B | C8B | N3B | 114.9(5) |
| N3 | C12 | C13 | 115.0(4) | N3B | C12B | C13B | 114.1(4) |
| C12 | C13 | N4 | 116.3(4) | C12B | C13B | N4B | 114.7(4) |

[a] Numbering scheme in Fig. S8b

**Table S9** Selected Least-Squares Planes Data for $[H_2\mathbf{L7}](ClO_4)_2$ (**4**).[a]

Least-Squares Planes

| Least-squares planes description | Abbreviation | Max. deviation/Å | Atom |
|---|---|---|---|
| Azaindol | Az | | |
| N1 C1 C2 C3 C4 C5 C6 N2 C7 | | 0.037(1) | C4 |
| Pyridine central | Py1 | | |
| N3 C8 C9 C10 C11 C12 | | 0.006(1) | C10 |
| Pyridine | Py2 | | |
| N4 C13 C14 C15 C16 C17 | | 0.014(1) | C13 |
| Azaindol B | AzB | | |
| N1B C1B C2B C3B C4B C5B C6B N2B C7B | | 0.049(1) | C5B |
| Pyridine central B | Py1B | | |
| N3B C8B C9B C10B C11B C12B | | 0.028(1) | C12B |
| Pyridine B | Py2B | | |
| N4B C13B C14B C15B C16B C17B | | 0.017(1) | N4B |

[a] Numbering scheme in Fig. S8b

Interplanar angles (°) (esd < 0.1°)

| | Py1 | Py2 |
|---|---|---|
| Az | 39.2 | 56.1 |
| Py1 | | 22.6 |

| | Py1B | Py2B |
|---|---|---|
| AzB | 32.2 | 54.4 |
| Py1B | | 25.2 |

**Table S10** Hydrogen bonds in $[H_2\mathbf{L7}](ClO_4)_2$ (**4**).[a]

| D-H···A | *d*(D-H)/Å | *d*(H···A)/Å | *d*(D···A)/Å | <(DHA)/° |
|---|---|---|---|---|
| N(1B)-H(1BA)...N(3B) [b] | 0.93(7) | 2.21(7) | 2.849(7) | 125(5) |
| N(1B)-H(1BA)...O(2Q) [c] | 0.93(7) | 2.21(7) | 2.926(7) | 133(6) |
| N(4B)-H(4B)...N(3B) [b] | 0.83(2) | 2.23(6) | 2.698(6) | 116(5) |
| N(4B)-H(4B)...O(5P)#1 [c] | 0.83(2) | 2.28(4) | 2.979(7) | 143(6) |
| N(4B)-H(4B)...O(2P)#1 [c] | 0.83(2) | 2.52(5) | 3.092(7) | 127(5) |
| N(1)-H(1A)...O(2) [c] | 0.84(2) | 2.07(4) | 2.831(6) | 150(6) |
| N(1)-H(1A)...N(3) [b] | 0.84(2) | 2.37(6) | 2.872(6) | 119(6) |
| N(4)-H(4)...O(3RB)#2 [c] | 0.84(2) | 2.11(3) | 2.901(18) | 159(6) |
| N(4)-H(4)...O(3RA)#2 [c] | 0.84(2) | 2.10(4) | 2.858(11) | 151(6) |

[a] Numbering scheme in Fig. S8b. Symmetry transformations used to generate equivalent atoms:

#1 *x*-1/2,-*y*+1/2,*z*-1/2 #2 *x*,-*y*+1,*z*+1/2. [b] Intramolecular hydrogen bonds between two nitrogen atoms of adjacent heterocyclic rings. [c] Intermolecular hydrogen bonds between the protonated N-atom of the heterocyclic rings and the oxygen atom of a perchlorate counter-anions.

**Table S11** Selected Bond Distances (Å), Bond Angles (°) in $[Li(\mathbf{L7})(OH_2)(ClO_4)]$ (**5**).[a]

Bond Distances (Å)

| Atom 1 | Atom 2 | Distance | Atom 1 | Atom 2 | Distance |
|---|---|---|---|---|---|
| Li | N1 | 2.038(5) | Li | O1W | 1.952(5) |
| Li | N3 | 2.156(5) | Li | O23A | 2.353(11) |
| Li | N4 | 2.053(5) | Li | O23B | 2.343(12) |

Angles (°)

| Atom 1 | Atom 2 | Atom 3 | Angle | Atom 1 | Atom 2 | Atom 3 | Angle |
|---|---|---|---|---|---|---|---|
| N1 | Li | N3 | 86.35(17) | N4 | Li | O1W | 98.2(2) |
| N1 | Li | O1W | 99.4(2) | | | | |
| N1 | Li | N4 | 161.8(2)) | | | | |
| N3 | Li | N4 | 80.16(18) | | | | |
| N3 | Li | O1W | 122.0(2) | | | | |

[a] Numbering scheme in Fig. S8c.

**Table S12** Selected Least-Squares Planes Data for [Li(**L7**)($OH_2$)($ClO_4$)] (**5**).[a]

Least-Squares Planes

| Least-squares planes description | Abbreviation | Max. deviation/Å | Atom |
|---|---|---|---|
| Azaindol | Az | | |
| N1 C1 C2 C3 C4 C5 C6 N2 C7 | | 0.012(3) | C1 |
| Pyridine central | Py1 | | |
| N3 C8 C9 C10 C11 C12 | | 0.013(3) | C12 |
| Pyridine | Py2 | | |
| N4 C13 C14 C15 C16 C17 | | 0.005(3) | C17 |

[a] Numbering scheme in Fig. S8c.

Interplanar angles (°) (esd < 0.1°)

| | Py1 | Py2 |
|---|---|---|
| Az | 1.16(11) | 9.80(12) |
| Py1 | | 9.46(14) |

**Table S13** Intermolecular Hydrogen bonds in [Li(**L7**)($OH_2$)($ClO_4$)] (**5**).[a]

| D-H···A | d(D-H)/Å | d(H···A)/Å | d(D···A)/Å | <(DHA)/° |
|---|---|---|---|---|
| O(1W)-H(1WA)...O(24A)#1 | 0.844(10) | 2.031(19) | 2846(7) | 162(4) |
| O(1W)-H(1WB)...O(2S)#2 | 0.846(10) | 1.933(18) | 2.779(14) | 177(4) |

[a] Numbering scheme in Fig. S8b. Symmetry transformations used to generate equivalent atoms: [1]-1+*x*,+*y*,+*z*; [2]1-*x*,1-*x*,2-*z*

**Table S14** Cumulative Thermodynamic Constants ($\log(\beta_{1,n}^{\mathrm{Mg,L7}})$), Associated Microscopic Affinities ($\log(f_{\mathrm{connect}}^{\mathrm{Mg,L7}})$ and $\Delta G_{\mathrm{connect}}^{\mathrm{Mg,L7}}$), Intramolecular Interligand ($\log(u_{\mathrm{Mg}}^{\mathbf{L7},\mathbf{L7}})$ and $\Delta G_{\mathrm{interaction}}^{\mathbf{L7},\mathbf{L7},\mathrm{Mg}}$) Obtained by $^1$H NMR Titrations of **L7** with $Mg(ClO_4)_2$ at variable Temperatures and Enthalpic $\Delta H_{1,n}^{\mathrm{Mg,L7}}$ and Entropic $\Delta S_{1,n}^{\mathrm{Mg,L7}}$ Contributions to Eqns (9)-(10).

| Metal | $Mg^{2+}$ | $Mg^{2+}$ | $Mg^{2+}$ | $Mg^{2+}$ |
|---|---|---|---|---|
| Solvent | $CD_3CN$/ $CDCl_3$ (1:1) | $CD_3CN$/ $CDCl_3$ (1:1) | $CD_3CN$ | $CD_3CN$ |
| *T* /*K* | 253 | 263 | 253 | 263 |
| $\log(\beta_{1,1}^{\mathrm{Mg,L7}})$ | 3.3(1) | 3.5(1) | 2.7(1) | 2.8(1) |
| $\log(\beta_{2,1}^{\mathrm{Mg,L7}})$ | 6.8(2) | 7.3(2) | 5.2(1) | 5.8(1) |
| $\log(f_{\mathrm{connect}}^{\mathrm{Mg,L7}})$ | 1.9(1) | 2.1(1) | 1.4(1) | 1.4(1) |
| $\Delta G_{\mathrm{connect}}^{\mathrm{M,L7}}$ / kJ·mol$^{-1}$ | -9.3(7) | -10.7(9) | -6.7(2) | -7.2(3) |
| $\log(u_{\mathbf{L7}}^{\mathrm{M,M}})$ | 1.6(3) | 1.7(2) | 1.1(2) | 1.6(2) |
| $\Delta E_{\mathrm{interaction}}^{\mathrm{M,M,L7}}$ / kJ·mol$^{-1}$ | -7.6(7) | -8.5(8) | -5.1(9) | -7.8(9) |
| $\Delta H_{1,1}^{\mathrm{Mg,L7}}$ / kJ·mol$^{-1}$ | 25.5(7.2) | - | 12.7(5.1) | - |
| $\Delta H_{1,2}^{\mathrm{Mg,L7}}$ / kJ·mol$^{-1}$ | 63.7(10.5) | - | 76.4(17.3) | - |
| $\Delta S_{1,1}^{\mathrm{Mg,L7}}$ / J·mol$^{-1\cdot\mathrm{K}-1}$ | 163(45) | - | 102(33) | - |
| $\Delta S_{1,2}^{\mathrm{Mg,L7}}$ / J·mol$^{-1\cdot\mathrm{K}-1}$ | 382(88) | - | 402(112) | - |

**Table S15** Summary of Crystal Data, Intensity Measurements and Structure Refinements for $Mg(\mathbf{L7})(OH_2)_3](ClO_4)_2$ (**6**), $[Zn(\mathbf{L7})(THF)(CF_3SO_3)_2]$ (**7**) and $[Zn(\mathbf{L7})_2](CF_3SO_3)_2\cdot 0.13H_2O$ (**8**).

| | **6** | **7** | **8** |
|---|---|---|---|
| Empirical formula | $C_{17}H_{18}Cl_2MgN_4O_{11}$ | $C_{23}H_{20}F_6N_4O_7S_2Zn$ | $C_{36}H_{24.25}F_6N_8O_{6.125}S_2Zn$ |
| Formula weight | 549.56 | 707.92 | 910.37 |
| Temperature /K | 180(2) | 180(2) | 180.1 |
| Wavelength /Å | 1.54184 | 1.54184 | 1.5417 |
| Crystal System, Space group | Triclinic<br>*P*-1 | Monoclinic<br>*P* $2_1$/c | Triclinic<br>*P*-1 |
| *a* /Å | 9.8604(4) | 10.06140(10) | 12.7973(4) |
| *b*/Å | 9.9680(5) | 15.2720(2) | 13.0890(3) |
| *c* /Å | 12.2159(4) | 19.2585(3) | 22.9289(7) |
| $\alpha$ /° | 74.510(3) | 90 | 76.931(2) |
| $\beta$ /° | 84.256(3) | 114.1500(10) | 86.061(2) |
| $\gamma$ /° | 73.945(4) | 90 | 84.064(2) |
| Volume / Å$^3$ | 1111.49(8) | 2700.22(6) | 3717.06(18) |
| *Z*, Calculated density / Mg·m$^{-3}$ | 2<br>1.642 | 4<br>1.741 | 4<br>1.627 |
| Absorption coefficient /mm$^{-1}$ | 3.539 | 3.573 | 2.767 |
| *F*(000) | 564 | 1432 | 1845 |
| Theta range for data collection /° | 3.76 to 73.29 | 3.83 to 73.31 | 3.48 to 73.29 |
| Limiting indices | -12<=*h*<=11<br>-11<=*k*<=12<br>-9<=*l*<=15 | -12<=*h*<=12<br>-18<=*k*<=18<br>-22<=*l*<=23 | -15<=*h*<=7<br>-16<=*k*<=15<br>-28<=*l*<=28 |
| Reflections collected / unique | 8511 / 4330 | 15579 / 5294 | 25902/14506 |
| *R*(int) | 0.0125 | 0.0266 | 0.0217 |
| Completeness to theta / °/ % | 66.97/ 99.9 | 66.97 / 99.9 | 67.00 / 99.9 |
| Data / restraints / parameters | 4330 / 1 / 330 | 5294 / 2 / 372 | 14506/ 290/ 1225 |
| Goodness-of-fit on $F^2$ | 1.042 | 1.028 | 1.027 |
| Final *R* indices [$I>2\sigma(I)$] | 0.0507<br>0.1323 | 0.0616<br>0.1604 | 0.0484<br>0.1237 |
| *R* indices (all data) | 0.0555<br>0.1368 | 0.0648<br>0.1633 | 0.0573<br>0.1313 |
| Largest diff. peak and hole / e.Å$^{-3}$ | 0.795 and -0.721 | 1.155 and -1.371 | 1.395 and -0.662 |

**Table S16** Selected Bond Distances (Å), Bond Angles (°) in [Mg(**L7**)$(OH_2)_3$]$(ClO_4)_2$ (**6**).[a]

Bond Distances (Å)

| Atom 1 | Atom 2 | Distance | Atom 1 | Atom 2 | Distance |
|---|---|---|---|---|---|
| Mg | N1 | 2.121(2) | Mg | O1W | 2.076(2) |
| Mg | N3 | 2.196(2) | Mg | O2W | 2.054(2) |
| Mg | N4 | 2.128(2) | Mg | O3W | 2.081(2) |

Angles (°)

| Atom 1 | Atom 2 | Atom 3 | Angle | Atom 1 | Atom 2 | Atom 3 | Angle |
|---|---|---|---|---|---|---|---|
| N1 | Mg | N3 | 87.41(9) | N3 | Mg | O3W | 93.32(9) |
| N1 | Mg | O1W | 91.66(9) | N4 | Mg | O1W | 92.30(9) |
| N1 | Mg | O2W | 98.63(9) | N4 | Mg | O2W | 97.44(9) |
| N1 | Mg | O3W | 88.90(9) | N4 | Mg | O3W | 88.70(9) |
| N1 | Mg | N4 | 163.68(10) | O1W | Mg | O2W | 86.14(9) |
| N3 | Mg | N4 | 76.62(10) | O1W | Mg | O3W | 174.44(10) |
| N3 | Mg | O1W | 92.23(9) | O2W | Mg | O3W | 88.31(9) |
| N3 | Mg | O2W | 173.78(10) | | | | |

[a] Numbering scheme in Fig. S20a

**Table S17** Selected Least-Squares Planes Data for [Mg(**L7**)$(OH_2)_3$]$(ClO_4)_2$ (**6**).[a]

Least-Squares Planes

| Least-squares planes description | Abbreviation | Max. deviation/Å | Atom |
|---|---|---|---|
| Azaindol | Az | | |
| N1 C1 C2 C3 C4 C5 C6 N2 C7 | | 0.1262(12) | C1 |
| Pyridine central | Py1 | | |
| N3 C8 C9 C10 C11 C12 | | 0.1101(11) | N3 |
| Pyridine | Py2 | | |
| N4 C13 C14 C15 C16 C17 | | 0.0059(12) | C13 |

[a] Numbering scheme in Fig. S20a

Interplanar angles (°) (esd < 0.1°)

| | Py1 | Py2 |
|---|---|---|
| Az | 14.80 | 20.74 |
| Py1 | | 6.14 |

**Table S18** Selected Bond Distances (Å), Bond Angles (°) in [Zn(**L7**)(THF)$(CF_3SO_3)_2$] (**7**).[a]

Bond Distances (Å)

| Atom 1 | Atom 2 | Distance | Atom 1 | Atom 2 | Distance |
|---|---|---|---|---|---|
| Zn | N1 | 2.050(3) | Zn | O(1S) | 2.134(3) |
| Zn | N3 | 2.163(3) | Zn | O(1T) | 2.167(3) |
| Zn | N4 | 2.078(3) | Zn | O(4T) | 2.206(3) |

Angles (°)

| Atom 1 | Atom 2 | Atom 3 | Angle | Atom 1 | Atom 2 | Atom 3 | Angle |
|---|---|---|---|---|---|---|---|
| N1 | Zn | N3 | 88.64(12) | N3 | Zn | O(4T) | 90.72(12) |
| N1 | Zn | O(1S) | 98.12(12) | N4 | Zn | O(1S) | 93.95(13) |
| N1 | Zn | O(1T) | 97.30(11) | N4 | Zn | O(1T) | 85.83(12) |
| N1 | Zn | O(4T) | 87.33(14) | N4 | Zn | O(4T) | 90.46(14) |
| N1 | Zn | N4 | 167.55(13) | O(1S) | Zn | O(1T) | 89.40(11) |
| N3 | Zn | N4 | 79.13(13) | O(1S) | Zn | O(4T) | 86.12(12) |
| N3 | Zn | O(1S) | 172.38(12) | O(1T) | Zn | O(4T) | 173.97(13) |
| N3 | Zn | O(1T) | 93.24(11) | | | | |

[a] Numbering scheme in Fig. S20b

**Table S19** Selected Least-Squares Planes Data for [Zn(**L7**)(THF)$(CF_3SO_3)_2$] (**7**).[a]

Least-Squares Planes

| Least-squares planes description | Abbreviation | Max. deviation/Å | Atom |
|---|---|---|---|
| Azaindol | Az | | |
| N1 C1 C2 C3 C4 C5 C6 N2 C7 | | 0.0370(11) | N2 |
| Pyridine central | Py1 | | |
| N3 C8 C9 C10 C11 C12 | | 0.0075(12) | C9 |
| Pyridine | Py2 | | |
| N4 C13 C14 C15 C16 C17 | | 0.0089(12) | C17 |

[a] Numbering scheme in Fig. S20b

Interplanar angles (°) (esd < 0.1°)

| | Py1 | Py2 |
|---|---|---|
| Az | 10.41 | 6.22 |
| Py1 | | 4.97 |

**Table S20** Selected Bond Distances (Å), Bond Angles (°) in $[Zn(\mathbf{L7})_2](CF_3SO_3)_2 \cdot 0.13H_2O$ (**8**).[a]

Bond Distances (Å)

| Atom 1 | Atom 2 | Distance | Atom 1 | Atom 2 | Distance |
|---|---|---|---|---|---|
| Zn2 | N1 | 2.144(2) | Zn2 | N5 | 2.172(2) |
| Zn2 | N3 | 2.157(2) | Zn2 | N7 | 2.202(2) |
| Zn2 | N4 | 2.153(2) | Zn2 | N8 | 2.129(2) |

Angles (°)

| Atom 1 | Atom 2 | Atom 3 | Angle | Atom 1 | Atom 2 | Atom 3 | Angle |
|---|---|---|---|---|---|---|---|
| N1 | Zn2 | N3 | 86.43(9) | N3 | Zn2 | N8 | 97.93(9) |
| N1 | Zn2 | N4 | 160.47(9) | N4 | Zn2 | N5 | 83.05(9) |
| N1 | Zn2 | N5 | 90.20(9) | N4 | Zn2 | N7 | 97.84(9) |
| N1 | Zn2 | N7 | 99.89(9) | N4 | Zn2 | N8 | 104.81(9) |
| N1 | Zn2 | N8 | 87.35(9) | N5 | Zn2 | N7 | 85.59(9) |
| N3 | Zn2 | N4 | 76.91(10) | N5 | Zn2 | N8 | 161.06(9) |
| N3 | Zn2 | N5 | 100.65(9) | N7 | Zn2 | N8 | 76.36(9) |
| N3 | Zn2 | N7 | 171.16(9) | | | | |

[a] Numbering scheme in Fig. S20c.

**Table S21** Selected Least-Squares Planes Data for $[Zn(\mathbf{L7})_2](CF_3SO_3)_2 \cdot 0.13H_2O$ (**8**).[a]

Least-Squares Planes

| Least-squares planes description | Abbreviation | Max. deviation/Å | Atom |
|---|---|---|---|
| Azaindol (A) | Az(A) | | |
| N1 C1 C2 C3 C4 C5 C6 N2 C7 | | 0.0280(11) | N1 |
| Pyridine central (A) | Py1(A) | | |
| N3 C8 C9 C10 C11 C12 | | 0.0276(12) | C8 |
| Pyridine (A) | Py2(A) | | |
| N4 C13 C14 C15 C16 C17 | | 0.0107(12) | C15 |
| Azaindol (B) | Az(A) | | |
| N8 C18 C19 C20 C21 C22 C23 N6 C24 | | 0.0264(11) | N5 |
| Pyridine central (B) | Py1(B) | | |
| N7 C25 C26 C27 C28 C29 | | 0.0162(12) | N7 |
| Pyridine (B) | Py2(B) | | |
| N8 C30 C31 C32 C33 C34 | | 0.0084(12) | C34 |

[a] Numbering scheme in Fig. S20c.

Interplanar angles (°) (esd < 0.1°)

| | Py1(A) | Py2(A) | Az(B) | Py1(B) | Py2(B) |
|---|---|---|---|---|---|
| Az(A) | 25.542 | 32.409 | 57.379 | 49.763 | 63.565 |
| Py1(A) | | 11.593 | 48.179 | 58.610 | 68.336 |
| Py2(A) | | | 37.138 | 52.648 | 60.184 |
| Az(B) | | | | 33.268 | 30.610 |
| Py1(B) | | | | | 14.680 |

**Table S22** Summary of Crystal Data, Intensity Measurements and Structure Refinements for $[Y(\mathbf{L7})_2Cl_2]I_3 \cdot CH_2Cl_2$ (**9**).

| | **9** |
|---|---|
| Empirical formula | $C_{35}H_{26}Cl_4I_3N_8Y$ |
| Formula weight | 1170.05 |
| Temperature /K | 180(2) |
| Wavelength /Å | 1.54184 |
| Crystal System, Space group | Triclinic |
| | *P*-1 |
| *a* /Å | 9.9524(4) |
| *b*/Å | 13.0566(5) |
| *c* /Å | 14.5815(6) |
| $\alpha$ /° | 91.029(3) |
| $\beta$ /° | 90.220(3) |
| $\gamma$ /° | 92.195(3) |
| Volume / Å$^3$ | 1893.07(14) |
| *Z*, Calculated density / Mg·m$^{-3}$ | 2 |
| | 2.053 |
| Absorption coefficient /mm$^{-1}$ | 24.289 |
| *F*(000) | 1116 |
| Theta range for data collection /° | 3.03 to 73.40 |
| Limiting indices | -12<=*h*<=11 |
| | -16<=*k*<=14 |
| | -18<=*l*<=15 |
| Reflections collected / unique | 12639 / 7379 |
| *R*(int) | [*R*(int) = 0.0264] |
| Completeness to theta / °/ % | 66.97 / 100 |
| Data / restraints / parameters | 7379 / 0 / 463 |
| Goodness-of-fit on $F^2$ | 1.119 |
| Final *R* indices [$I>2\sigma(I)$] | 0.0573 |
| | 0.1658 |
| *R* indices (all data) | 0.0607 |
| | 0.1689 |
| Largest diff. peak and hole / e.Å$^{-3}$ | 2.667 and -2.018 |

**Table S23** Selected Bond Distances (Å), Bond Angles (°) in $[Y(\mathbf{L7})_2Cl_2]I_3 \cdot CH_2Cl_2$ (**9**).[a]

Bond Distances (Å)

| Atom 1 | Atom 2 | Distance | Atom 1 | Atom 2 | Distance |
|---|---|---|---|---|---|
| Y | N1 | 2.535(5) | Y | N7 | 2.604(5) |
| Y | N3 | 2.613(5) | Y | N8 | 2.464(6) |
| Y | N4 | 2.462(6) | Y | Cl3 | 2.6520(16) |
| Y | N5 | 2.532(6) | Y | Cl4 | 2.6569(16) |

Angles (°)

| Atom 1 | Atom 2 | Atom 3 | Angle | Atom 1 | Atom 2 | Atom 3 | Angle |
|---|---|---|---|---|---|---|---|
| N1 | Y | N3 | 69.96(17) | N4 | Y | N7 | 143.99(19) |
| N1 | Y | N4 | 118.73(19) | N4 | Y | N8 | 147.35(19) |
| N1 | Y | N5 | 124.36(17) | N4 | Y | Cl3 | 82.63(14) |
| N1 | Y | N7 | 71.50(17) | N4 | Y | Cl4 | 74.90(14) |
| N1 | Y | N8 | 77.30(18) | N5 | Y | N7 | 69.47(18) |
| N1 | Y | Cl3 | 150.62(13) | N5 | Y | N8 | 118.40(19) |
| N1 | Y | Cl4 | 77.80(13) | N5 | Y | Cl3 | 77.48(13) |
| N3 | Y | N4 | 65.46(18) | N5 | Y | Cl4 | 151.18(13) |
| N3 | Y | N5 | 71.90(17) | N7 | Y | N8 | 65.86(19) |
| N3 | Y | N7 | 89.87(17) | N7 | Y | Cl3 | 103.83(12) |
| N3 | Y | N8 | 144.23(18) | N7 | Y | Cl4 | 139.27(13) |
| N3 | Y | Cl3 | 139.38(13) | N8 | Y | Cl3 | 74.55(14) |
| N3 | Y | Cl4 | 104.22(12) | N8 | Y | Cl4 | 81.97(15) |
| N4 | Y | N5 | 77.77(18) | Cl3 | Y | Cl4 | 90.04(5) |

[a] Numbering scheme in Fig. S26.

**Table S24** Selected Least-Squares Planes Data for in $[Y(\mathbf{L7})_2Cl_2]I_3 \cdot CH_2Cl_2$ (**9**).[a]

Least-Squares Planes

| Least-squares planes description | Abbreviation | Max. deviation/Å | Atom |
|---|---|---|---|
| Azaindol (A) | Az(A) | | |
| N1 C1 C2 C3 C4 C5 C6 N2 C7 | | 0.0588(11) | N1 |
| Pyridine central (A) | Py1(A) | | |
| N3 C8 C9 C10 C11 C12 | | 0.0330(12) | C12 |
| Pyridine (A) | Py2(A) | | |
| N4 C13 C14 C15 C16 C17 | | 0.0105(12) | C13 |
| Azaindol (B) | Az(A) | | |
| N8 C18 C19 C20 C21 C22 C23 N6 C24 | | 0.0680(11) | N5 |
| Pyridine central (B) | Py1(B) | | |
| N7 C25 C26 C27 C28 C29 | | 0.0371 | C29 |
| Pyridine (B) | Py2(B) | | |
| N8 C30 C31 C32 C33 C34 | | 0.0092 | C33 |

[a] Numbering scheme in Fig. S26.

Interplanar angles (°) (esd < 0.1°)

| | Py1(A) | Py2(A) | Az(B) | Py1(B) | Py2(B) |
|---|---|---|---|---|---|
| Az(A) | 23.32 | 27.33 | 5.85 | 20.99 | 32.76 |
| Py1(A) | | 12.06 | 19.91 | 31.63 | 32.39 |
| Py2(A) | | | 26.43 | 26.16 | 21.96 |
| Az(B) | | | | 27.80 | 35.92 |
| Py1(B) | | | | | 15.25 |

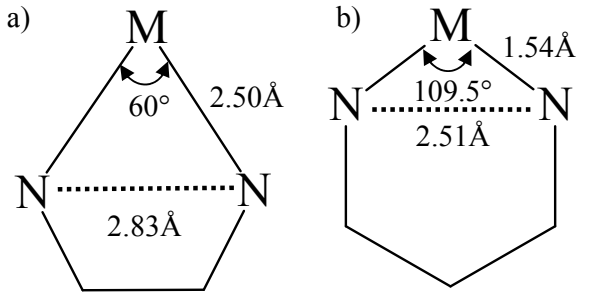


**Figure S1** The lowest strain energy geometry calculated using molecular mechanics for a) a five-membered aliphatic chelate ring and b) a six-membered aliphatic chelate ring. Adapted from reference 1b.

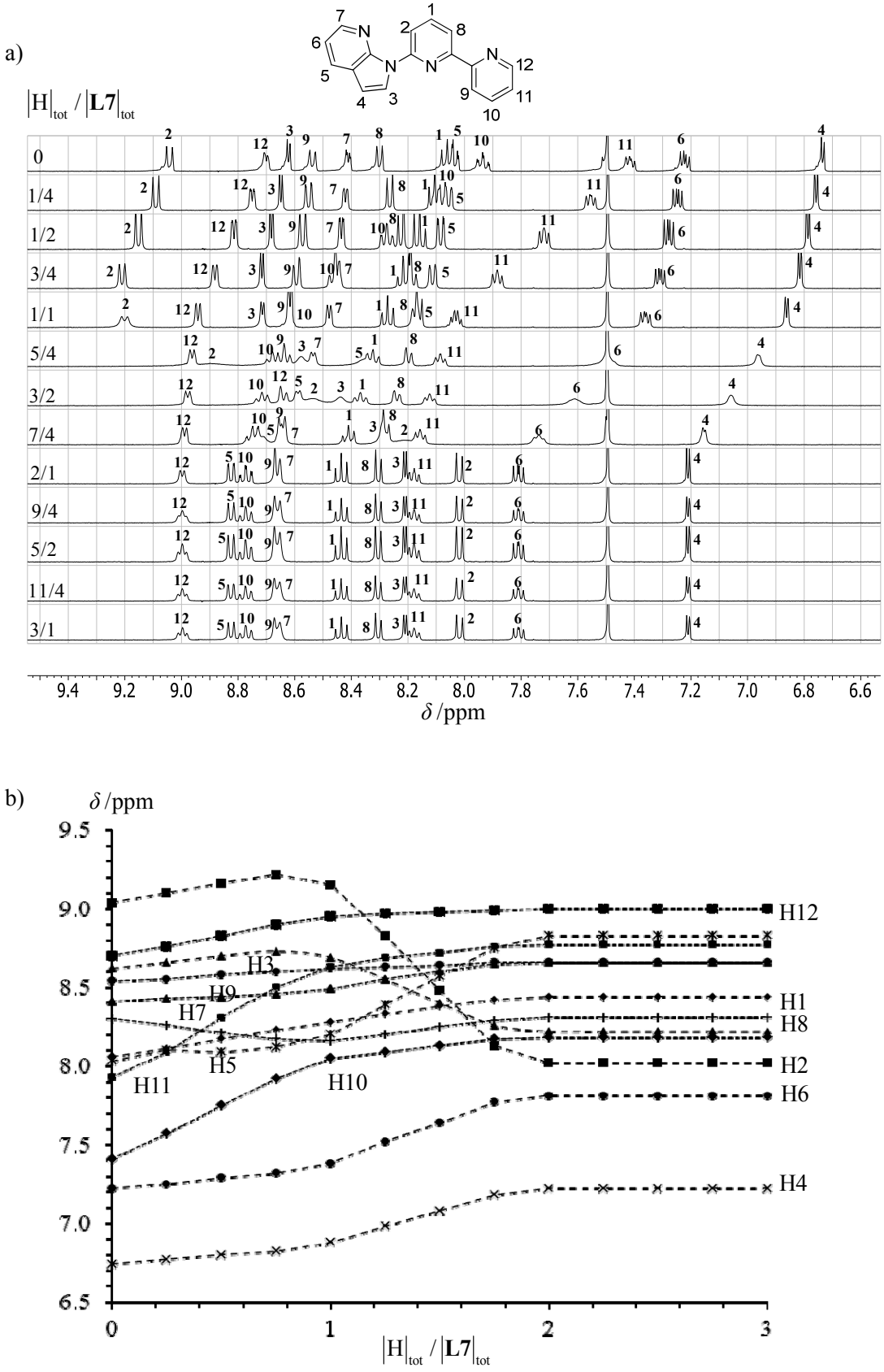


**Figure S2** Variation of a) $^1$H NMR spectra and b) $^1$H NMR chemical shifts for the titration of **L7** with $CF_3SO_3H$ in $CD_3CN/CDCl_3$ (1:1) at 298 K ($|\mathbf{L7}|_{tot} = 7.5 \cdot 10^{-3}$ M).

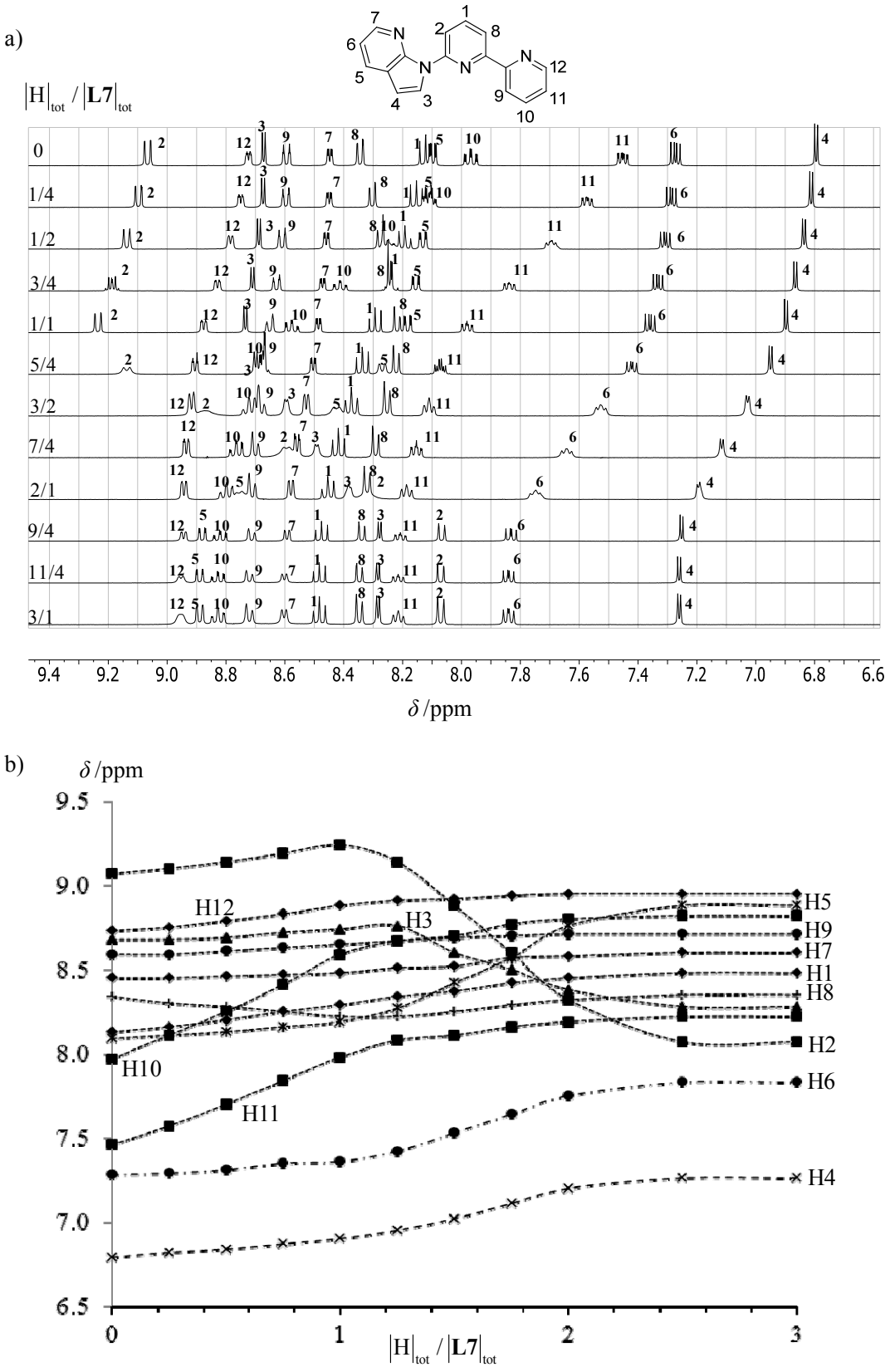


**Figure S3** Variation of a) $^1$H NMR spectra and b) $^1$H NMR chemical shifts for the titration of **L7** with $CF_3SO_3H$ in $CD_3CN$ at 298 K ($|\mathbf{L7}|_{tot} = 7.5 \cdot 10^{-3}$ M).

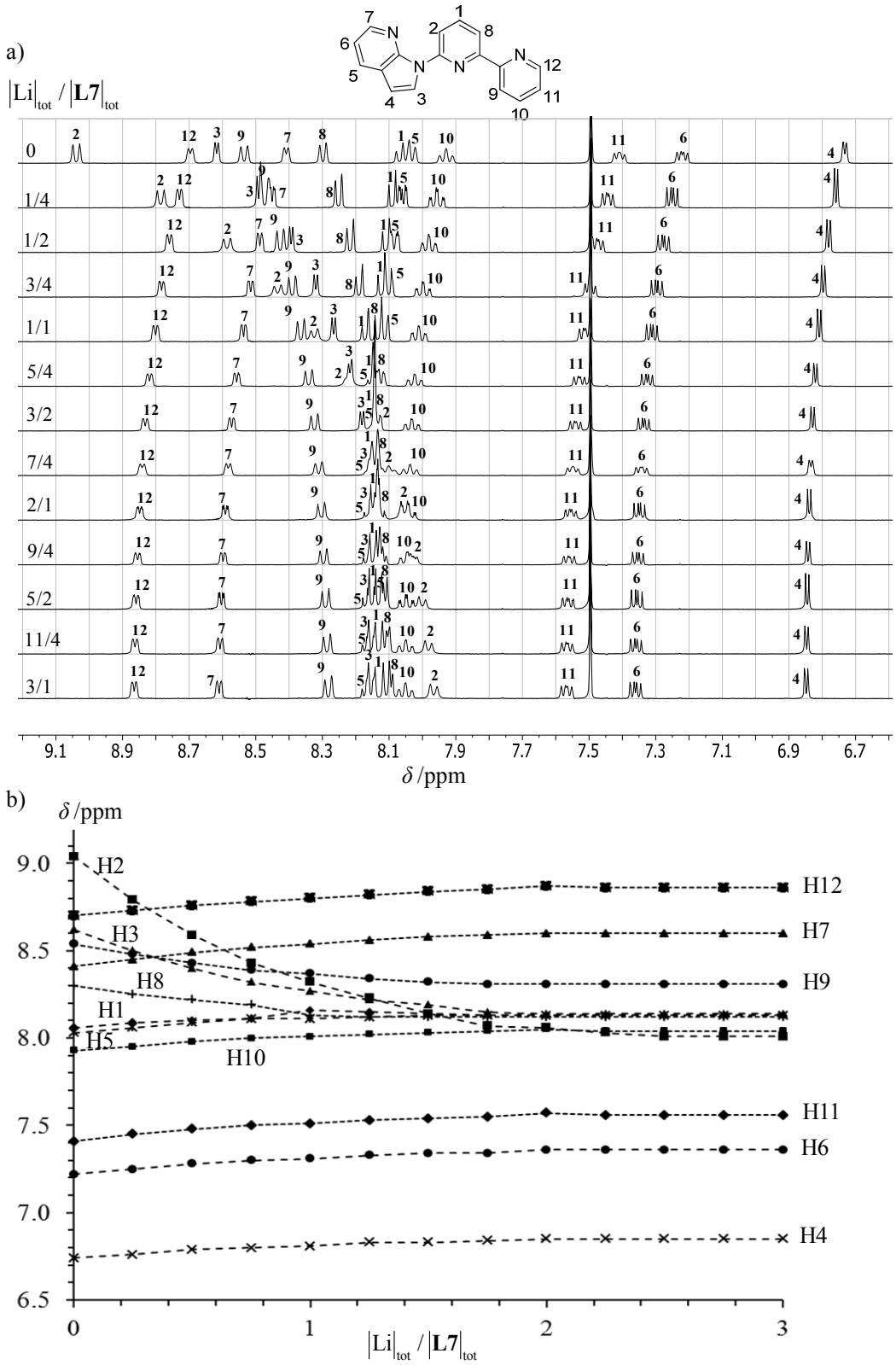


**Figure S4** Variation of a) $^1$H NMR spectra and b) $^1$H NMR chemical shifts for the titration of **L7** with $LiClO_4$ in $CD_3CN/CDCl_3$ (1:1) at 298 K ($|\mathbf{L7}|_{tot} = 7.5 \cdot 10^{-3}$ M).

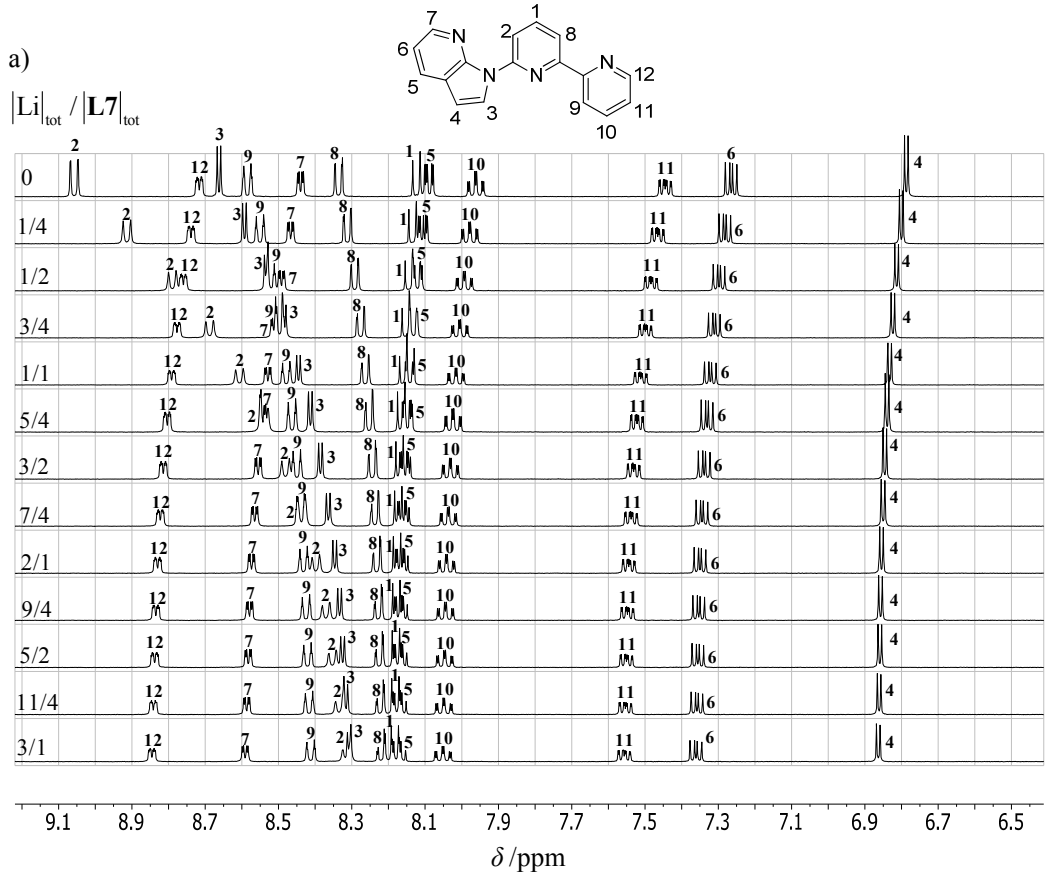


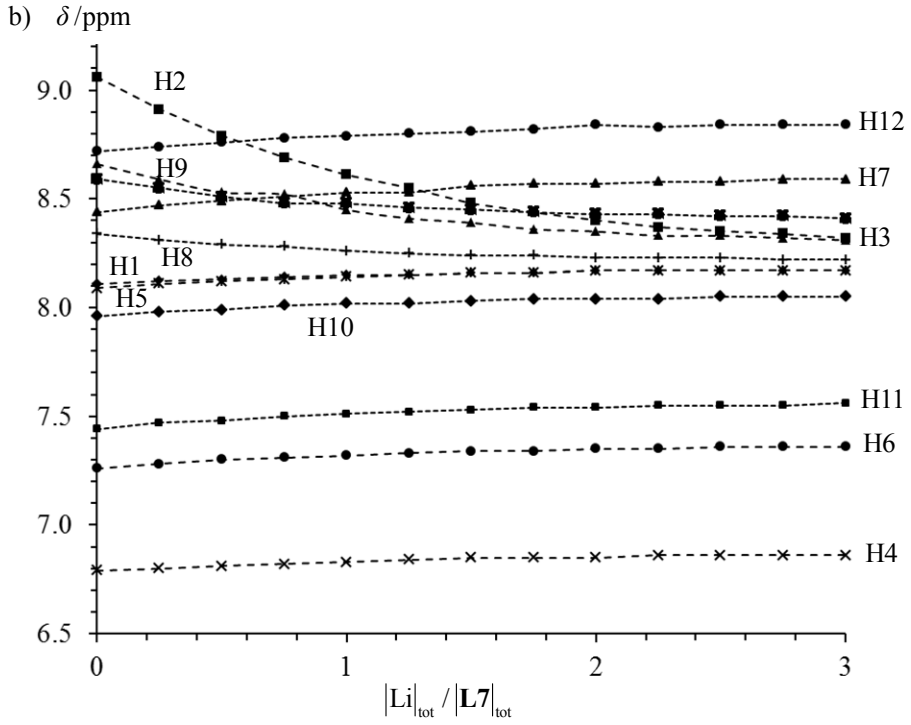


**Figure S5** Variation of a) $^1$H NMR spectra and b) $^1$H NMR chemical shifts for the titration of **L7** with $LiClO_4$ in $CD_3CN$ at 298 K ($|\mathbf{L7}|_{tot} = 7.5 \cdot 10^{-3}$ M).

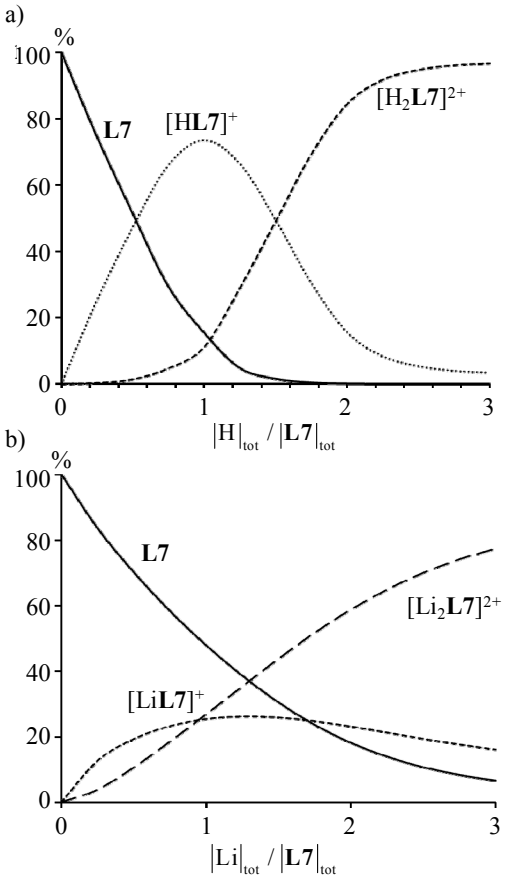


**Figure S6** Computed ligand speciation for the titrations of **L7** with (a) $CF_3SO_3H$ and (b) $LiClO_4$ in $CD_3CN$. Total ligand concentration $|\mathbf{L7}|_{tot} = 7.5 \cdot 10^{-3}$ M.

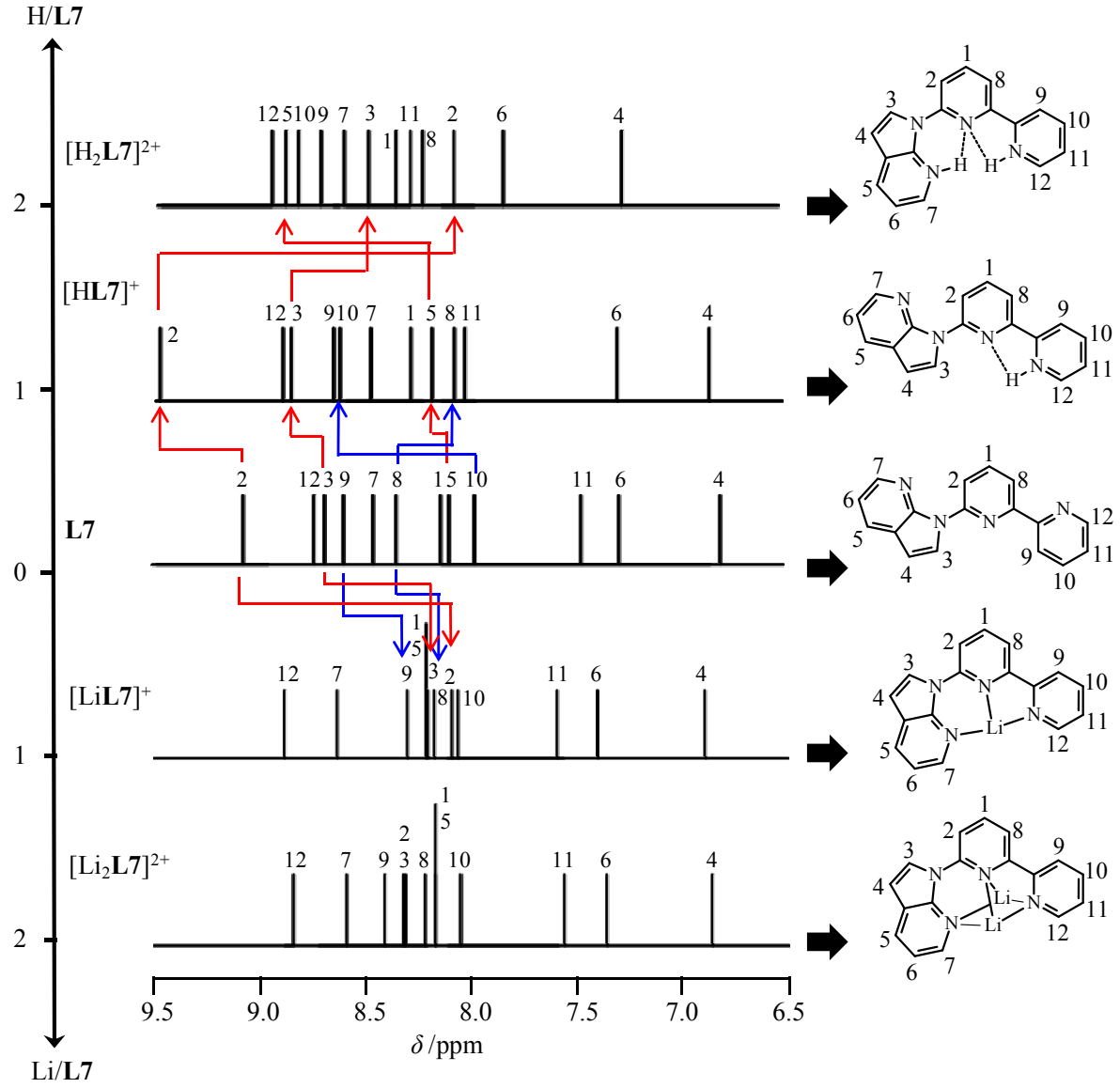


**Figure S7** Computed individual $^{1}$H NMR spectra for **L7** (middle), [H**L7**]$^{+}$ and [$H_2$**L7**]$^{2+}$ (top), and [Li**L7**]$^{+}$ and [$Li_2$**L7**]$^{2+}$ (down) in $CD_3CN$ with associated solution structures. Red arrows highlight chemical shifts variations diagnostic for establishing the conformation of the azaindol-pyridine unit, whereas blue arrows hold for the bipyridine unit (see text).

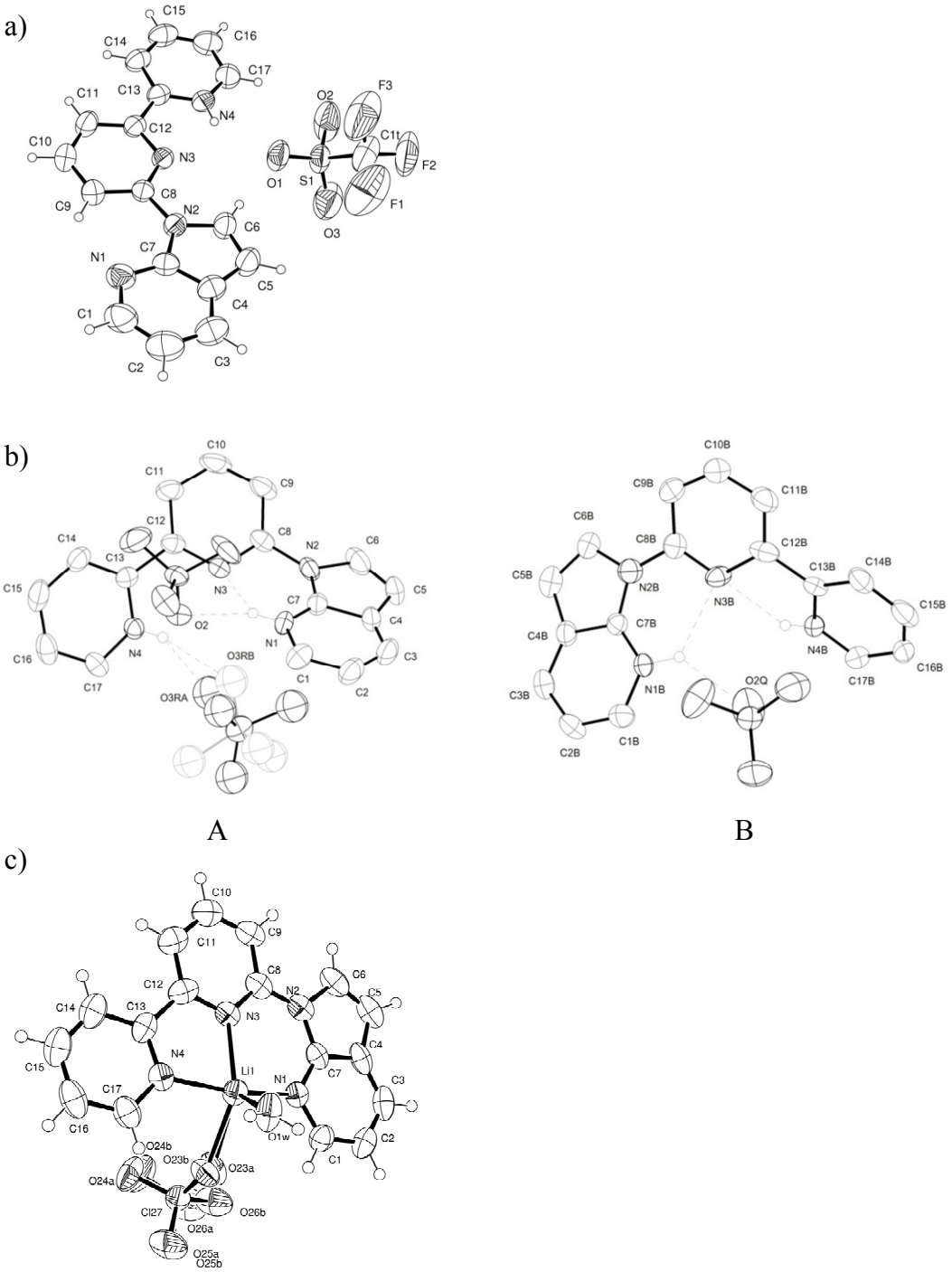


**Figure S8** ORTEP views of (a) [H**L7**]$^{+}$, (b) [$H_2$**L7**]$^{2+}$ (two independent A and B molecules per unit cell) and (c) [Li(**L7**)($OH_2$)($ClO_4$)] observed in the crystal structures of [H**L7**]($CF_3SO_3$) (**1**), [$H_2$**L7**]($ClO_4$)$_2$ (**2**) and [Li(**L7**)($ClO_4$)($H_2O$)] (**3**) with atomic numbering schemes. Thermal ellispoids are represented at the 50% probability level.

Microspecies

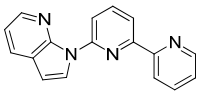
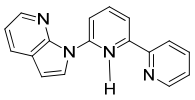

$$H^+ + \mathbf{L7} \underset{\beta^{H,\mathbf{L7}}_{1,1(Npycentral)}}{\rightleftharpoons} [H\mathbf{L7}]^+$$

| Point groups: | $R_3$ | $C_s$ | $C_s$ |
|---|---|---|---|
| $\sigma^{ext}$: | 1 | 1 | 1 |
| $\sigma^{int}$: | 1 | 1 | 1 |
| $\sigma^{chiral}$: | 1 | 1 | 1 |

$$\omega^{H,\mathbf{L7}}_{1,1(Npycentral)} = \frac{\left(\sigma^{ext}_H \sigma^{int}_H \sigma^{chiral}_H\right)\cdot\left(\sigma^{ext}_{\mathbf{L7}} \sigma^{int}_{\mathbf{L7}} \sigma^{chiral}_{\mathbf{L7}}\right)}{\left(\sigma^{ext}_{H\mathbf{L7}} \sigma^{int}_{H\mathbf{L7}} \sigma^{chiral}_{H\mathbf{L7}}\right)} = 1$$

$$\Rightarrow \beta^{H,\mathbf{L7}}_{1,1(Npycentral)} = f^{H,\mathbf{L7}}_{(Npycentral)}$$

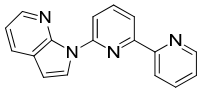
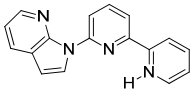

$$H^+ + \mathbf{L7} \underset{\beta^{H,\mathbf{L7}}_{1,1(Npydistal)}}{\rightleftharpoons} [H\mathbf{L7}]^+$$

| Point groups: | $R_3$ | $C_S$ | $C_S$ |
|---|---|---|---|
| $\sigma^{ext}$: | 1 | 1 | 1 |
| $\sigma^{int}$: | 1 | 1 | 1 |
| $\sigma^{chiral}$: | 1 | 1 | 1 |

$$\omega^{H,\mathbf{L7}}_{1,1(Npydistal)} = \frac{\left(\sigma^{ext}_H \sigma^{int}_H \sigma^{chiral}_H\right)\cdot\left(\sigma^{ext}_{\mathbf{L7}} \sigma^{int}_{\mathbf{L7}} \sigma^{chiral}_{\mathbf{L7}}\right)}{\left(\sigma^{ext}_{H\mathbf{L7}} \sigma^{int}_{H\mathbf{L7}} \sigma^{chiral}_{H\mathbf{L7}}\right)} = 1$$

$$\Rightarrow \beta^{H,\mathbf{L7}}_{1,1(Npydistal)} = f^{H,\mathbf{L7}}_{(Npydistal)}$$

Macrospecies

$$\beta^{H,\mathbf{L7}}_{1,1} = \beta^{H,\mathbf{L7}}_{1,1(Npydistal)} + \beta^{H,\mathbf{L7}}_{1,1(Npycentral)} = f^{H,\mathbf{L7}}_{(Npydistal)} + f^{H,\mathbf{L7}}_{(Npycentral)} = 2 f^{H,\mathbf{L7}}_{connect} \qquad (5)$$

**Figure S9** Application of the site binding model[21] showing the determination of symmetry numbers ($\sigma^{ext}$, $\sigma^{int}$, $\sigma^{chiral}$)[22] for the two microspecies contributing to equilibrium (1) with M = H. The symmetry point groups are those expected for coplanar arrangements of the heterocyclic rings.

## Microspecies

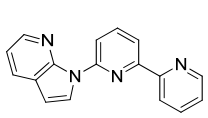
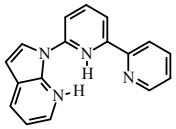

$$2H^+ \quad + \quad \mathbf{L7} \quad \rightleftharpoons \quad [H_2\mathbf{L7}]^{2+} \qquad \beta^{H,\mathbf{L7}}_{2,1(\text{Naza-Npycentral})}$$

| Point groups: | $R_3$ | $C_s$ | $C_s$ |
|---|---|---|---|
| $\sigma^{ext}$: | 1 | 1 | 1 |
| $\sigma^{int}$: | 1 | 1 | 1 |
| $\sigma^{chiral}$: | 1 | 1 | 1 |

$$\omega^{H,\mathbf{L7}}_{2,1(\text{Naza-Npycentral})} = \frac{\left(\sigma^{ext}_{H}\sigma^{int}_{H}\sigma^{chiral}_{H}\right)^2 \cdot \left(\sigma^{ext}_{\mathbf{L7}}\sigma^{int}_{\mathbf{L7}}\sigma^{chiral}_{\mathbf{L7}}\right)}{\left(\sigma^{ext}_{H2\mathbf{L7}}\sigma^{int}_{H2\mathbf{L7}}\sigma^{chiral}_{H2\mathbf{L7}}\right)} = 1$$

$$\Rightarrow \beta^{H,\mathbf{L7}}_{2,1(\text{Naza-Npycentral})} = f^{H,\mathbf{L7}}_{(\text{Naza})} f^{H,\mathbf{L7}}_{(\text{Npycentral})} u^{H,H}_{\mathbf{L7}(\text{Naza-Npycentral})}$$

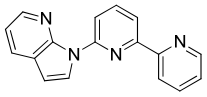
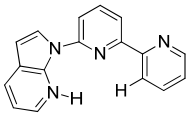

$$2H^+ \quad + \quad \mathbf{L7} \quad \rightleftharpoons \quad [H_2\mathbf{L7}]^{+} \qquad \beta^{H,\mathbf{L7}}_{2,1(\text{Naza-Npydistal})}$$

| Point groups: | $R_3$ | $C_S$ | $C_S$ |
|---|---|---|---|
| $\sigma^{ext}$: | 1 | 1 | 1 |
| $\sigma^{int}$: | 1 | 1 | 1 |
| $\sigma^{chiral}$: | 1 | 1 | 1 |

$$\omega^{H,\mathbf{L7}}_{2,1(\text{Naza-Npydistal})} = \frac{\left(\sigma^{ext}_{H}\sigma^{int}_{H}\sigma^{chiral}_{H}\right)^2 \cdot \left(\sigma^{ext}_{\mathbf{L7}}\sigma^{int}_{\mathbf{L7}}\sigma^{chiral}_{\mathbf{L7}}\right)}{\left(\sigma^{ext}_{H2\mathbf{L7}}\sigma^{int}_{H2\mathbf{L7}}\sigma^{chiral}_{H2\mathbf{L7}}\right)} = 1$$

$$\Rightarrow \beta^{H,\mathbf{L7}}_{2,1(\text{Naza-Npydistal})} = f^{H,\mathbf{L7}}_{(\text{Naza})} f^{H,\mathbf{L7}}_{(\text{Npydistal})} u^{H,H}_{\mathbf{L7}(\text{Naza-Npydistal})}$$

## Macrospecies

$$\beta^{H,\mathbf{L7}}_{2,1} = \beta^{H,\mathbf{L7}}_{2,1(\text{Naza-Npydistal})} + \beta^{H,\mathbf{L7}}_{2,1(\text{Naza-Npycentral})} = 2\left(f^{H,\mathbf{L7}}_{\text{connect}}\right)^2 u^{H,H}_{\mathbf{L7}} \qquad (6)$$

**Figure S10** Application of the site binding model[21] showing the determination of symmetry numbers ($\sigma^{ext}$, $\sigma^{int}$, $\sigma^{chiral}$)[22] for the two microspecies contributing to equilibrium (2) with M = H. The symmetry point groups are those expected for coplanar arrangements of the heterocyclic rings.

Microspecies = Macrospecies

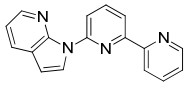

$$[Li(CH_3CN)_4]^+ \quad + \quad \mathbf{L7} \quad \rightleftharpoons^{\beta_{1,1}^{Li,\mathbf{L7}}} \quad [Li\mathbf{L7}(CH_3CN)_2]^+ \quad + \quad 2CH_3CN$$

| Point groups: | *Td* | $C_s$ | | $C_s$ | $C_{3v}$ |
|---|---|---|---|---|---|
| $\sigma^{ext}$: | 12 | 1 | | 1 | 3 |
| $\sigma^{int}$: | $3^4$ | 1 | | $3^2$ | 1 |
| $\sigma^{chiral}$: | 1 | 1 | | 1 | 1 |

$$\omega_{1,1}^{Li,\mathbf{L7}} = \frac{\left(\sigma_{Li}^{ext}\sigma_{Li}^{int}\sigma_{Li}^{chiral}\right)\cdot\left(\sigma_{\mathbf{L7}}^{ext}\sigma_{\mathbf{L7}}^{int}\sigma_{\mathbf{L7}}^{chiral}\right)}{\left(\sigma_{Li\mathbf{L7}}^{ext}\sigma_{Li\mathbf{L7}}^{int}\sigma_{Li\mathbf{L7}}^{chiral}\right)\cdot\left(\sigma_{CH_3CN}^{ext}\sigma_{CH_3CN}^{int}\sigma_{CH_3CN}^{chiral}\right)^2} = \frac{\left(12\cdot 3^4\right)}{3^2\cdot 3^2} = 12$$

$$\Rightarrow \beta_{1,1}^{Li,\mathbf{L7}} = 12 f_{connect}^{Li,\mathbf{L7}} \qquad (7)$$

Microspecies = Macrospecies

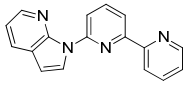

$$2Li^+(CH_3CN)_4 \quad + \quad \mathbf{L7} \quad \rightleftharpoons^{\beta_{2,1}^{Li,\mathbf{L7}}} \quad [Li_2\mathbf{L7}(CH_3CN)_4]^{2+} + 4CH_3CN$$

| Point groups: | *Td* | $C_s$ | | $C_s$ | $C_{3v}$ |
|---|---|---|---|---|---|
| $\sigma^{ext}$: | 12 | 1 | | 1 | 3 |
| $\sigma^{int}$: | $3^4$ | 1 | | $3^4$ | 1 |
| $\sigma^{chiral}$: | 1 | 1 | | 1 | 1 |

$$\omega_{2,1}^{Li,\mathbf{L7}} = \frac{\left(\sigma_{Li}^{ext}\sigma_{Li}^{int}\sigma_{Li}^{chiral}\right)^2\cdot\left(\sigma_{\mathbf{L7}}^{ext}\sigma_{\mathbf{L7}}^{int}\sigma_{\mathbf{L7}}^{chiral}\right)}{\left(\sigma_{Li2\mathbf{L7}}^{ext}\sigma_{Li2\mathbf{L7}}^{int}\sigma_{Li2\mathbf{L7}}^{chiral}\right)\cdot\left(\sigma_{CH_3CN}^{ext}\sigma_{CH_3CN}^{int}\sigma_{CH_3CN}^{chiral}\right)^4} = \frac{\left(12\cdot 3^4\right)^2}{3^4\cdot 3^4} = 144$$

$$\Rightarrow \beta_{2,1}^{Li,\mathbf{L7}} = 144\left(f_{connect}^{Li,\mathbf{L7}}\right)^2 u_{\mathbf{L7}}^{Li,Li} \qquad (8)$$

**Figure S11** Application of the site binding model[21] showing the determination of symmetry numbers ($\sigma^{ext}$, $\sigma^{int}$, $\sigma^{chiral}$)[22] for the microspecies contributing to equilibria (1)-(2) with M = Li. The symmetry point groups are those expected for coplanar arrangements of the heterocyclic rings.

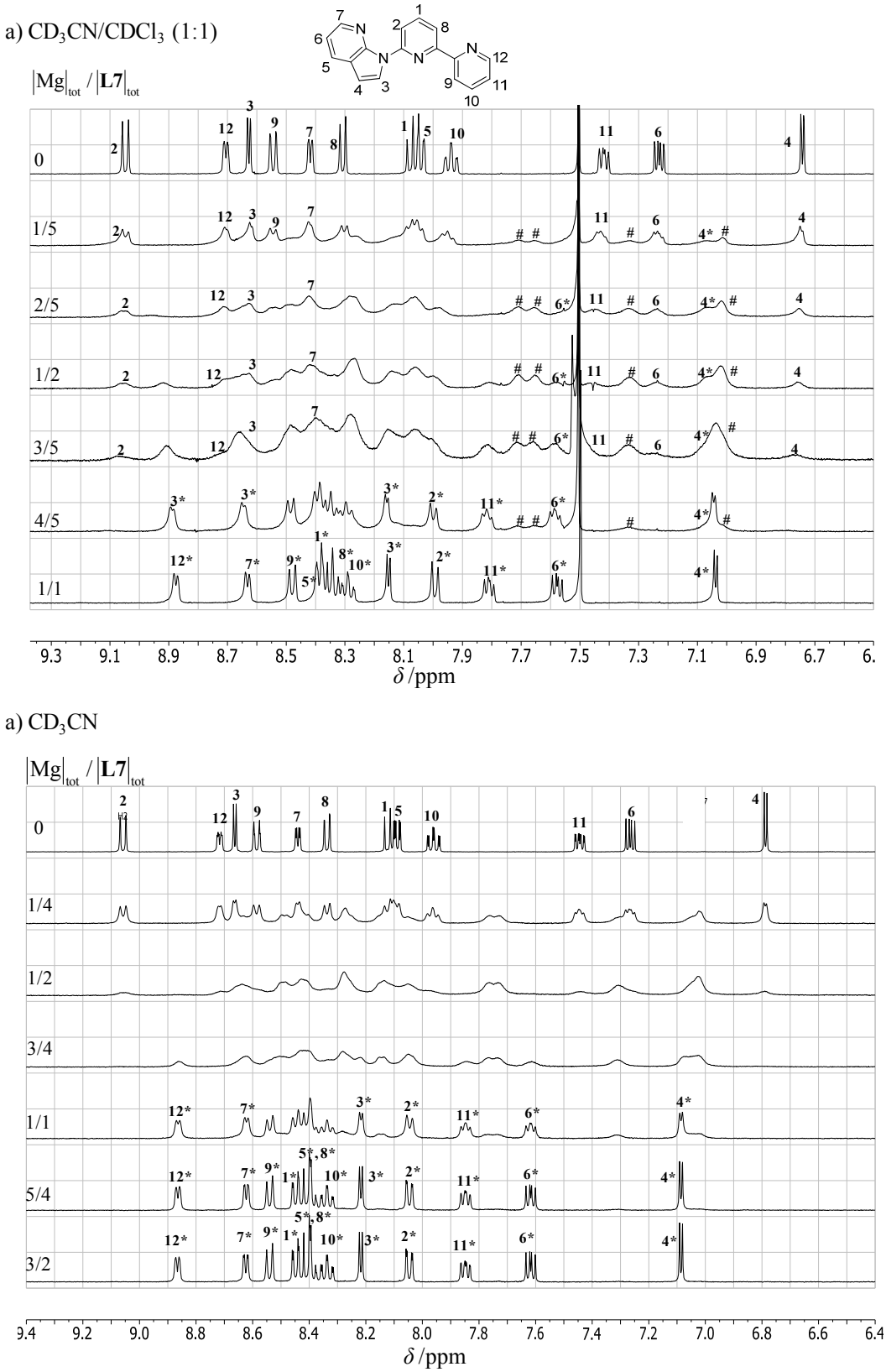


**Figure S12** Variation of $^1$H NMR spectra for the titration of **L7** with $Mg(ClO_4)_2$ in (a) $CD_3CN/CDCl_3$ (1:1) and (b) $CD_3CN$ at 298 K ($|\mathbf{L7}|_{tot}$ = $7.5\cdot10^{-3}$ M). Code: # = $[Mg(\mathbf{L7})_2]^{2+}$, * = $[Mg(\mathbf{L7})]^{2+}$.

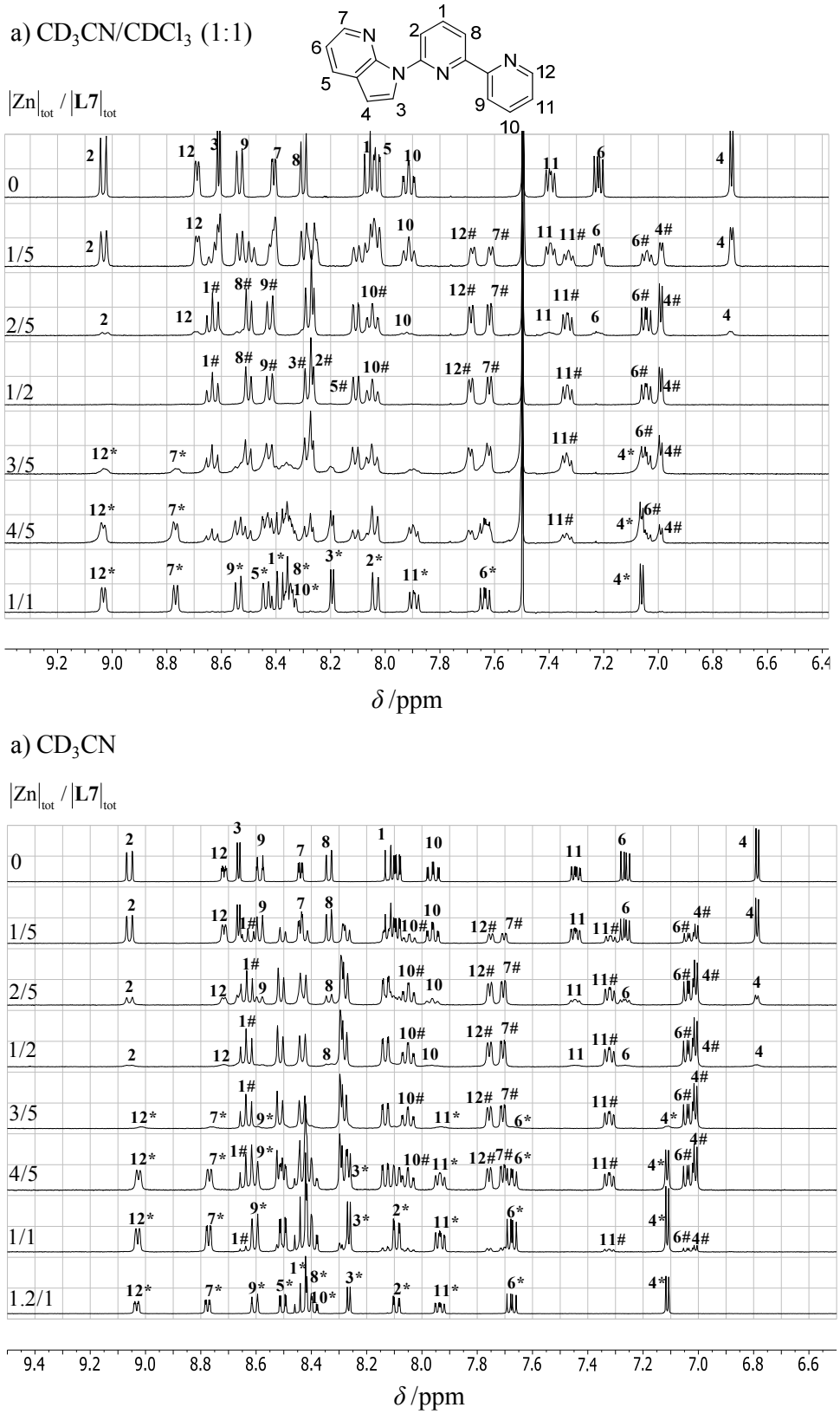


**Figure S13** Variation of $^1$H NMR spectra for the titration of **L7** with $Zn(CF_3SO_3)_2$ in (a) $CD_3CN/CDCl_3$ (1:1) and (b) $CD_3CN$ at 298 K ($|\mathbf{L7}|_{tot}$ = $7.5\cdot10^{-3}$ M). Code: # = $[Zn(\mathbf{L7})_2]^{2+}$, * = $[Zn(\mathbf{L7})]^{2+}$.

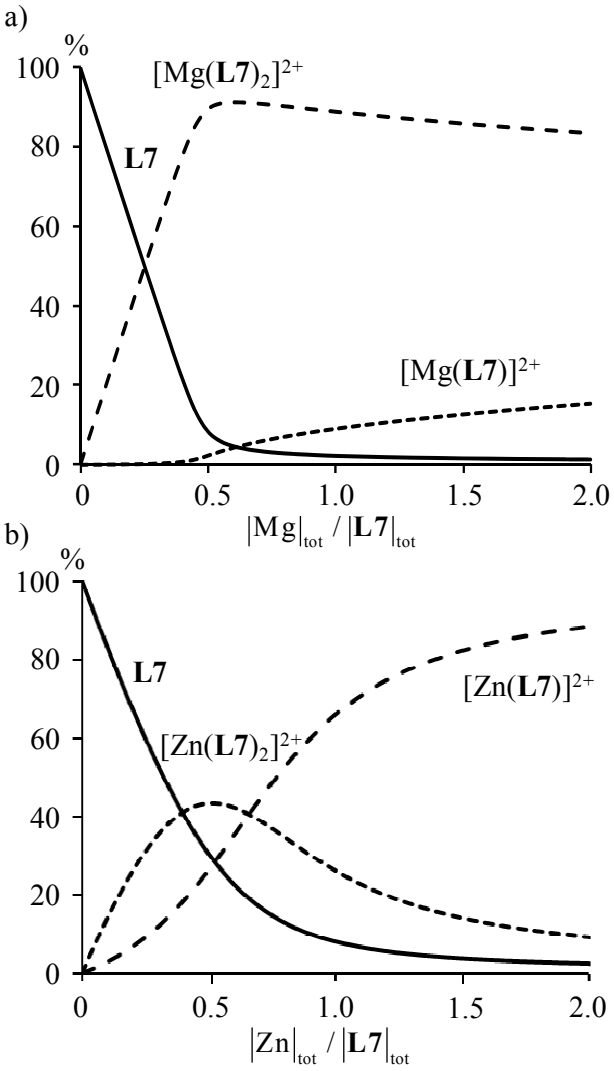


**Figure S14** Computed ligand speciation for the titrations of **L7** with (a) $Mg(ClO_4)_2$ and (b) $Zn(CF_3SO_3)_2$ in $CD_3CN$ at 298K. Total ligand concentration $|\mathbf{L7}|_{tot} = 7.5 \cdot 10^{-3}$ M.

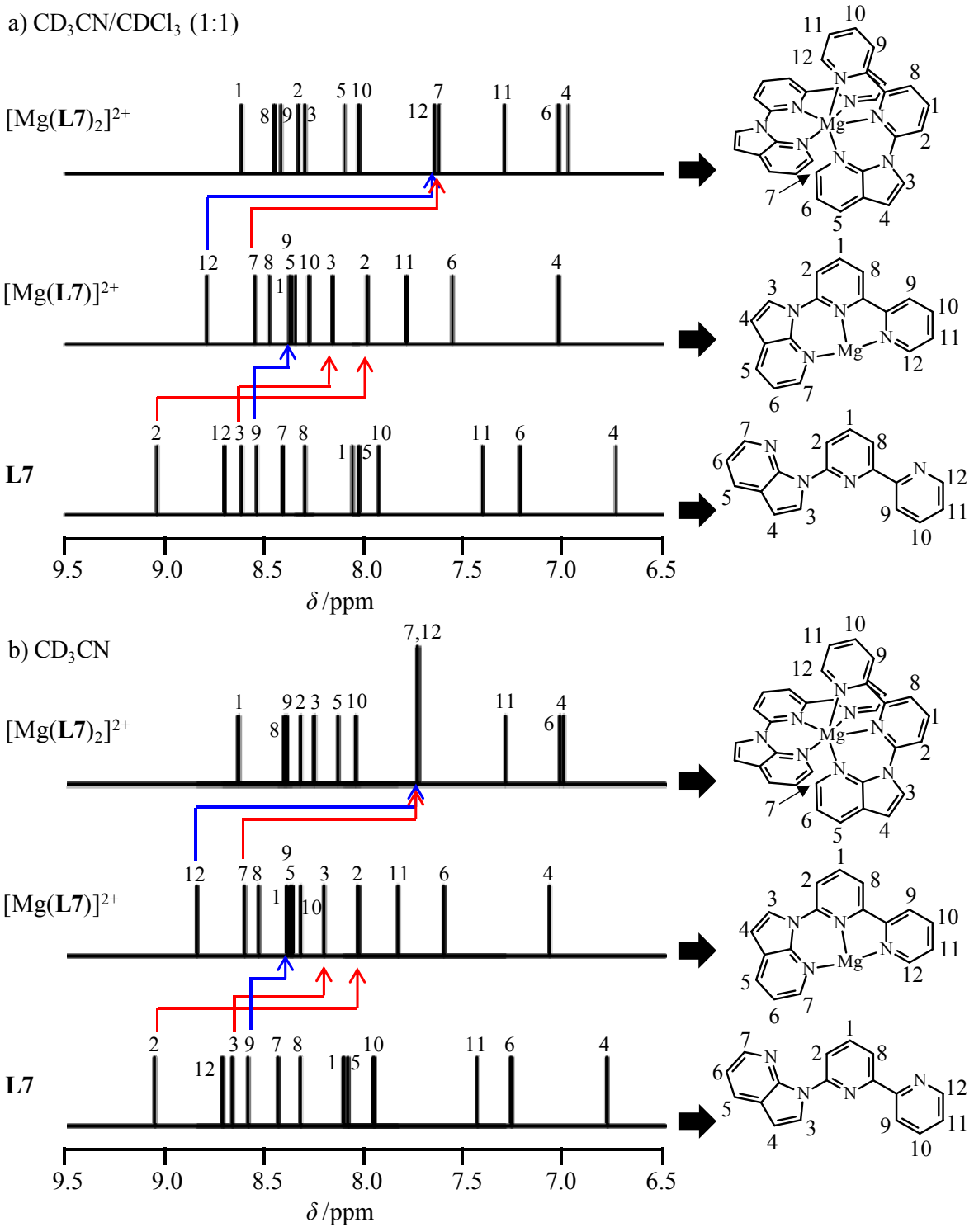


**Figure S15** Computed individual $^{1}$H NMR spectra for **L7**, [Mg(**L7**)]$^{2+}$ and [Mg(**L7**)$_2$]$^{2+}$ in (a) $CD_3CN/CDCl_3$ (1:1) and (b) $CD_3CN$ with associated solution structures. Red arrows highlight chemical shifts variations diagnostic for establishing the conformation of the azaindol-pyridine unit, whereas blue arrows hold for the bipyridine unit (see text).

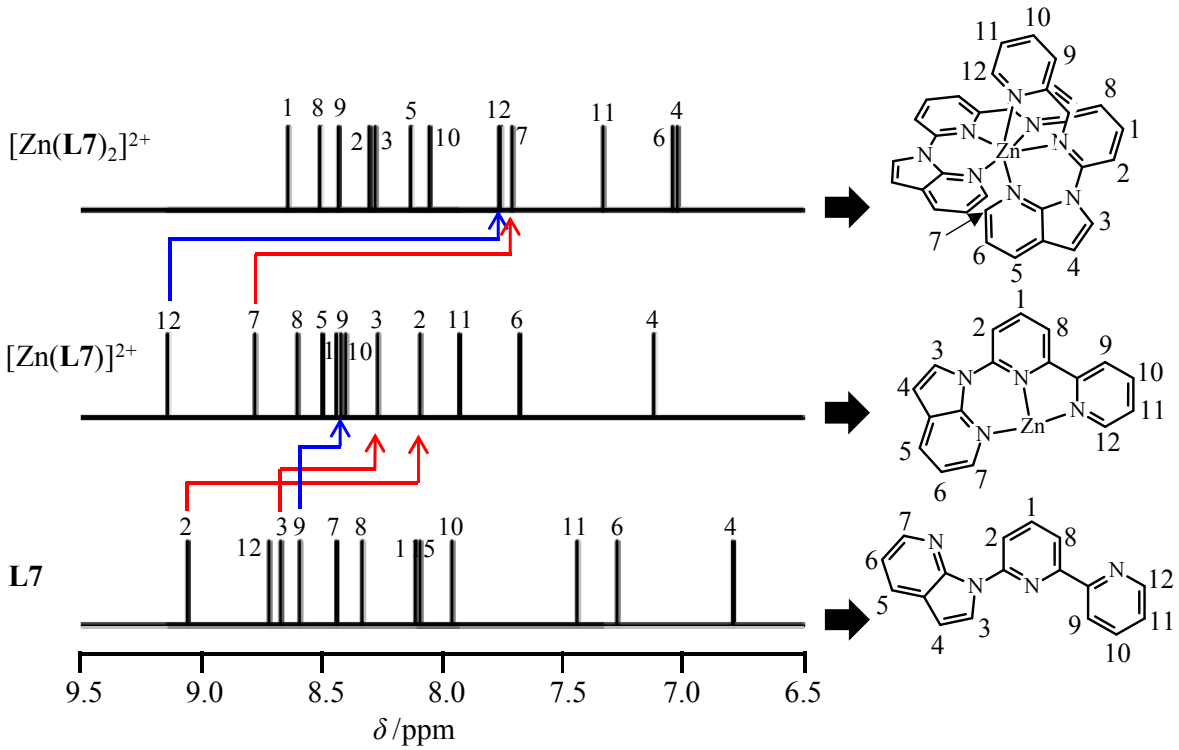


**Figure S16** Computed individual $^{1}$H NMR spectra for **L7**, [Zn(**L7**)]$^{2+}$ and [Zn(**L7**)$_2$]$^{2+}$ in $CD_3CN$ with associated solution structures. Red arrows highlight chemical shifts variations diagnostic for establishing the conformation of the azaindol-pyridine unit, whereas blue arrows hold for the bipyridine unit (see text).

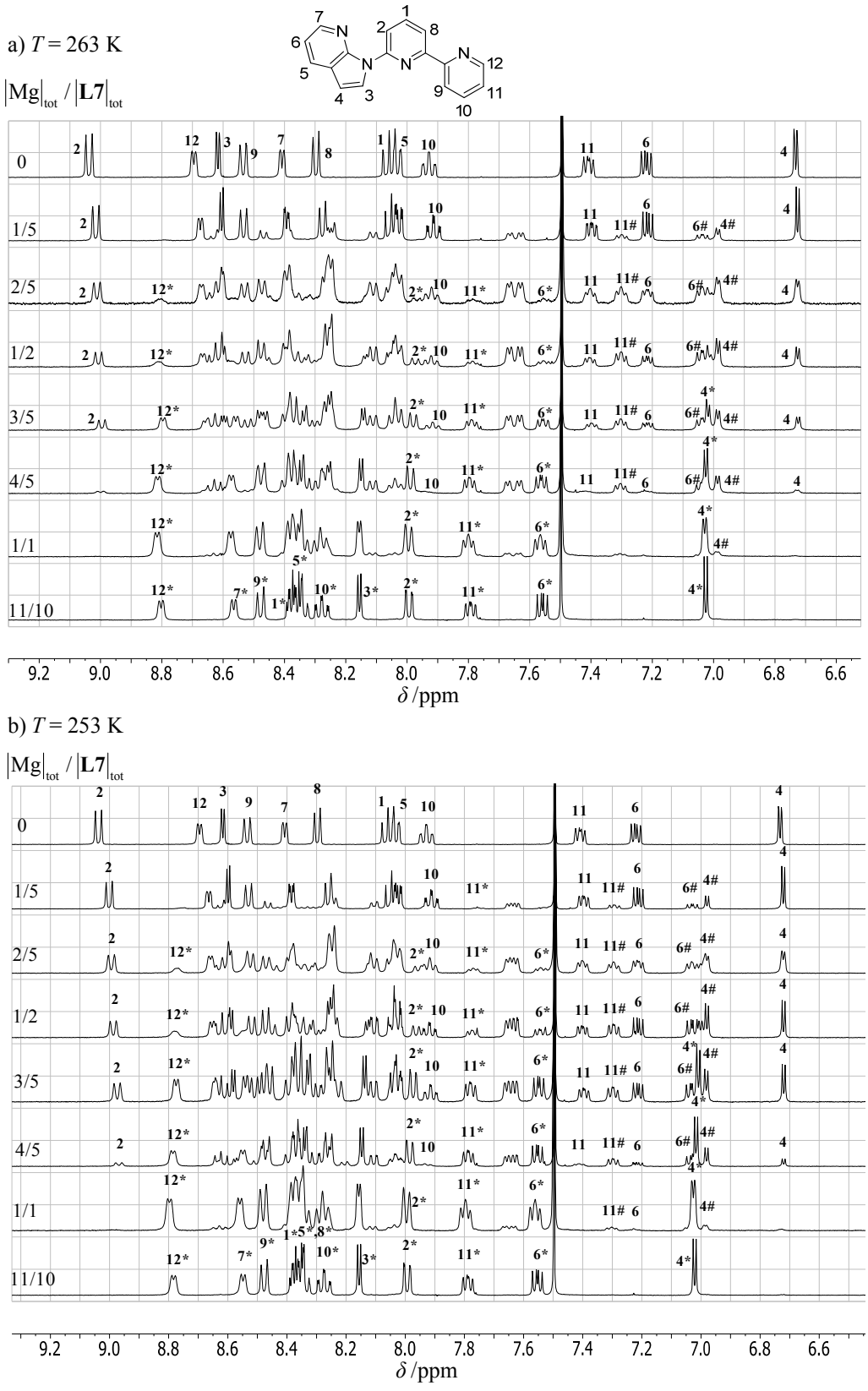


**Figure S17** Variation of $^1$H NMR spectra for the titration of **L7** with $Mg(ClO_4)_2$ in $CD_3CN/CDCl_3$ (1:1) at (a) 263 K and (b) 253 K ($|\mathbf{L7}|_{tot}$ = 7.5·10$^{-3}$ M). Code: # = $[Mg(\mathbf{L7})_2]^{2+}$, * = $[Mg(\mathbf{L7})]^{2+}$.

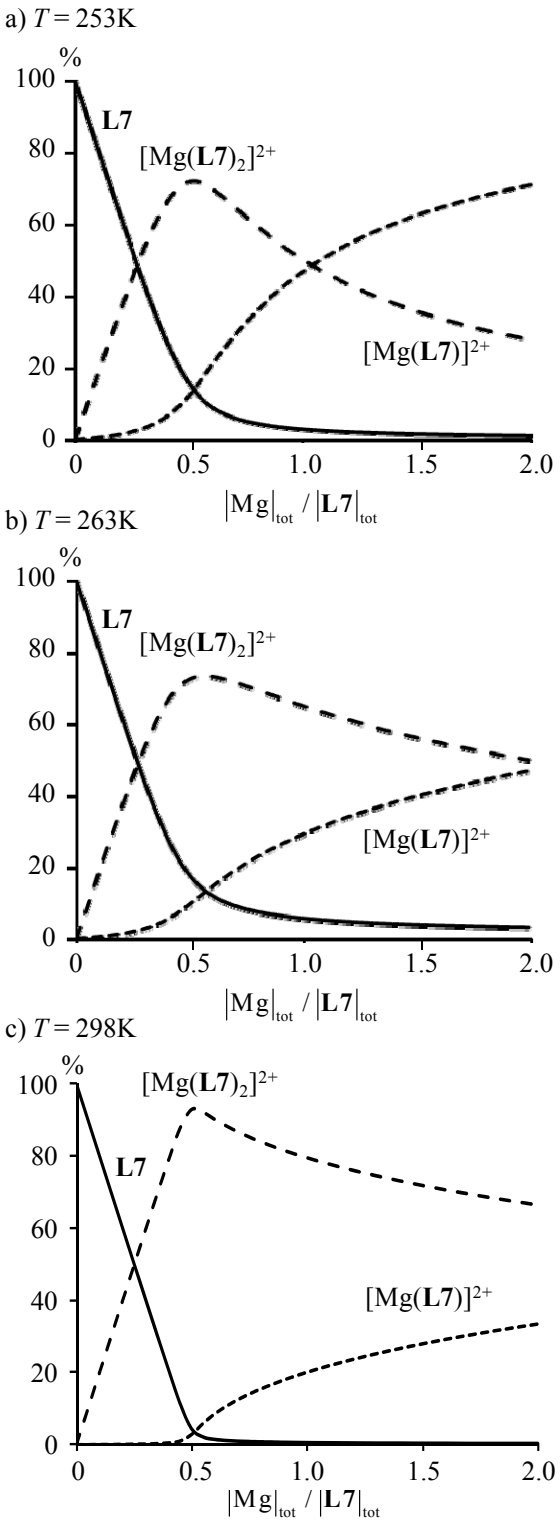


**Figure S18** Computed ligand speciation for the titrations of **L7** with $Mg(ClO_4)_2$ at various temperatures in $CD_3CN$:$CDCl_3$ (1:1). Total ligand concentration $|\mathbf{L7}|_{tot} = 7.5 \cdot 10^{-3}$ M.

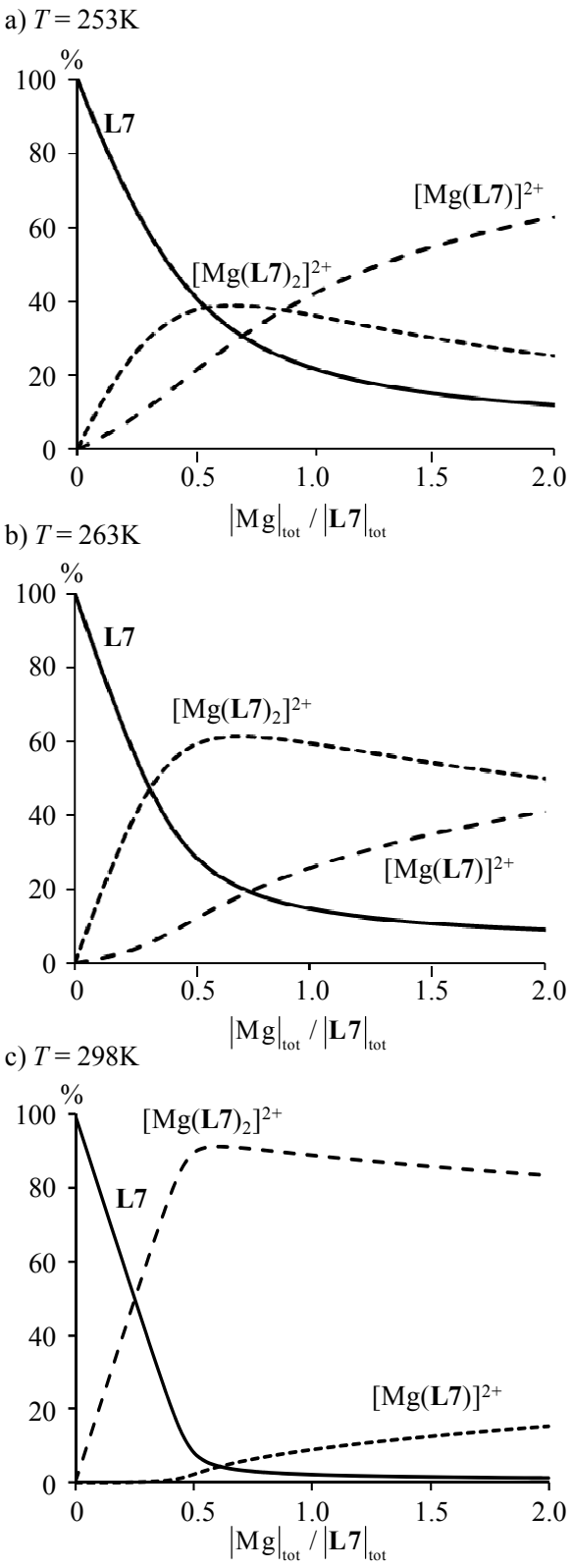


**Figure S19** Computed ligand speciation for the titrations of **L7** with $Mg(ClO_4)_2$ at various temperatures in $CD_3CN$. Total ligand concentration $|\mathbf{L7}|_{tot} = 7.5 \cdot 10^{-3}$ M.

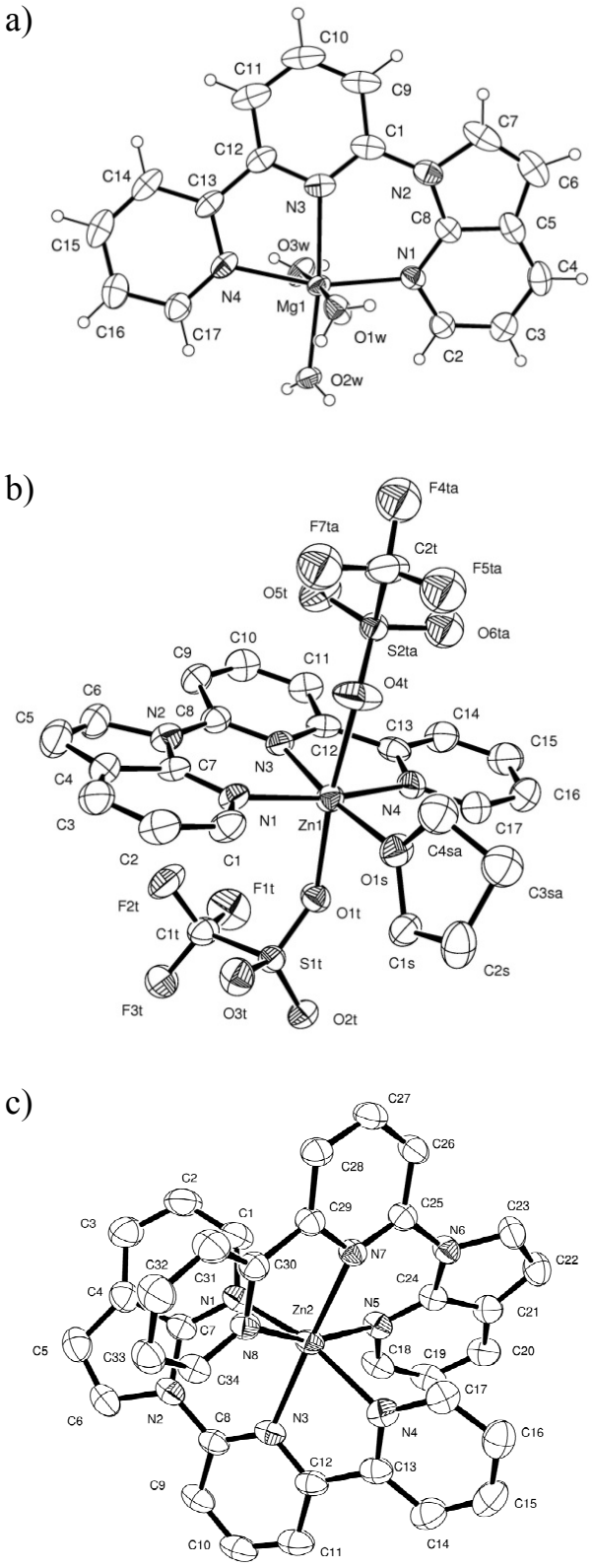


**Figure S20** ORTEP views of (a) $[Mg(\mathbf{L7})(OH_2)_3]^{2+}$, (b) $[Zn(\mathbf{L7})(THF)(CF_3SO_3)_2]$ and (c) $[Zn(\mathbf{L7})_2]^{2+}$ observed in the crystal structures of $[Mg(\mathbf{L7})(OH_2)_3](ClO_4)_2$ (**4**), $[Zn(\mathbf{L7})(THF)(CF_3SO_3)_2]$ (**5**) and $[Zn(\mathbf{L7})_2](CF_3SO_3)_2 \cdot 0.13\ H_2O$ (**6**) with atomic numbering scheme. Thermal ellispoids are represented at the 50% probability level.

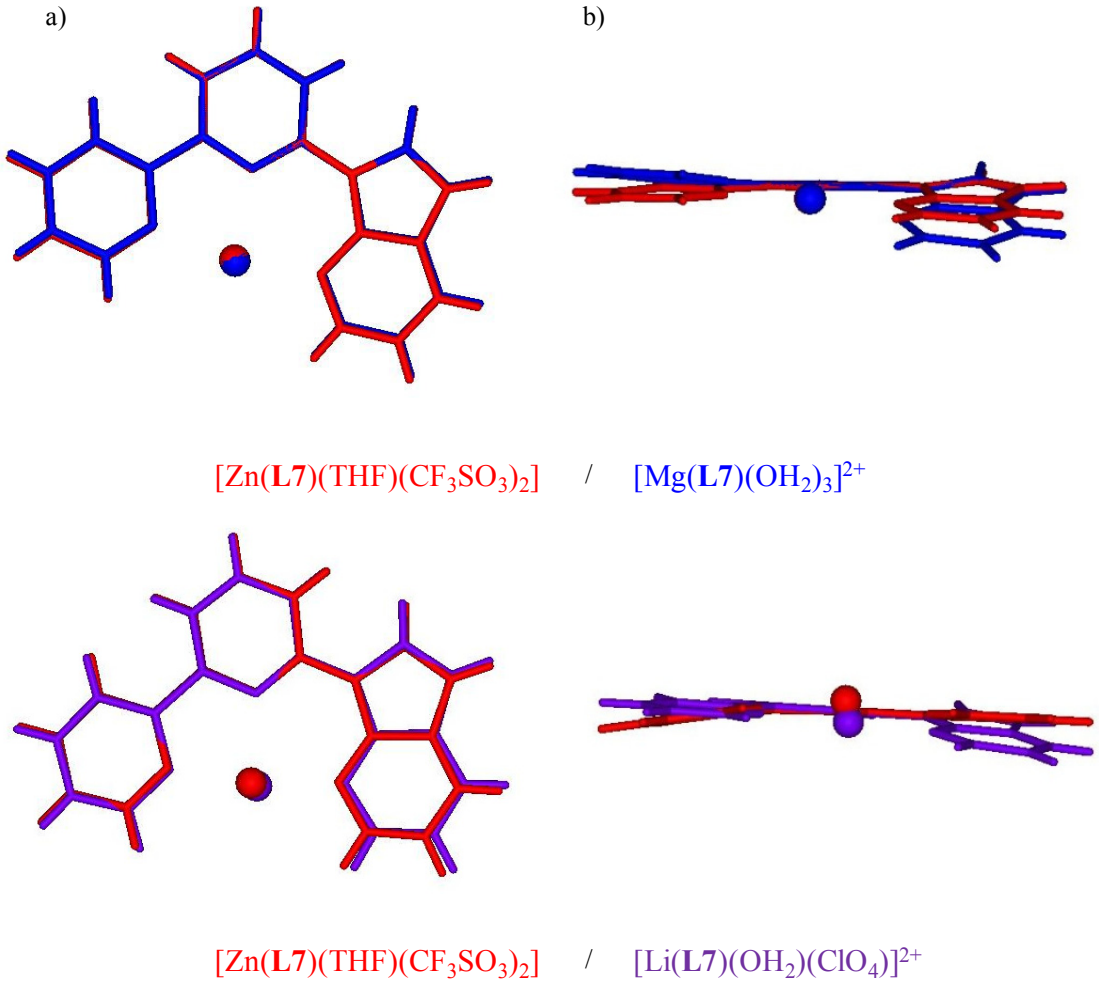


**Figure S21** Perspective views (a) perpendicular and (b) parallel to the central pyridine ring of the superimposition of the molecular structures of the polyaromatic M(**L7**) cores in [Zn(**L7**)(THF)($CF_3SO_3$)$_2$] (red) versus [Mg(**L7**)($OH_2$)$_3$]$^{2+}$ (blue, top), and [Zn(**L7**)(THF)($CF_3SO_3$)$_2$] (red) versus [Li(**L7**)($OH_2$)($ClO_4$)] (cyan, bottom).

Microspecies = Macrospecies

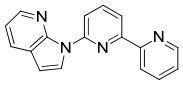

$$[M(CH_3CN)_6]^{2+} + \mathbf{L7} \rightleftharpoons[\beta_{1,1}^{M,\mathbf{L7}}] [M(\mathbf{L7})(CH_3CN)_3]^{2+} + 3CH_3CN$$

| Point groups: | $O_h$ | $C_s$ | $C_s$ | $C_{3v}$ |
|---|---|---|---|---|
| $\sigma^{ext}$: | 24 | 1 | 1 | 3 |
| $\sigma^{int}$: | $3^6$ | 1 | $3^3$ | 1 |
| $\sigma^{chiral}$: | 1 | 1 | 1 | 1 |

$$\omega_{1,1}^{M,\mathbf{L7}} = \frac{\left(\sigma_M^{ext}\sigma_M^{int}\sigma_M^{chiral}\right)\cdot\left(\sigma_{\mathbf{L7}}^{ext}\sigma_{\mathbf{L7}}^{int}\sigma_{\mathbf{L7}}^{chiral}\right)}{\left(\sigma_{M\mathbf{L7}}^{ext}\sigma_{M\mathbf{L7}}^{int}\sigma_{M\mathbf{L7}}^{chiral}\right)\cdot\left(\sigma_{CH_3CN}^{ext}\sigma_{CH_3CN}^{int}\sigma_{CH_3CN}^{chiral}\right)^3} = \frac{\left(24\cdot 3^6\right)}{3^3\cdot 3^3} = 24$$

$$\Rightarrow \beta_{1,1}^{M,\mathbf{L7}} = 24 f_{connect}^{M,\mathbf{L7}} \qquad (11)$$

Microspecies = Macrospecies

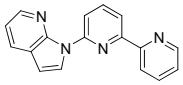

$$[M(CH_3CN)_6]^{2+} + 2\,\mathbf{L7} \rightleftharpoons[\beta_{1,2}^{M,\mathbf{L7}}] [M(\mathbf{L7})_2]^{2+} + 6\,CH_3CN$$

| Point groups: | $O_h$ | $C_s$ | $C_2$ | $C_{3v}$ |
|---|---|---|---|---|
| $\sigma^{ext}$: | 24 | 1 | 2 | 3 |
| $\sigma^{int}$: | $3^6$ | 1 | 1 | 1 |
| $\sigma^{chiral}$: | 1 | 1 | 1/2 | 1 |

$$\omega_{1,2}^{M,\mathbf{L7}} = \frac{\left(\sigma_M^{ext}\sigma_M^{int}\sigma_M^{chiral}\right)\cdot\left(\sigma_{\mathbf{L7}}^{ext}\sigma_{\mathbf{L7}}^{int}\sigma_{\mathbf{L7}}^{chiral}\right)^2}{\left(\sigma_{M(\mathbf{L7})2}^{ext}\sigma_{M(\mathbf{L7})2}^{int}\sigma_{M(\mathbf{L7})2}^{chiral}\right)\cdot\left(\sigma_{CH_3CN}^{ext}\sigma_{CH_3CN}^{int}\sigma_{CH_3CN}^{chiral}\right)^6} = \frac{\left(24\cdot 3^6\right)}{2\cdot 1/2\cdot 3^6} = 24$$

$$\Rightarrow \beta_{1,2}^{M,\mathbf{L7}} = 24\left(f_{connect}^{M,\mathbf{L7}}\right)^2 u_M^{\mathbf{L7},\mathbf{L7}} \qquad (12)$$

**Figure S22** Application of the site binding model[21] showing the determination of symmetry numbers ($\sigma^{ext}$, $\sigma^{int}$, $\sigma^{chiral}$)[22] for the microspecies contributing to equilibria (9)-(10) with M = Mg or Zn. The symmetry point groups are those expected for coplanar arrangements of the heterocyclic rings.

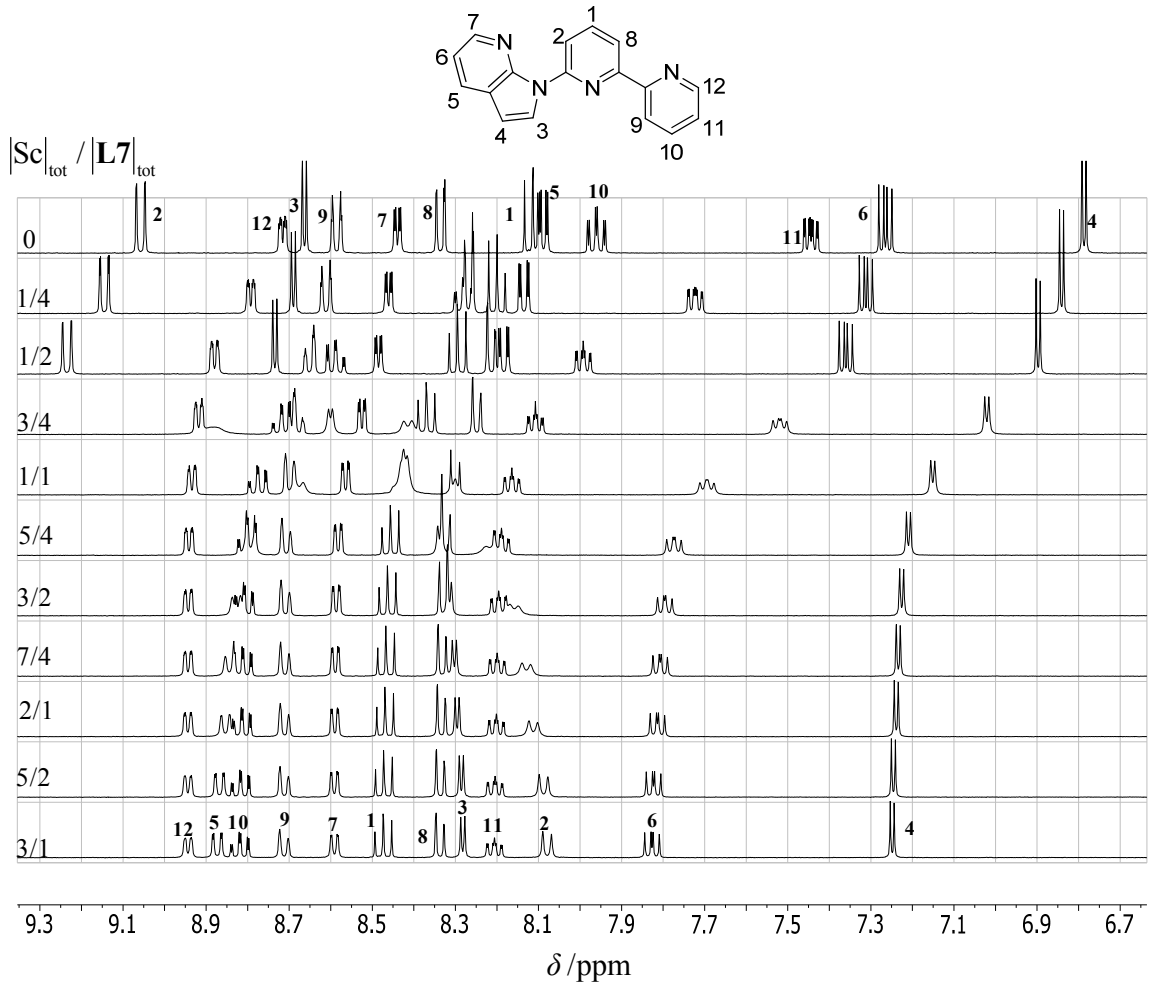


**Figure S23** Variation of $^1$H NMR spectra for the titration of **L7** with $Sc(CF_3SO_3)_3$ in $CD_3CN$ at 298 K ($|\mathbf{L7}|_{tot} = 7.5 \cdot 10^{-3}$ M).

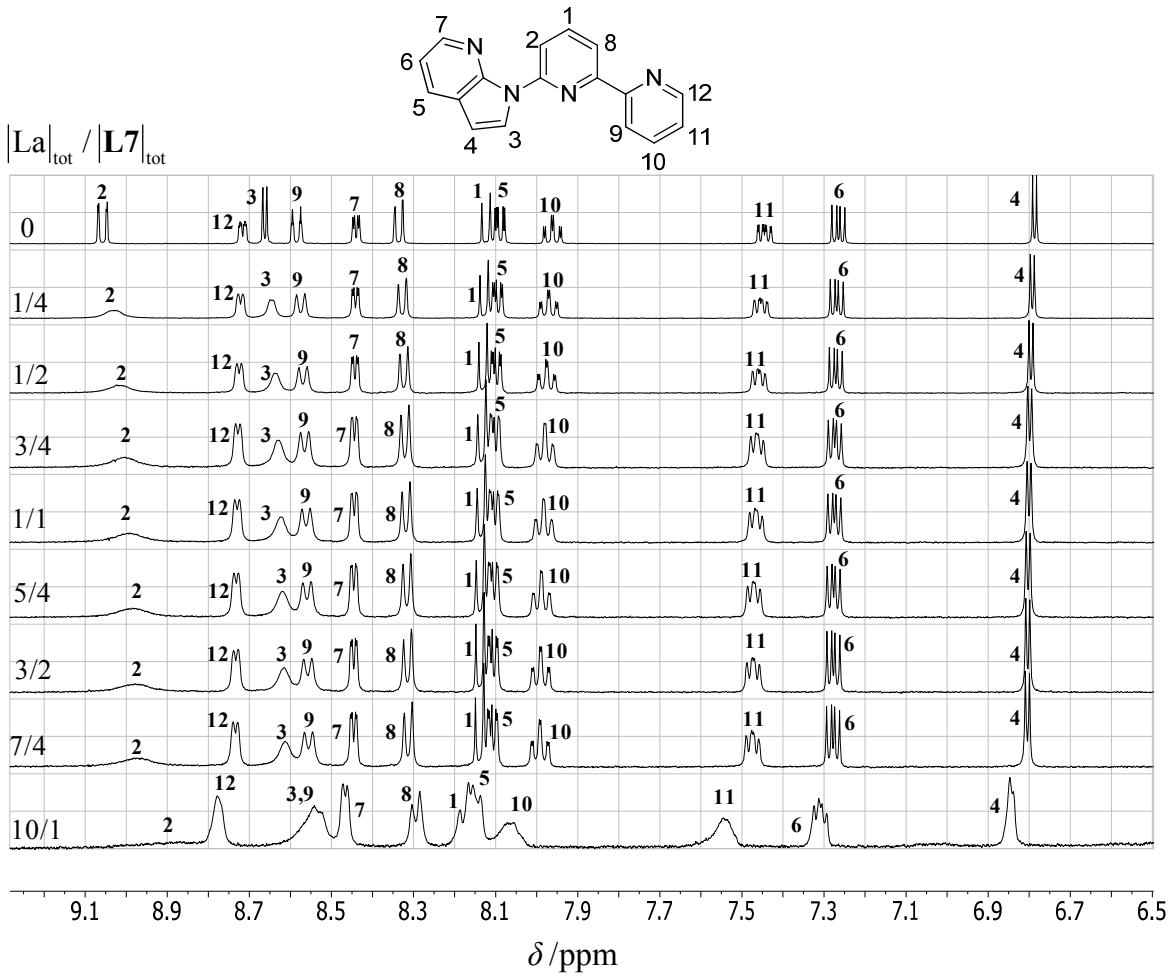


**Figure S24** Variation of $^{1}$H NMR spectra for the titration of **L7** with [La(hfac)$_3$(diglyme)] in $CD_3CN$ at 298 K ($|\mathbf{L7}|_{tot}$ = 7.5·10$^{-3}$ M).

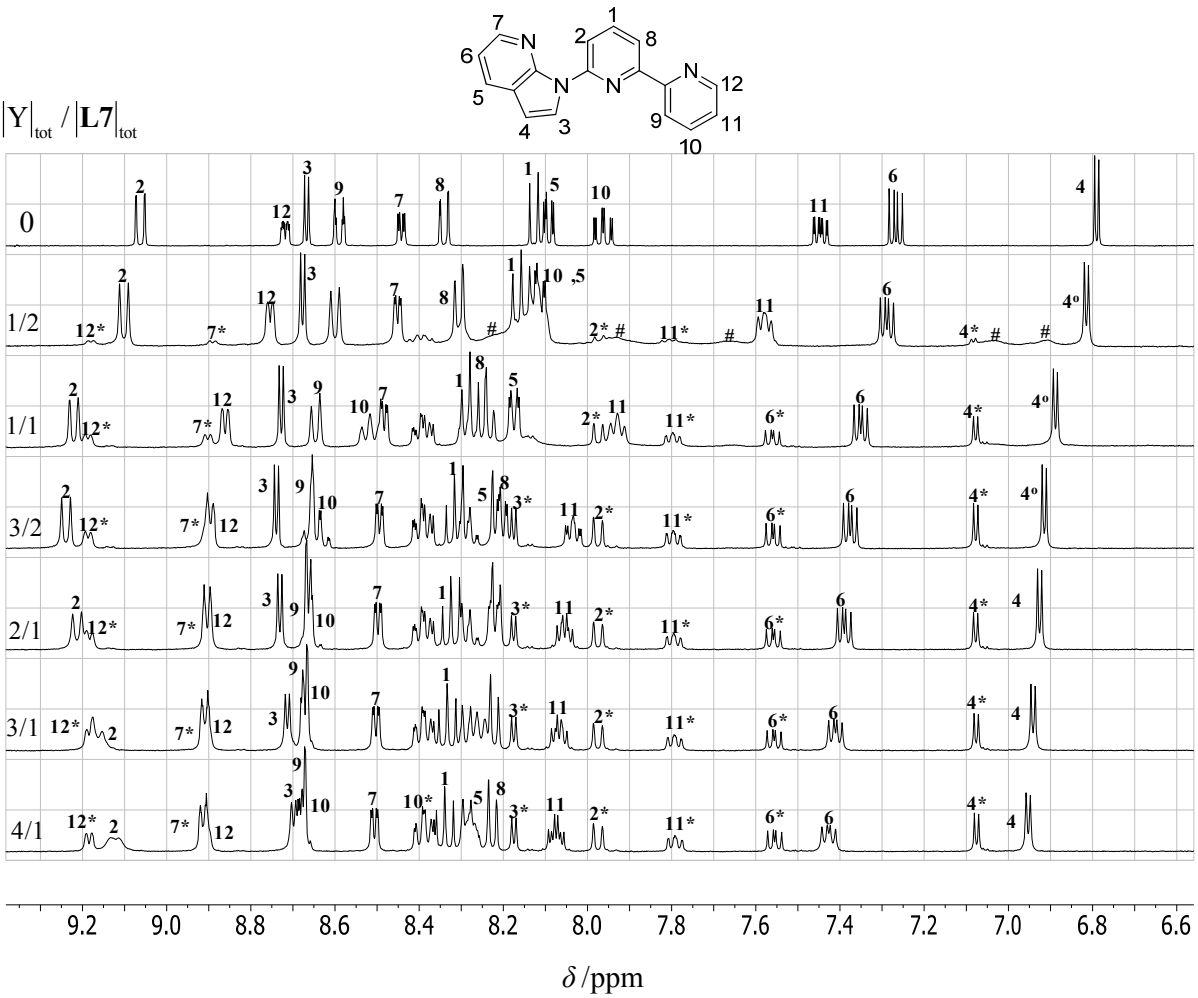


**Figure S25** Variation of $^1$H NMR spectra for the titration of **L7** with $[Y(CF_3SO_3)_3(diglyme)]$ in $CD_3CN$ at 298 K ($|\mathbf{L7}|_{tot} = 7.5\cdot10^{-3}$ M). Code: # = $[Y(\mathbf{L7})_2]^{3+}$, * = $[Y(\mathbf{L7})]^{3+}$.

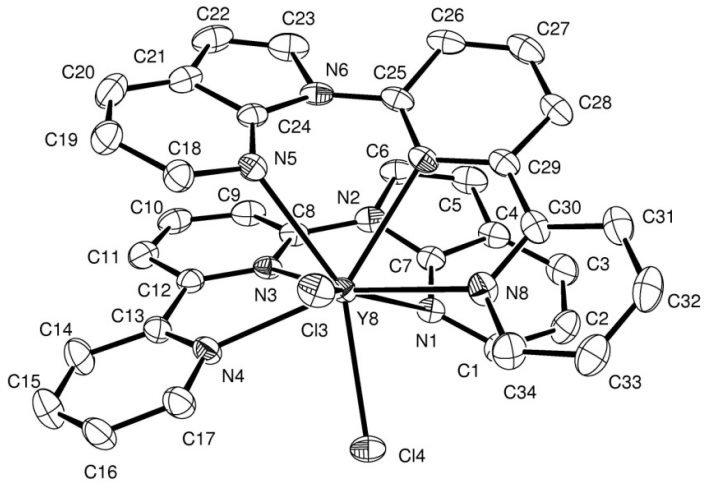


**Figure S26** ORTEP view of $[Y(\mathbf{L7})_2Cl_2]^+$ observed in the crystal structure of $[Y(\mathbf{L7})_2Cl_2]I_3\cdot CH_2Cl_2$ (**7**) with atomic numbering scheme. Thermal ellispoids are represented at the 50% probability level.

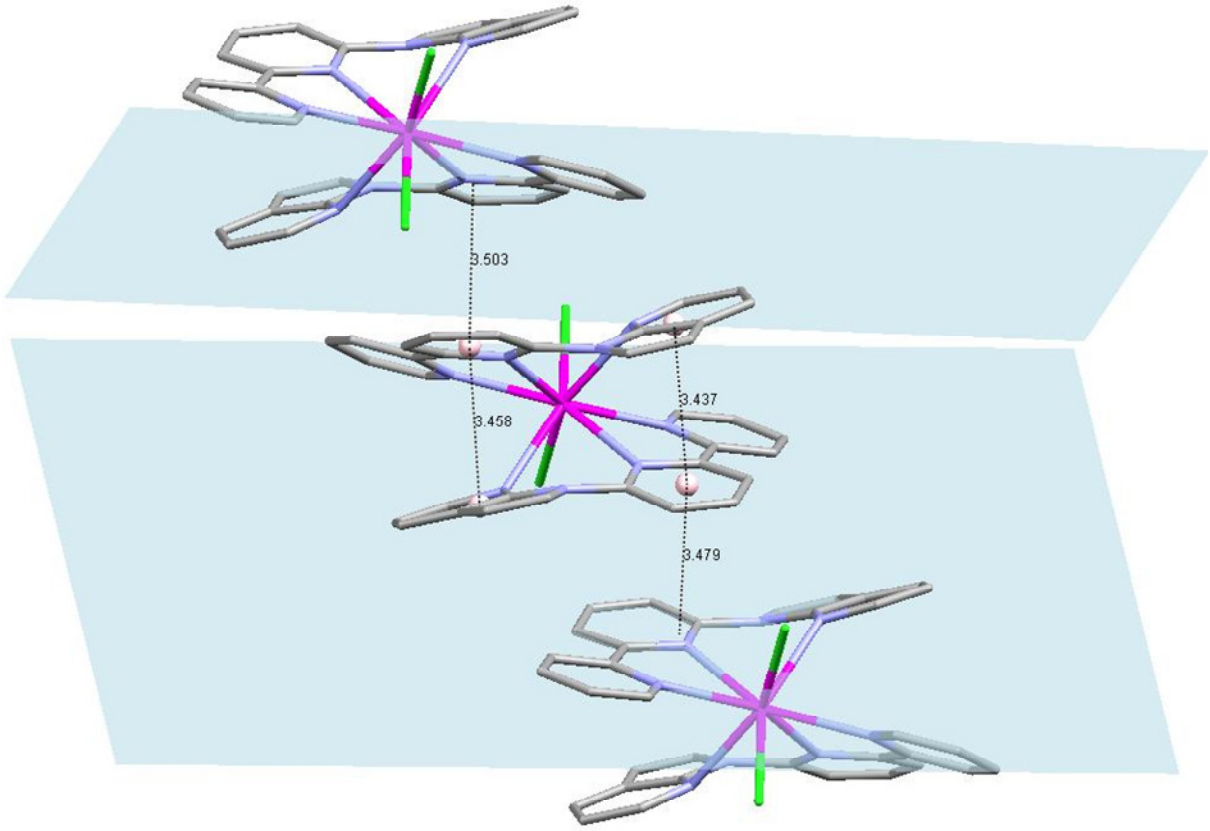


**Figure S27** π-stacking interactions operating in the crystal structure of $[Y(\mathbf{L7})_2Cl_2]I_3 \cdot CH_2Cl_2$ (**7**). Intramolecular: Py1(N3 C8 C9 C10 C11 C12)···Az2(N5 C24 C6 C18 C19 C20 C21 C22 C23) $d_{centroid\text{-}centroid}$ = 3.46 Å, Interplanar angle = 21.0°; Py2(N7 C25 C26 C27 C28 C29)···Az1(N1 C7 N2 C1 C2 C3 C4 C5 C6) $d_{centroid\text{-}centroid}$ = 3.44 Å, Interplanar angle = 19.9°.

Intermolecular: Py1···Py1'(' = 2-*x*, 2-*y*, 1-*z*) $d_{centroid\text{-}centroid}$ = 3.50 Å, Interplanar angle = 0°; Py2···Py2''('' =2-*x*, 2-*y*, -*z*) $d_{centroid\text{-}centroid}$ = 3.48 Å, Interplanar angle = 0°.

Microspecies = Macrospecies

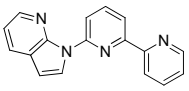

$$[Ln(CH_3CN)_9]^{2+} + \mathbf{L7} \rightleftharpoons[\beta_{1,1}^{Ln,\mathbf{L7}}] [M(\mathbf{L7})(CH_3CN)_6]^{3+} + 3CH_3CN$$

| Point groups: | $D_{3h}$ | $C_s$ | $C_s$ | $C_{3v}$ |
|---|---|---|---|---|
| $\sigma^{ext}$: | 6 | 1 | 1 | 3 |
| $\sigma^{int}$: | $3^9$ | 1 | $3^6$ | 1 |
| $\sigma^{chiral}$: | 1 | 1 | 1 | 1 |

$$\omega_{1,1}^{Ln,\mathbf{L7}} = \frac{\left(\sigma_{Ln}^{ext}\sigma_{Ln}^{int}\sigma_{Ln}^{chiral}\right)\cdot\left(\sigma_{\mathbf{L7}}^{ext}\sigma_{\mathbf{L7}}^{int}\sigma_{\mathbf{L7}}^{chiral}\right)}{\left(\sigma_{Ln\mathbf{L7}}^{ext}\sigma_{Ln\mathbf{L7}}^{int}\sigma_{Ln\mathbf{L7}}^{chiral}\right)\cdot\left(\sigma_{CH_3CN}^{ext}\sigma_{CH_3CN}^{int}\sigma_{CH_3CN}^{chiral}\right)^3} = \frac{\left(6\cdot 3^9\right)}{3^6\cdot 3^3} = 6$$

$$\Rightarrow \beta_{1,1}^{Ln,\mathbf{L7}} = 6 f_{connect}^{Ln,\mathbf{L7}} \qquad (20)$$

Microspecies = Macrospecies

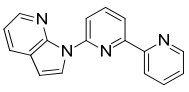

$$[Ln(CH_3CN)_9]^{2+} + 2\,\mathbf{L7} \rightleftharpoons[\beta_{1,2}^{Ln,\mathbf{L7}}] [M(\mathbf{L7})_2(CH_3CN)_3]^{3+} + 6\,CH_3CN$$

| Point groups: | $D_{3h}$ | $C_s$ | $C_2$ | $C_{3v}$ |
|---|---|---|---|---|
| $\sigma^{ext}$: | 6 | 1 | 2 | 3 |
| $\sigma^{int}$: | $3^9$ | 1 | $3^3$ | 1 |
| $\sigma^{chiral}$: | 1 | 1 | 1/2 | 1 |

$$\omega_{1,2}^{Ln,\mathbf{L7}} = \frac{\left(\sigma_{Ln}^{ext}\sigma_{Ln}^{int}\sigma_{Ln}^{chiral}\right)\cdot\left(\sigma_{\mathbf{L7}}^{ext}\sigma_{\mathbf{L7}}^{int}\sigma_{\mathbf{L7}}^{chiral}\right)^2}{\left(\sigma_{Ln(\mathbf{L7})2}^{ext}\sigma_{Ln(\mathbf{L7})2}^{int}\sigma_{Ln(\mathbf{L7})2}^{chiral}\right)\cdot\left(\sigma_{CH_3CN}^{ext}\sigma_{CH_3CN}^{int}\sigma_{CH_3CN}^{chiral}\right)^6} = \frac{\left(6\cdot 3^9\right)}{2\cdot 1/2\cdot 3^6\cdot 3^6} = 6$$

$$\Rightarrow \beta_{1,2}^{Ln,\mathbf{L7}} = 6\left(f_{connect}^{Ln,\mathbf{L7}}\right)^2 u_{Ln}^{\mathbf{L7},\mathbf{L7}} \qquad (21)$$

**Figure S28** Application of the site binding model[21] showing the determination of symmetry numbers ($\sigma^{ext}$, $\sigma^{int}$, $\sigma^{chiral}$)[22] for the microspecies contributing to equilibria (16)-(17) with Ln = Y. The symmetry point groups are those expected for coplanar arrangements of the heterocyclic rings.